April 2018

Experimental and Theoretical Optimization of BiI3 Selective-Contact Solar Cell Materials

Andrew Neil Callahan
Worcester Polytechnic Institute

Danielle L. Cote
Worcester Polytechnic Institute

Gina Rose Capobianco
Worcester Polytechnic Institute

Michaella Balicki
Worcester Polytechnic Institute

Follow this and additional works at: https://digitalcommons.wpi.edu/mqp-all

Experimental and Theoretical Optimization of BiI₃ Selective-Contact Solar Cell Materials

A Major Qualifying Project

Submitted to the Faculty and Staff of

WORCESTER POLYTECHNIC INSTITUTE

in partial fulfillment of the requirements for the
Degrees of Bachelor of Science in Chemical Engineering
and Bachelor of Science in Professional Writing

By:

_____
Michaella Balicki

_____
Andrew Callahan

_____
Gina Capobianco

_____
Danielle Cote

Abstract

BiI_3 is an n-type semiconductor, synthesized in thin layers through the solution deposition techniques of spin-coating and thermal annealing. Although the material has a favorable optical band gap of 1.8 eV, researchers have not yet been able to raise the power conversion efficiency to a point where it contends with current manufactured semiconductor materials like silicon. We hypothesize that this is attributed to the high resistivity of BiI_3 combined with an insufficient carrier lifetime. To address this, we sought to improve the light absorption and carrier collection by optimizing the thickness, morphology, and chemical composition of each layer. The BiI_3 cell contained the following layers, in order: Glass/FTO/TiO_2/BiI_3/ P3HT/Gold, where we optimized the BiI_3 and TiO_2 layers. For the TiO_2 layer optimization, it was found that compact (c) TiO_2 with an additional layer of mesoporous (m) TiO_2 facilitated charge collection and therefore increased the short-circuit current density (J_{SC}) of the cells. As for our semiconductor layer, we found through experimental results that annealing BiI_3 in air oxidizes its surface, improving open-circuit voltage (V_{OC}). This benefit of using oxidized BiI_3 as the semiconductor layer was also confirmed through computational modeling. Additionally, a heat treatment of BiI_3 using solvent vapor annealing (SVA) in dimethylformamide (DMF) increased grain sizes, increased carrier mobility and lifetime, and improved the V_{OC}. Finally, we combined these modifications with an additional 10-minute 100°C post-anneal after the gold evaporation stage, which we found to enhance interlayer contact and therefore the overall J_{SC}. Achieving a maximum power conversion efficiency of 0.23%, we affirm that BiI_3 is a promising material that requires a more in-depth characterization to better discern areas of improvement.

Acknowledgements

Authorship

Under the advisement of Professors Aaron Deskins and Pratap Rao, all members of our MQP team contributed equally to the design, implementation, and analysis of our experimental research. Michaella Balicki and Gina Capobianco conducted the theoretical simulations that are outlined and analyzed in Sections 3.3 and 4.2 respectively. Advised by Professor Brenton Faber, Andrew Callahan proposed a technology acceptance model for solar energy technologies in the United States, as discussed in Section 6.0.

Table of Contents

1.0 Introduction

This Major Qualifying Project (MQP) is part of a larger effort to characterize and advance the potential of thin-film selective contact solar cells. Though these photovoltaic (PV) materials are in their research and development stage, we believe that there is a hopeful and promising future for them. There are many benefits to pursuing second generation solar materials as global efforts toward the integration of clean energy practices continues.

In terms of current manufacturing prices, silicon solar cells have high costs due to high temperature production requirements (~1500 °C), which are required to achieve high efficiency. Additionally, because the silicon cells are nearly perfected, it is difficult to reduce the associated pricing beyond lean manufacturing improvements. Therefore, researchers are now focusing on alternative materials.

Presently, there is relatively little background research focused on second generation solar cell materials, such as bismuth triiodide (BiI_3), the material of interest in this research study. As a semiconductor material, BiI_3 serves as a nontoxic alternative to lead-based thin film solar materials. It also has many favorable photovoltaic properties, such as a near-ideal band gap of 1.8 eV, and a high optical absorption coefficient of $>10^5$ cm^{-1}. Another benefit of BiI_3, addressed more comprehensively in the background section, includes a theoretical efficiency of ~44% when placed in tandem with a silicon cell (see Section 2.5.1).

Accordingly, the goal for this MQP is to synthesize BiI_3 thin-film solar cells and analyze how altering variables in the synthesis process affect solar cell performance. In order to reach this goal, we had the following objectives:

1. Synthesize BiI_3 solar cells using a reproducible method.
2. Benchmark solar cell layers by measuring cell efficiency.
3. Use experimental data to provide a basis on improving the material and optimizing its production process.
4. Study the BiI_3 absorber using the density functional theory.
5. Use theoretical data to explain important features of experimental data.

2.0 Background

This section contains background information for understanding methodologies and results detailed in later sections. It begins more broadly with the larger implications and promising future of solar energy and then narrows to physical and theoretical terminology and concepts of photovoltaic (PV) materials such as bismuth triiodide (BiI_3).

2.1 The Promise of Solar Power

Solar energy was first harnessed over a century ago, but only in the past few decades have people begun to use it as a viable energy option. As a renewable energy source, solar energy is environmentally friendly and has seen a steady decline in cost over the past decade. Although solar energy grows increasingly relevant each year, it still faces the challenge of contending with fossil fuel energy sources, such as oil and gas. This section aims to address the fundamental challenges created through current energy practices, and affirms the promise and potential of solar energy.

2.1.1 The Human-Enhanced Greenhouse Effect

The United States and many other first world countries rely heavily on resources such as coal, oil, and natural gas for their energy needs. Although these resources are inexpensive and convenient for many, they are finite in nature and tax the environment when used on a large scale. From petrochemical refineries and oil wells to gasoline-powered vehicles, there are many ways by which fossil fuels have an adverse effect on the environment. This damaging effect is achieved, in part, from the retrieval of these resources - for example, the drilling and extraction of natural gases - however, the most prominent source of environmental harm are the emissions from combustion, such as greenhouse gases or other toxic pollutants.

Our planet's atmosphere contains different gases that trap heat, called greenhouse gases; many of these gases are a result of burning fossil fuels. Carbon dioxide and methane are the most abundant greenhouse gases - they account for an accumulated 92% of global greenhouse gas emissions.[1] Other, less prevalent greenhouse gases include nitrous oxide, ozone, and chlorofluorocarbons (CFCs). As a result of the presence of these gases, Earth's transparent atmosphere undergoes the greenhouse effect. When sunlight warms the Earth's masses of land and

---

[1] Environmental Protection Agency, *Overview of Greenhouse Gases* (EPA, April 2016).

oceans, these warmed surfaces release infrared radiation, in the form of heat, back into the atmosphere. Greenhouse gases prevent infrared radiation from passing back through the atmosphere. They instead absorb this infrared light and prevent it from reflecting back into space. This trapped heat is emitted as radiation back to the surface of the Earth, which in turn heats the surface.[2] The result - planetwide climate change.

2.1.2 Solar as a Renewable Energy Source

According to a Massachusetts Institute of Technology (MIT) research study, *The Future of Solar Energy*, researchers believe that the large-scale implementation of solar energy is "likely to be an essential component of any serious strategy to mitigate global climate change."[3] Given that present day issues like global warming are directly attributed to current energy practices, solar energy is a promising energy source for the future. Solar power has large scale potential for mitigation of global climate change and the ability to meet the global energy demand. According to the United States Energy Information Administration (EIA), the total world energy consumption, as of 2015, is 575 quadrillion British thermal units (Btu). This number is projected to grow to 736 quadrillion Btu in 2040, a 28% rise.[4] Solar energy can keep up with this energy demand because the sun delivers more energy to Earth in one hour than the world consumes over the course of a year.[5]

From *Energy Informative*, solar energy has the potential to save United States families thousands of dollars, increase the value of homes, create energy independence, and save the environment.[6] Figure 1 illustrates the price of solar power over time, which has traditionally been a factor which hinders adoption. Based on the graph, the median price of residential, non-residential, and utility-scale solar technologies has decreased substantially since 2010. The y-axis of the graph represents values of 2015 $/Watt (W)$_{DC}$, or dollar value per unit of direct current power, indicating a tangible decline in price.

---

[2] University of Pittsburgh Physics and Astronomy, *Environmental Problems with Coal, Oil, and Gas* (The Nuclear Energy Option, Ch. 3).

[3] Massachusetts Institute of Technology, *The Future of Solar Energy*. (MIT, 2015).

[4] U.S. Energy Information Administration, *International Energy Outlook 2017* (EIA, September 2017).

[5] MIT Technology Review. *Solar Power Will Make a Difference - Eventually* (2009).

[6] Meahlum, Mathias Aarre, *Top 10 Benefits of Going Solar* (Energy Informative, 2017).
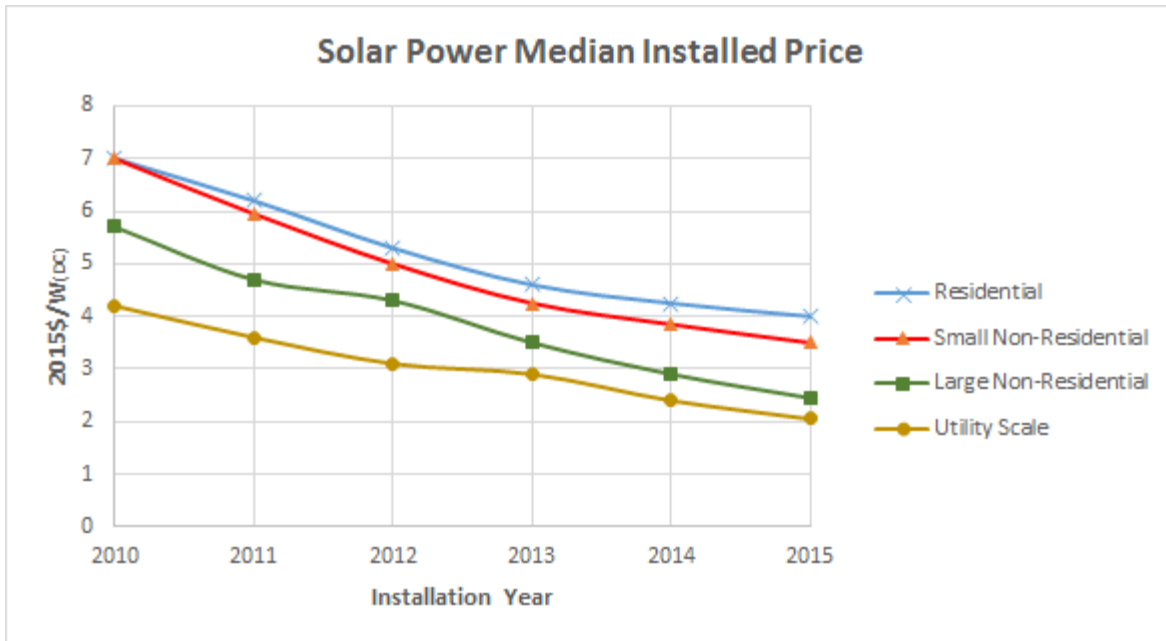
Figure 1. Installment cost of solar electricity (per watt) from 2010 –2015.[7]

With this decrease in installment price has come an increase in usage, and thus growth of the solar industry. According to a *Science Magazine* article, the global solar electricity market is presently valued at more than $10 billion annually and continues to experience industrial growth of at least 30% each year.[8] Figure 2 illustrates the growth of solar energy based on yearly energy consumption. Based on the graph, there is a promising trend in solar growth rate that is projected to continue in the future. Each year the adoption of solar grows, but there are challenges that the industry must overcome to compete with other energy sources, such as petroleum, coal, and natural gas.

---

[7] Weiner, Jon, *Median Installed Price of Solar in the United States Fell by 5-12% in 2015* (Berkeley Lab, 2016).
[8] Lewis, Nathan S., *Toward Cost-Effective Solar Use* (Science Magazine, 2007).
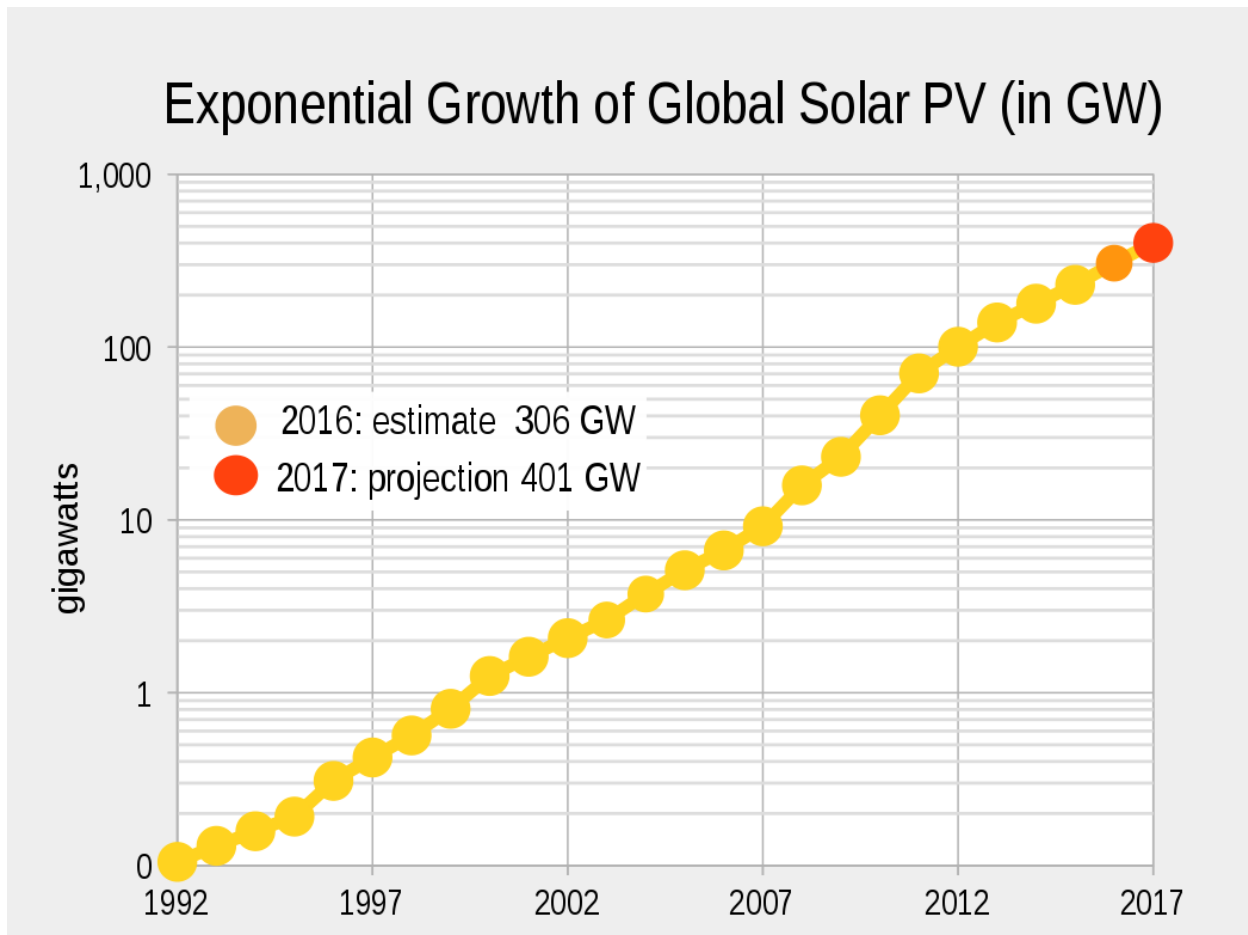
Figure 2. Steady growth of solar PV renewable energy.[9]

2.1.3 The Challenges of Solar Energy

Although solar energy is growing, fossil fuels continue to serve as the dominant energy source. Presently, fossil fuels are inexpensive, available, reliable, and convenient.[10] Industries have been created for the purpose of retrieving underground deposits of these resources. They are convenient for homeowners to use and provide instant and reliable energy on demand. Finally, in terms of reliability, the capacity factor, or the average power generated divided by the rated peak power, is notably greater for fossil fuels than solar energy devices. While coal power stations operate at 70-80% maximum capacity, solar panels often operate at a capacity factor of around 15%.[11] This means that solar energy sources are less reliable than fossil fuels, which can be

---

[9] Wikimedia Commons, *PV cume semi log chart 2014 estimate.svg* (Wikimedia Commons, 2014).

[10] Distributed Generation Limited, *Fossil Fuels - Cheap, Available, Reliable, & Convenient* (Dec 2017).

[11] Mathiesen, Karl, *What is holding back the growth of solar power?* (The Guardian, 2016).

attributed to the scarcity of consistent sunlight during different seasons or in different regions of the globe.

Another challenge that solar energy faces is low usage in many regions of the globe, especially in developing countries. Only a limited number of first world countries, particularly those in Europe such as Germany, Italy, and the United Kingdom, utilize solar energy significantly. The price of solar (\$260/m^2 for silicon PV cells)[12] far exceeds the economic limits of developing countries, such as India and those in Africa, where experts argue that the price per unit area would need to be reduced by one order of magnitude in order to be implemented in widespread fashion.[13] Fortunately, as solar prices decline and growth expands, poorer countries are more likely to begin implementing PV units.

To expedite solar commercial implementation on a large scale, researchers argue that solar energy must be captured, converted, and stored in an economically-sound manner.[14] This would mean harnessing solar energy in a manner that is comparable to fossil fuels. This is a challenge that all renewable energy industries are facing; although scientists believe that this will one day be a feasible objective, there is still much research and collaboration to be done before it becomes a reality. Fortunately, there are certain realities that benefit the future of solar energy. For instance, the most obvious and substantial drawback of fossil fuels is that they are not replenishable. In this sense, solar energy has a fundamental advantage since it is renewable, which serves as its main selling point. In addition, there is reason to believe that other factors, such as solar cell efficiency and price will come together to bring about an opportune time for solar power. In order to understand how to improve these factors, photovoltaics as well as their materials must be understood as well.

2.2 Governing Principles of Photovoltaic Materials

Photovoltaic devices, also known as solar cells, are made up of materials that are able to harness light energy from the sun and transform it into electricity. This section articulates these photovoltaic materials, their importance in the structure of solar cells, and how they allow the cells to operate.

---

[12] Rao, Pratap, *Solar Energy - Photovoltaics*. (Worcester Polytechnic Institute Mechanical Engineering, 2017).
[13] Ibid.
[14] Ibid.

2.2.1 Semiconductors

The main component of a solar cell is the semiconductor material. Semiconductors provide an efficient system for converting solar energy into electrical energy. This is because semiconductors absorb light and create photoexcited electrons. The energy of these photoexcited electrons can be extracted to produce electricity. There are two types of semiconductors based on whether the dominant charge is a hole (p-type) or an electron (n-type). Holes and electrons are both carriers within the solar cell, while holes carry a positive charge and electrons carry a negative charge. Semiconductor materials become p or n type when they are doped or an impurity is added to it.[15] Doping semiconductor materials enhances the electronic properties, therefore allowing it to be used as a photovoltaic material. These doping techniques are shown below in Figures 3 and 4, where a group IV element (such as Si) is being doped, for example. In n-type doping group V elements, such as phosphorus or arsenic, are used because they have five valence electrons and group IV has four. In Figure 3, this is shown as the red atom. When the red atom replaces a semiconductor atom, there is an extra negative electron, creating an n-type material. Although, the negative electron is also paired with an extra proton from the nucleus of the impurity, so there is still an overall neutral charge on the material. The extra negative electrons become free electrons within the material because they are not bound to a nucleus. As a result, n-type materials have an increased concentration of free electrons.
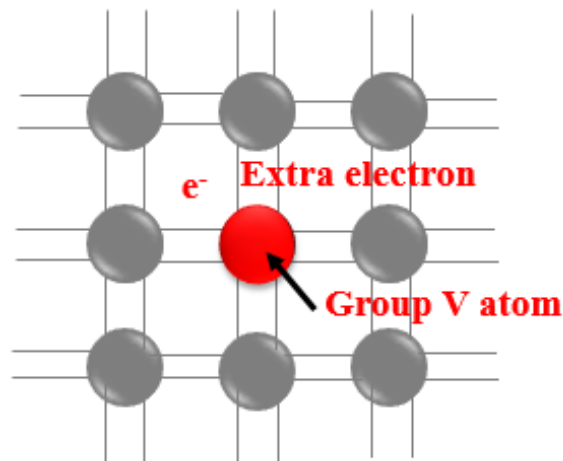
Figure 3. N-Type Doped Semiconductor

---

[15] Honsberg, C. and Bowden, S., *Doping*, (PVEducation, 2016).

In p-type doping, a group III element, such as boron or gallium, is added to the semiconductor because they have three valence electrons, compared to four electrons of group IV elements like Si. In Figure 4 this is shown as a blue atom. Since the dopant atom only has 3 electrons, compared to four electrons of neighboring atoms, there is a deficiency of charge on the dopant. If a nearby atom donates a charge to the dopant, this leaves behind a net positive charge on the donating atom, or a hole. These holes are a lack of full electrons on atoms. Similar to n-type, the material has an overall neutral charge, although in p-type there are an excess amount of free holes instead of free electrons.[16] Holes are positively charged carriers within the cell.
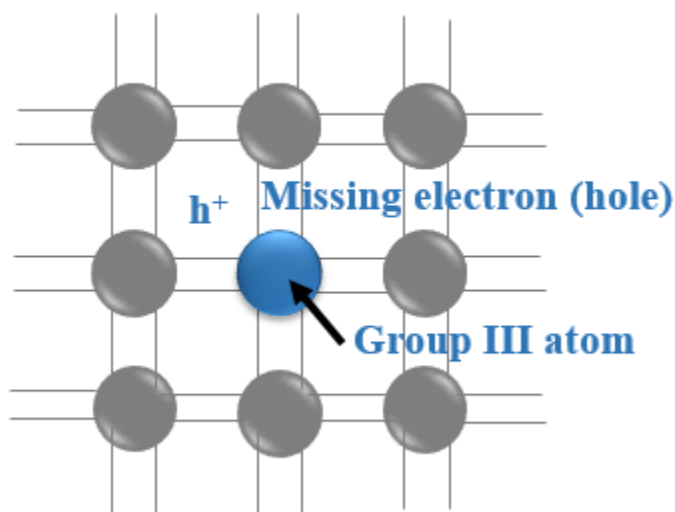
Figure 4. P-Type Doped Semiconductor

These materials are important to photovoltaics because when junctioned together, they allow the flow of electricity necessary for the cell to function.

2.2.2 Semiconductor Junctions

Semiconductors harness light energy from the sun and transform it into electricity by converting electromagnetic energy of the photons from the light into electrical potential energy. The potential energy is raised when the electrons are excited and then allowed to move from the ground state to the excited state, as shown in Figure 5 below. In the ground state, there is an

---

[16] Honsberg, C. and Bowden, S., *Light Generated Current*, (PVEducation, 2016).

electron hole pair, which is a positive and negative charge together, and in the excited state they separate.

Photon

Ground State
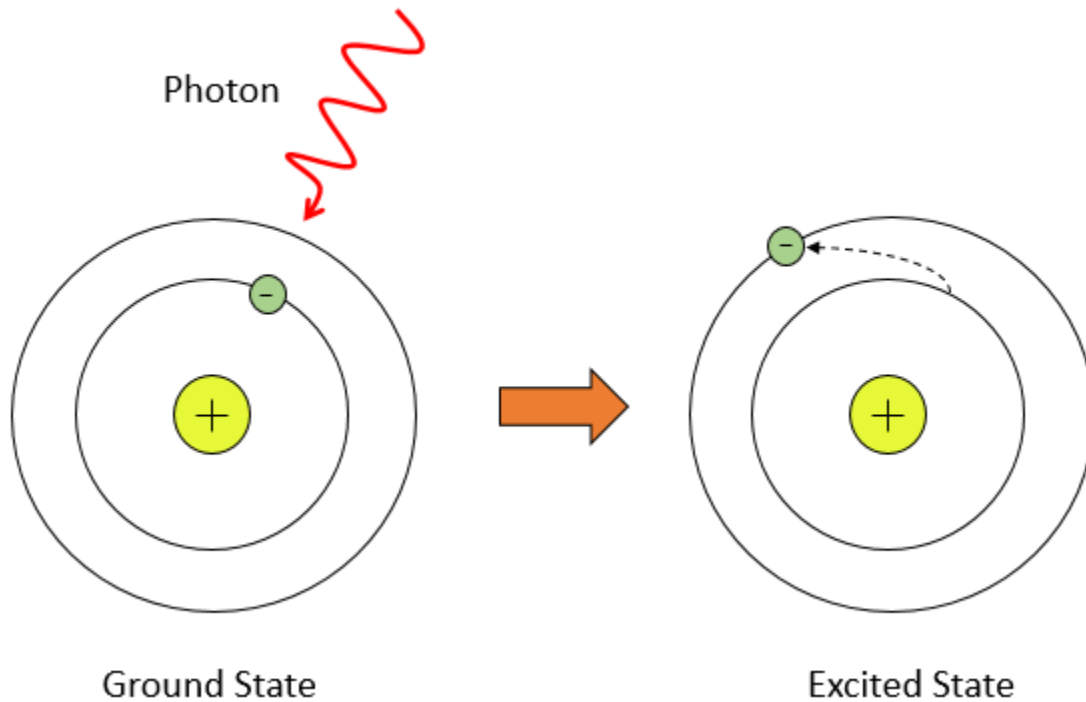
Excited State

Figure 5. Sunlight in the form of photons increase the electrons in the cell to an excited state therefore increasing the electrical potential energy. Only light with a certain wavelength (the difference in energy between the two electronic states) is able to excite the electron.

In order for the light to generate electrical power, a voltage across the cell must be produced. Solar cells are made up of materials with different concentrations of free holes and electrons, creating an electric field at the junction of the materials. The electric field is created when the electrons diffuse into the other material and leave behind ion cores. This concept of electron deficiency in p-type and n-type materials to create an electric field which is like a concentration gradient, shown in Figure 6 below. Electrons diffusing from the n-type to the p-type material leave behind uncompensated donor ions (N_d^+) and holes diffusing from the p-type to n-type material leave behind uncompensated acceptor ions (N_a^+).[17] However, because of the

---

[17] Valkenburg, Mac E. VAN, *Reference Data for Engineers: Radio, Electronics, Computer, and Communications* (Technology & Engineering, 2001).

fundamental concentration gradient that exists in the semiconductor material, an electric field at the junction is generated.
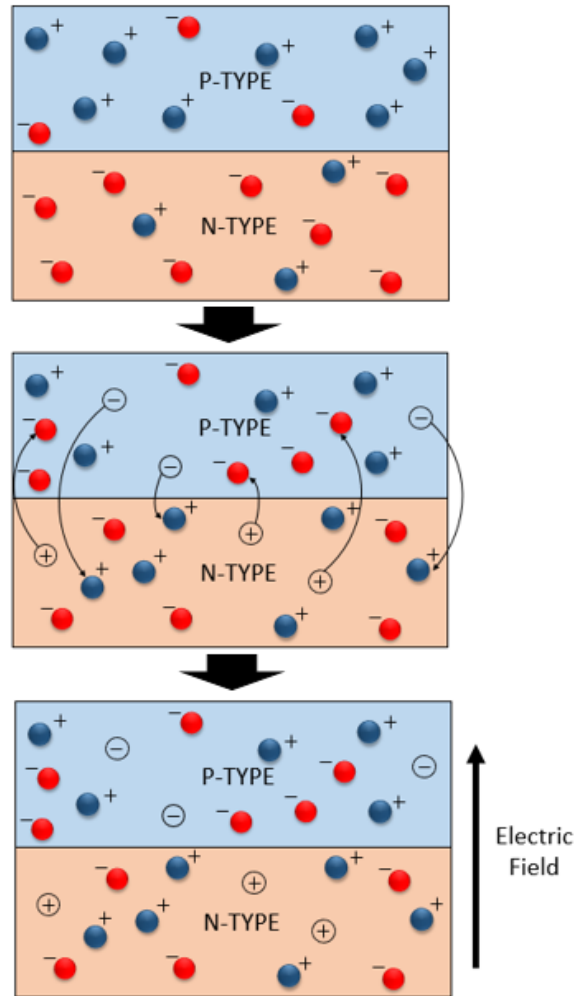
Figure 6. The formation of an electric field can be thought of as a concentration gradient. Once there is motion of the charges, the holes leave behind positive ion cores on the n side and the electrons leave behind negative ion cores on the p side, forming the electric field.

If there is no difference in concentration among the carriers in the semiconductor, then there is no net motion of charge through the material. However, in n-type materials like BiI_3, electrons are the majority carrier (while holes are the minority carrier) and therefore there is a difference in concentration between the n-type and the p-type materials. Accordingly, a larger difference in concentration between p-type and n-type materials results in a greater amount of diffusion, which in turn, yields a stronger electric field. Inversely, a smaller difference in

concentration ultimately results in a weaker electric field. As electrons diffuse across the p-n junction, there is a point where the electric field's negative charge repels any further diffusion. The electric field acts as a barrier, and is referred to as the depletion region. This phenomena can be used to explain the behavior of electrons and holes as they diffuse through semiconductor materials, such as ours. The potential difference needed to move electrons through the electric field is called the barrier potential. Equation 1 outlines the equation of the barrier potential.

$$V_0 = \frac{kT}{q} \ln\left(\frac{p_p}{p_n}\right)$$

Equation 1. Barrier Potential

In the above equation, kT is equal to room temperature thermal energy (~0.025 eV) and q represents the electron charge, while variables p_p and p_n are the hole concentrations on the p and n-side, respectively. Qualitatively, this means that the higher the concentration of holes on the p-side of the material, the greater the barrier potential. Because n-type materials have a low concentration of holes that when placed in tandem with a p-type material, which has a higher concentration of holes, the strength of the electric field would increase with increasing amount of holes. The difference in electrical potential of the electrons and holes across these materials creates the voltage.

The electric field at the junction between these materials drives the electric current in one direction, allowing for the operation of the device. The general operation of a solar cell starts with the light entering the cell, and exciting electron-hole pairs. The electrons then diffuse in the direction of the electric field. Once the electrons diffuse to the current collector layer, they move horizontally toward the external circuit. The electrons move through the external circuit and dissipate their energy into the load, and then they move back to the cell, entering through the transparent current collecting layer. An electron meets back with a hole in the cell to complete the circuit.[18] This is known as the photovoltaic effect.

---

[18] Honsberg, C. and Bowden, S., *Solar Cell Structure*, (PVEducation, 2016).

2.2.3 Structure of Solar Cells

In order for solar cells to operate as described above, the cells must have the correct structure. The most common structure of photovoltaics contain p-n junctions, although this is not the only existing structure of a solar cell. An alternative structure is a selective-contact solar cell, which is the structure that we will be studying in this report. Both structures follow the same general operation as described in 2.2.2, although there are a few differences depending on the layers included in each structure which will be outlined within this section.

2.2.3.1 P-n Junction Solar Cells

The most common structure of a solar cell includes a p-n junction. A p-n junction is formed when p-type and n-type semiconductors are placed next to each other. The p-type and n-type materials are the main component in the structure of these types of cells and are located in the middle of the cell. A common semiconductor for these layers is silicon. Just as was shown in Section 2.2.1, silicon can be doped to become p-type or n-type. On top of the p-type semiconductor is a transparent current collector layer. This is transparent to allow light through and into the semiconductor layers. Below the n-type material is the current collector layer, where the electrons are collected before they move into the external circuit. Some other examples of p-n junction solar cells are thin-film cells including cadmium telluride (CdTe) and copper indium gallium selenide (CIGS) cells. In CdTe cells, the p-type material is the CdTe and the n-type material is Cadmium Sulfide (CdS). In CIGS solar cells, the p-type material is the CIGS and the n-type material is also CdS. The general structure of a p-n junction cell is shown in each step of Figure 7 below.
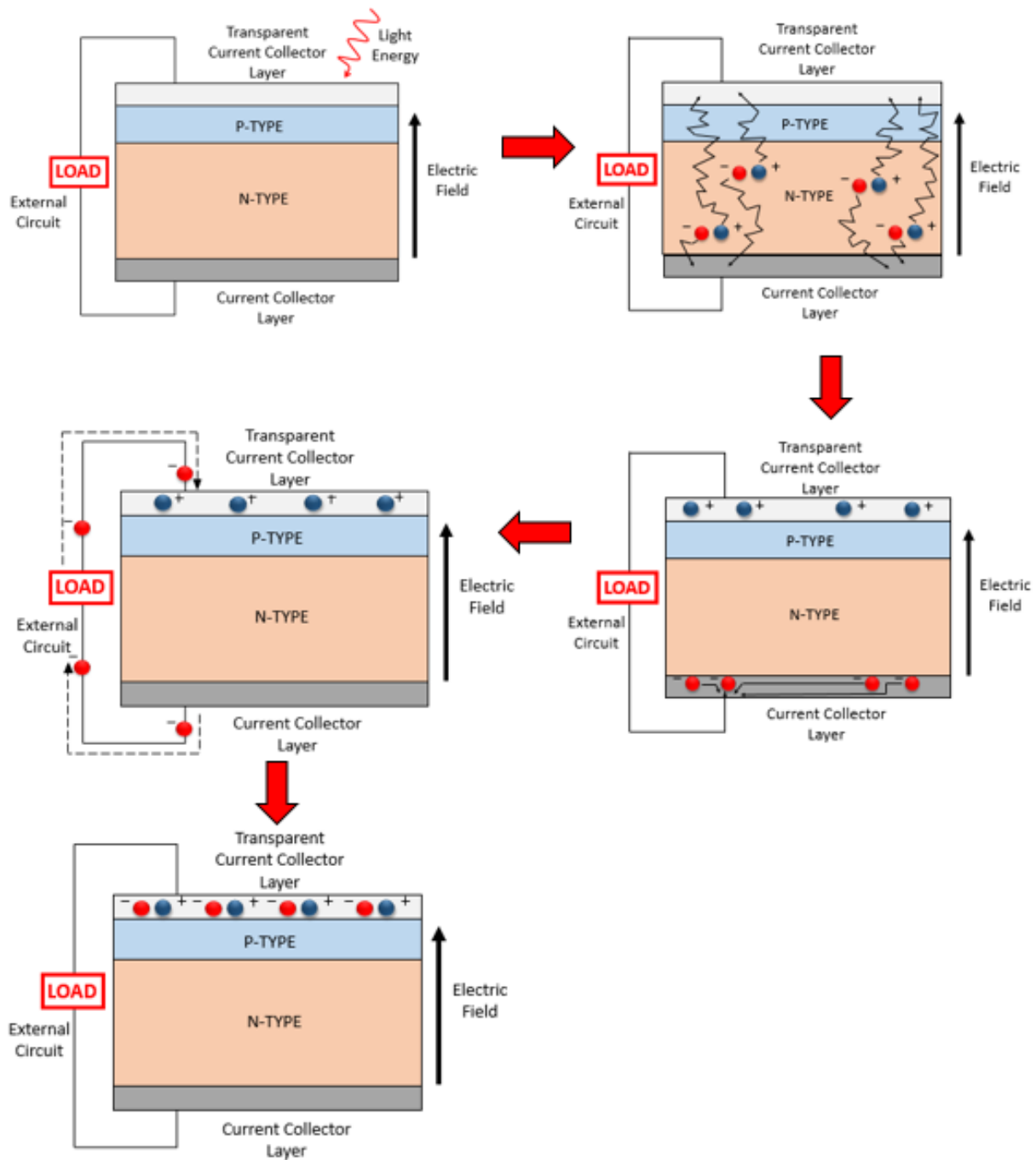
Figure 7. A p-n junction is created when p-type and n-type materials are next to each other. Once the light enters the cell, the electron hole pairs get excited and the electric field forces the charge to flow in one direction. The solid line show how the electrons and holes diffuse through the cell and the dotted line in this figure shows how the charge flows through the circuit. When the electrons meet back with a hole in the transparent current collector layer, the circuit is completed.

As described in 2.2.2, an electric field occurs because of electron diffusion between a p-type and n-type material. Because of this, the electric field occurs at the junction between the p-type and n-type material. The electric field forces the charge to flow in one direction, allowing electricity to flow through the cell. As shown in Figure 7, p-n junction solar cell operation starts with light energy from the sun entering the cell at the top. Once the electron hole pairs are excited, the electrons will diffuse through the n-type material towards the current collector layer, then horizontally to the external circuit. The electrons will re-enter through the transparent current collecting layer and then meet with a hole there to complete the circuit. The hole reached the transparent current collector layer by first diffusing through the n-type, then the p-type material. The carriers diffuse by moving in random straight lines until they hit defects or atoms in the cell to cause them to bounce in a different direction. This diffusion continues, as shown in the top of Figure 7, until they reach their respective destinations.

2.2.3.2 Selective-Contact Solar Cells

Another type of solar cell structure is a selective-contact solar cell, which is illustrated in Figure 8 below. Figure 8 shows the cell in the orientation that it is built, although it operates with the glass layer as the top contact in relation to the sun. These photovoltaics contain a semiconductor in the center of the structure, where the absorption of light occurs. They also include Hole Transport Layers (HTLs) and Electron Transport Layers (ETLs), and these layers serve the same purpose as the p-n junction. The HTL, which is the layer directly below the semiconductor layer, is usually made of PEDOT:PSS (poly(3,4-ethylenedioxythiophene) polystyrene sulfonate), Spiro-OMeTAD (2,2',7,7'-Tetrakis-(N,N-di-4-methoxyphenylamino)-9,9'-spirobifluorene), or P3HT (poly(3-hexylthiophene-2,5-diyl)). This layer is selective, meaning that it only allows holes through. Additional polymers that the HTL can be made up of include poly-triarylamine (PTAA) or poly-indacenodithiophene-difuorobenzothiadiazole (PIDT-DFBT).[19] On the top side of the semiconductor is the Electron Transport Layer, or the ETL. This layer is usually made of TiO_2 and it is also selective in order to only allow electrons through. It is important that the HTL and the ETL are selective because otherwise, recombination of the electrons and holes could occur at the interfaces. Below the HTL is a 100 nm thick layer of gold, which a current collector layer. Above the ETL is a transparent conductive electrode layer which is usually made up of fluorine doped tin

---

[19] Lehner, Anna, et al, *Electronic structure and photovoltaic application of BiI₃, Applied Physics Letters (2015)*

oxide (FTO) or Indium Tin Oxide (ITO) or. The final layer on the top of the solar cell is a 2 mm layer of clear glass.
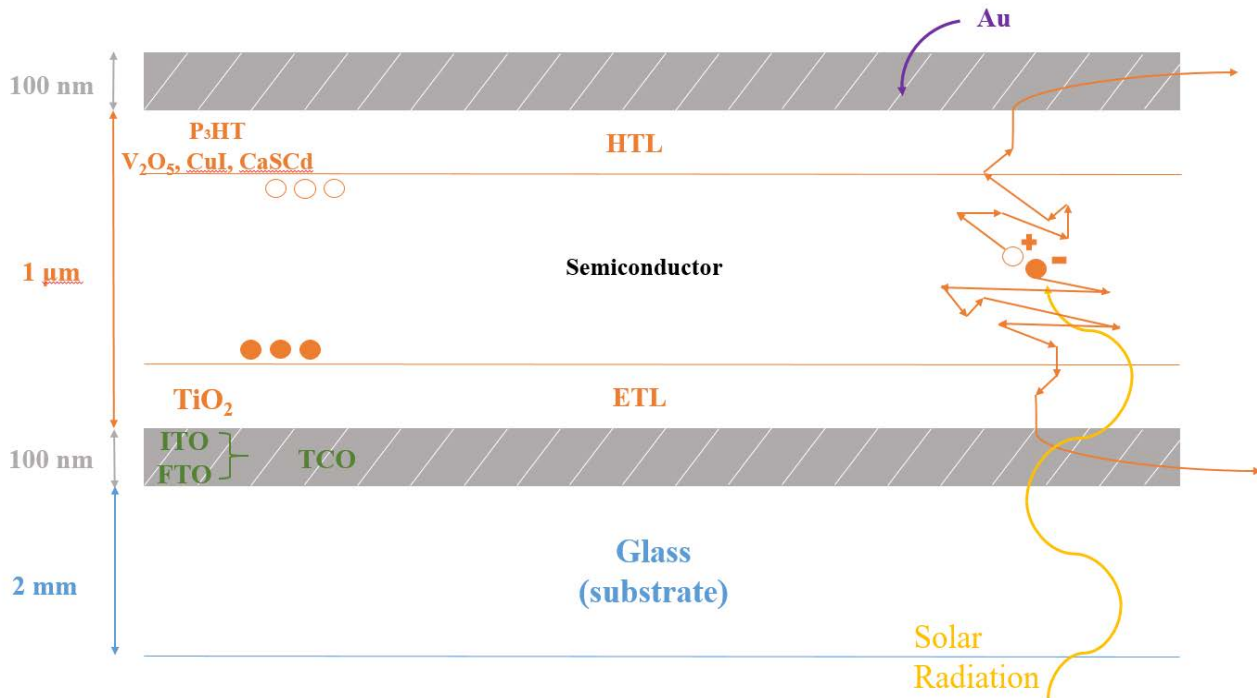
Figure 8. The structure of a selective-contact solar cell shown in the orientation that it is built. The sunlight entering the cell excites the electron-hole pairs in the semiconductor layer. The charges separate and diffuse toward their own selective layers, the HTL (hole transport layer) and ETL (electron transport layer). These layers only allow their respective charges to diffuse through them. The electrons reach the transparent conductive electrode layer then move through an external circuit and recombine with the holes in the current collector layer. Selective contact solar cells also include a glass layer which is the substrate that the cell is built upon. It is transparent to allow light into the cell.

The operation of the selective-contact solar cells begins with light entering the top of the cells through the transparent glass. Once the light reaches the semiconductor layer excited electron and hole pairs are created. Once the pairs are separated they diffuse around the semiconductor layer until they find their selective layers. This diffusion of charges creates electric fields at the interfaces between the semiconductor and the selective layers. The ETL serves as the n-type component, the HTL serves as the p-type component, and the semiconductor can be either p-type or n-type. In the case that the semiconductor is more n-type, a series of p-n-n would be created, with electric fields at both of the junctions. Both of these fields are pointing in the same direction, which makes the ETL selective to only electron carriers and the HTL to only hole carriers. The electrons move through the ETL, then toward the transparent conductive layer, as shown in Figure

8 above. Once they reach this layer, they start moving horizontally toward the end of the cell. Meanwhile, the holes diffuse through the HTL and into the gold layer. The electrons move through the external circuit, re-enter the cell through the gold layer and meet a hole here. This re-pairing of an electron and hole completes the circuit, allowing for the electricity to be produced.[20]

One very important feature of the electrons and holes in the semiconductor material are their diffusion lengths. Depending on the wavelength of the light that is entering the cell, the excited electron hole pair will be created in different locations of the semiconductor layer. For example, light with a long wavelength will travel deeper into the cell before photoexcitation occurs and in this case the electron in the pair will be farther away from the ETL, but the hole will be close to the HTL. On the other hand, light with a shorter wavelength will land at the top of the semiconductor layer, so the electron will be very close to the ETL, while the hole will be farther away from the HTL. In order for these carries to reach their respective transport layers, the carrier must have a long enough diffusion length.[21] This is illustrated below in Figure 9.
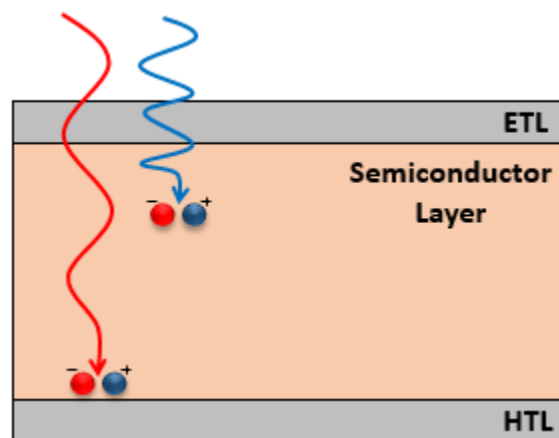
Figure 9. Different wavelengths of light will absorb into the cell at different depths. Longer wavelengths will be closer to the HTL and shorter wavelengths will be closer to the ETL.

Other properties of the carriers as well as the material itself are important in determining how well the cell will operate. These properties will be discussed further in the next section.

---

[20] Rao, Pratap, *Engineering Light Absorption and Charge Transport in Nanostructured Solar Energy Conversion Materials* (Rutgers Mechanical and Aerospace Engineering, 2017)
[21] Ibid.

2.3 Critical Optoelectronic Properties of Solar Cell Materials

To best approach how to optimize the efficiency of a solar cell, the nature and relation of its optical and optoelectronic properties need to be understood. To facilitate this understanding, the next section discusses different optical and optoelectronic properties involved with the composition of a solar cell, such as the band gap, lifetime, carrier mobility, and the absorption coefficient. Knowledge about these characteristics will allow the the analysis of trends and how semiconductor modification can occur.

2.3.1 The Shockley-Queisser Limit and Band Gap

The most important feature of semiconductors as solar cell materials is their band gap. The band gap is the minimum energy required to excite an electron in its bound state into a free state where it can participate in conduction.[22] Semiconductors have band gaps within a certain range, from 0 to about 3 eV. The Shockley-Queisser Limit, also known as the detailed balance limit, indicates the maximum theoretical efficiency of a solar cell with one semiconductor based on its own band gap. As shown in Figure 10, the most efficient solar cells contain semiconductors with a narrower band gap in the range of about 1.1 to 1.3 eV. The band gap is important because it determines the overall efficiency of the cell, therefore determining how well the cell will perform and how efficiently it will be able to turn light energy into electrical energy.

---

[22] Honsberg, C. and Bowden, S., "Band Gap", (PVEducation, 18 September, 2017).
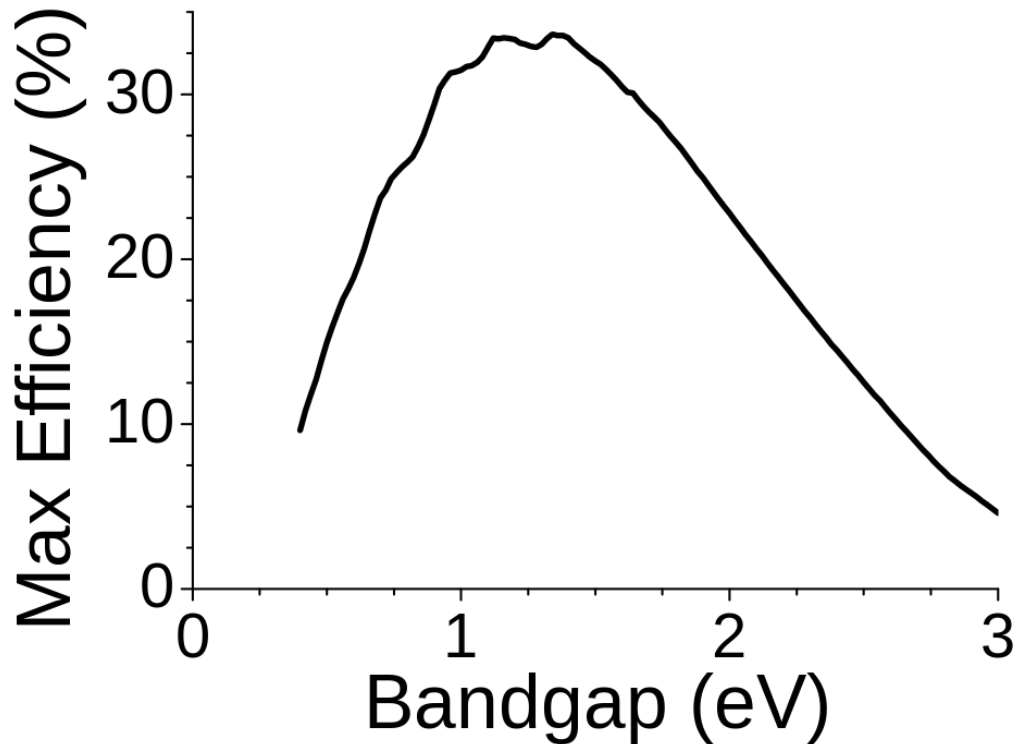
Figure 10. The Shockley-Queisser Limit shows the maximum efficiency of a solar cell in percent versus the band gap of the semiconductor in electron volts.[23]

Photons with energy less than the band gap cannot be absorbed by the solar cell so they do not contribute to the energy produced.[24] Each absorbed photon can only contribute one electron to the conduction band so high energy photons can only contribute a fraction of their energy to the cell. Two other properties that are significant to the function of a solar cell are discussed in the next section.

2.3.2 Introduction of Lifetime and Carrier Mobility

A property which affects the overall efficiency of a semiconductor material is that of diffusion length. For this project, modifications will be made on other optoelectronic properties of BiI$_3$ to optimize the diffusion length and other properties of the semiconductor material. Diffusion length is primarily determined by carrier lifetime and mobility, as described below. This is given

---

[23] *Shockley-Queisser limit* (Wikipedia, 2017)
[24] Friedlein, Jake, "The Shockley-Queisser Limit", (2012)

by the diffusion equation derived from Einstein relations where $L_{n,p}$ is the diffusion length, μ represents carrier mobility, *k* is the Boltzmann constant, T is room temperature, *e* is the charge of the carrier, and τ_{life} is the carrier lifetime:

$$L_{n,p} = \sqrt{\frac{\mu kT}{e} * \tau_{life}}$$

Equation 2. Diffusion Equation

The carrier mobility represents how quickly a charge carrier (electrons or holes) can move through a semiconductor or metal.[25] The farther a carrier can travel in a specified period of time, the greater the diffusion length will be. Carrier lifetime indicates the amount of time an excited, mobile positive or negative charge carrier—either a hole or electron— will travel before recombining with their counterpart, which makes them lose their excited energy and become immobile. The longer the carrier lifetime is, the more ideal because this gives the hole or electron more time to travel, (i.e. diffuse) and reach their respective transport layers; otherwise, they would simply recombine and give off heat or emit the photon as wasted energy. Therefore, if the diffusion length is increased, the carrier lifetime will correspondingly increase.The electron/hole pair will separate where and when the photon is absorbed by the material and begin to diffuse towards the ETL and HTL, respectively.[26] As stated previously, these transport layers provide electric fields that selectively collect the charges and deliver them to the current collectors, which lead the charges to the load being supplied with the energy. Decreasing defects in the material improves the carrier lifetime. This further allows for optimization of the diffusion length. [27]The concepts regarding carrier lifetime and the relationships associated with the property are discussed in the following section.

---

[25] "Electron and Hole Mobility", (Physics and Radio Electronics, n.d.)

[26] Rao, Pratap, *Engineering Light Absorption and Charge Transport in Nanostructured Solar Energy Conversion Materials* (Rutgers Mechanical and Aerospace Engineering, 2017)

[27] "Understanding the Implication of Carrier Diffusion Length in Photovoltaic Cells", *The Journal of Physical Chemistry Letters"* (American Chemical Society, 2015), 4090.

2.3.3 Carrier Lifetime

This project investigates the optimization of what is known as an n-type semiconductor. An n-type semiconductor inherently has a concentration of electrons in the semiconductor layer of the solar cell higher than the concentration of free holes. In an n-type semiconductor, the carrier lifetime--more specifically, the hole lifetime--is affected by the greater concentration of free electrons in the cell. Since the ratio of electrons to holes is greater within the solar cell, the probability of a hole pairing up (i.e. recombining) with an electron is greater than the probability of an electron pairing up with a hole, therefore. If the hole recombines with an electron before it reaches the HTL, then it will give off wasted energy because it will either recombine and give off heat or it will emit the energy as radiation.

Therefore, to maximize the lifetime of holes in an n-type semiconductor, the recombination rate should be minimized. In an n-type semiconductor, the recombination mechanism is known as "band-to-band recombination". This entails the electron, which occupies the conduction band, settling directly into the valence band, with a loss in energy equivalent to the band gap.[28] The electron transitions directly into the valence band because there is no third party catalyst. In an n-type semiconductor the minority carriers are the holes, and the recombination rate of the majority carrier depends upon the excess-minority-carrier-density (i.e. the holes). For this recombination mechanism and type of semiconductor, the expression for the recombination rate of holes and electrons is as follows:

$$U_{b-b} = b(np - n_i^2)$$

Equation 3. Band-to-band Net Recombination Rate of Holes and Electrons in an n-type Semiconductor[29]

In the above expression, the thermal equilibrium that is present during band-to-band recombination is represented by the capture coefficient, b, multiplied by the difference in the product of the concentration of electrons, n, and the concentration of holes, p, with n_i^2, the electron concentration in intrinsic semiconductors at the equilibrium temperature. The expression represents the concept that although the concentrations of electrons and holes are different in an n-type semiconductor,

---

[28] B. Van Zeghbroeck, "Band-to-band recombination" *Principles of Semiconductor Devices* (Boulder, August 2007).
[29] Ibid.

the net recombination rate is 0. That is, the rate of generation is equal to the rate of recombination. This is a result of the back process of the energy of the electrons falling down to the valence band from the conduction band occurring at the same rate as they are being generated by the thermal energy, establishing equilibrium. This generation can occur through thermal energy or light which would result in more electrons in the conduction band and more holes in the valence band. Without the light, the concentration of the holes and electrons would be static, however, new pairs are always being created as a result of the thermal energy.

When the recombination rate is discussed individually, however, the concentration of the electrons and holes do affect it. The concentration of the charge carriers, n and p, and recombination rate, R, as demonstrated above in Equation 3 and Equation 4 below, are directly correlated. Equation 4 also demonstrates how an increase in charge carrier concentration indirectly affects the lifetime of the charge carriers. That is, as the concentration increases, the lifetime decreases.

$$R_n = R_p = R = \frac{\delta n}{\tau_n} + \frac{\delta p}{\tau_p}$$

Equation 4. Band-to-band Recombination Equation Including Lifetime[30]

Although the recombination rates for electrons and holes are not equal in trap-assisted recombination, the effects of increasing charge carrier concentration still apply. Trap-assisted recombination involves a defect that provides energy between the conduction and valence band to catalyze the recombination of the electron and hole. The following equation summarizes the effects affiliated with net trap-assisted recombination:

$$U_{SHR} = \frac{pn - n_i^2}{p + n + 2n_i cosh(\frac{E_i - E_t}{kT})} N_t v_{th} \sigma$$

Equation 5. Net Recombination Rate for Trap-Assisted Recombination[31]

---

[30] Volovichev, I. N. "Recombination and lifetimes of charge carriers in semiconductors" in *Journal of Applied Physics* (© 2004 American Institute of Physics, 15 April 2004), 4495.
[31] B. Van Zeghbroeck, " Trap assisted recombination" *Principles of Semiconductor Devices* (Boulder, August 2007).

While the above equation presents multiple variables and relationships that determine the net recombination rate with traps, there are particular variables that are of primary concern. The numerator, with p and n again representing the charge carrier concentrations, indicates that more electrons or holes will increase recombination as they are directly proportional. The variables E_i and E_t denote the halfway energy between the valence and conduction bands, and the actual energy of the trap, respectively. If E_t is close to E_i then it will serve as a recombination site, and if the E_t is close to the conduction or valence band then it will serve as a trapping site. Additionally, due to how it will increase the trap-assisted recombination rate, it will also decrease the lifetime of the charge carriers. The faster the charge carriers are trapped, the less time they have as excited electrons and unpaired holes. Another property that contributes to the lifetime of the charge carriers is the charge mobility which will be discussed in the next subsection.

2.3.4 Carrier Mobility

Another factor to consider with an absorber material is the mobility of the electrons and holes. For n-type, however, hole mobility is more of a focus because it is the minority carrier (i.e. the more frequently unpaired carrier) and therefore, the limiting carrier. It is important to note the electron and hole mobility is dependent on the collision time, or the mean time between collision of particles. If the amount of electrons within the semiconductor is large, then the amount of time between collisions of the particles will decrease. With more electrons, the collision time for electrons will decrease. This is due to electrons colliding with each other, stationary atoms, and defects more often. A small time between collisions indicates greater collision frequency and lower electron mobility. This relation can be demonstrated below where q is the charge, τ_c is the collision time, and $m_{n,p}$ is the mass of the electron or hole:

$$\mu_{n,p} = \frac{q * \tau_c}{2 * m_{n,p}}$$

Equation 6. Mobility of an Electron or Hole[32]

---

[32] "Carrier Transport" in *Semiconductor Physics (II)* (Massachusetts Institute of Technology, Spring 2007), 5.

If the carrier mobility can be optimized, the diffusion length can be improved. The diffusion factor (or diffusivity) for diffusion length is directly proportional to the carrier mobility as shown before in Equation 2.

Before charge carrier mobility can be considered, however, the absorption of the incoming photons must be considered. The relationship between that principle and solar cell performance is discussed in the next section.

2.3.5 Absorption Coefficient

The absorption coefficient of a semiconductor material is indicative of the degree of a specific wavelength of light being absorbed into the material. The lower the absorption coefficient, the greater the absorption depth of that wavelength of light.[33] This can be explained by the relation of the absorption coefficient to the absorption depth; the depth (i.e. the average distance the photon penetrates into the material prior to absorption) is the reciprocal of the absorption coefficient as shown below in Equation 7.

$$\delta_p = \frac{1}{\alpha}$$

Equation 7. Relationship between Absorption Depth and Absorption Coefficient

Quantitatively, this translates to the lesser the divisor, (absorption coefficient) the greater the quotient (absorption depth).[34] This optic property has an impact on the thickness of the semiconductor layer in the solar cell. The specifics of this impact is discussed in the following section.

2.3.6 Absorption Coefficient and Semiconductor Material Thickness

If the energy of the photon(s) is at or above the band gap, then there is adequate energy to excite the electron from the valence band of the material into the conduction band, correspondingly.[35] The absorption coefficient and energy of the photon and gap are directly proportional as demonstrated by the relations for direct and indirect band gaps below:

---

[33] Honsberg, C. and Bowden, S., "Absorption Coefficient", (PVEducation, 18 September, 2017).
[34] Skorupska, K., "Optical Properties of Semiconductors", (University of Wyoming).
[35] Honsberg, C. and Bowden, S., "Band Gap", (PVEducation, 18 September, 2017).

$$\alpha(hv) \propto A(E_{photon} - E_g)^2$$

Equation 8. Direct Semiconductors' Absorption Coefficient Dependence on Photon and Band Gap Energy

$$\alpha(hv) \propto B(E_{photon} - E_g)^2$$

Equation 9. Indirect Semiconductors' Absorption Coefficient Dependence on Photon and Band Gap Energy[36]

The larger the energy of the photon is compared to the energy of the band gap, the higher the absorption coefficient. Since the absorption depth is the inverse of the coefficient, the absorption depth is also going to be less. If the semiconductor material is too thin, then the light of long wavelengths will perceive it as being transparent.[37]

The absorption coefficient, along with the other optical and optoelectronic properties that have been discussed and are involved in a solar cell, impact the electric properties that are indicative of solar cell efficiency. Such electric properties include the open circuit voltage and short circuit current. These relationships are discussed in the following subsections.

2.3.7 Current-Voltage Curves

Current-voltage (I-V) curves provide insight on solar cell conversion ability and efficiency. These curves will be useful for assessing how synthesized BiI_3 cells respond to light. Figure 11 illustrates a standard I-V curve. When light shines on a solar cell, both a current and a voltage are produced that yield electric power. The current is produced via the absorption of photons to create electron-hole pairs and the collection of carriers by the p-n junction.[38] As for the voltage, it is essentially a potential difference, or pressure, that directs the motion of electrons through the external circuit.

[36] Skorupska, Katarzyna, "Optical Properties of Semiconductors", (University of Wyoming).

[37] Honsberg, C. and Bowden, S., "Absorption Depth", (PVEducation, September 18, 2017).

[38] Honsberg, C. and Bowden, S., "Solar Cell Structure", (PVEducation, Dec 2017).
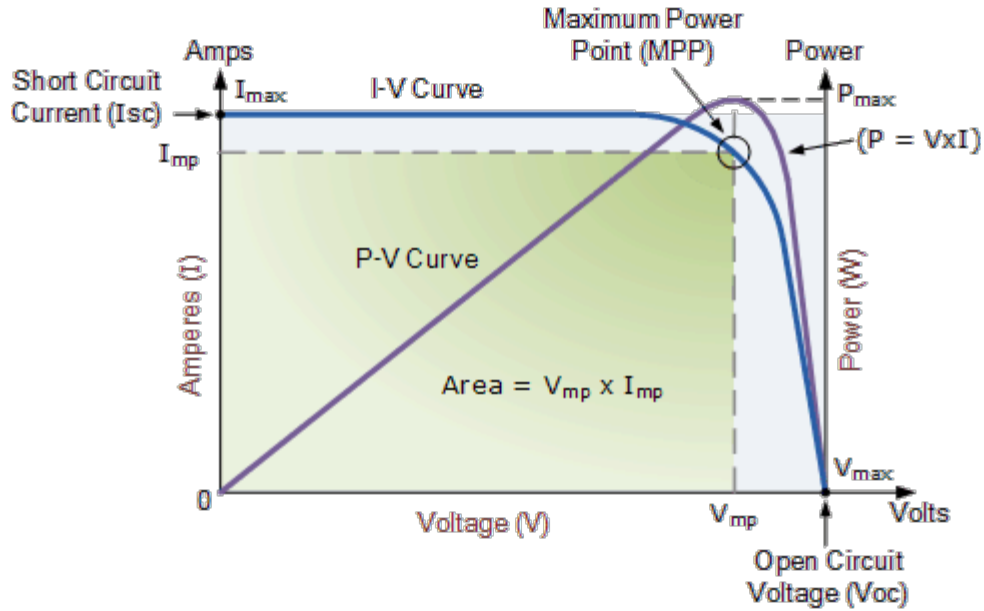
Figure 11. I-V curve depicting open-circuit voltage and short-circuit current.[39]

2.3.7.1 Short-Circuit Current

Short-circuit current density, J_{SC}, is the current through a solar cell when the voltage across the device is zero.[40] The graph above depicts this phenomenon; short-circuit current is attributed to the generation and subsequent collection of light-generated carriers. In fact, the short-circuit current and light-generated current are often identical in value.[41]

Short-circuit current is dependent upon the following factors: the area of the solar cell, the number of photons, the spectrum of the incident light, the optical properties, and the collection probability of the cell.[42] Equation 10 may be used to calculate the short-circuit current of a PV device.

$$J_{SC} = qG(L_n + L_p)$$

Equation 10. The short-circuit current expressed as a function of the generation rate and the electron and hole diffusion lengths.

---

[39] "Solar Cell I-V Characteristic", Alternative Energy Tutorials.
[40] Honsberg, C. and Bowden, S., "Short-Circuit Current", (PVEducation, Dec 2017).
[41] Ibid.
[42] Ibid.

In the above equation, the variable G represents the generation rate of carriers in the cell, and L_n and L_p are the electron and hole diffusion lengths. As more pairs are generated in a solar cell via photon absorption and subsequent carrier excitation, there is more opportunity for carrier diffusion and collection, and thus increased light-generated current. Additionally, higher diffusion lengths correspond to longer carrier lifetimes, and therefore an increase in short-circuit current. Increasing the diffusion length via altering the material structure or thickness of a cell may prove to be beneficial to improving the solar cell.

2.3.7.2 Open-Circuit Voltage

The open-circuit voltage, V_{OC}, is the maximum available voltage from a solar cell that occurs when there is zero net current.[43] It is used in the equation to determine overall solar cell efficiency, which can be found in Appendix C5. Equation 11 can be used to determine the open-circuit voltage of a given PV device.

$$V_{OC} = \frac{nkT}{q} ln\left(\frac{I_L}{I_0} + 1\right)$$

Equation 11. The open-circuit voltage expressed as a function of the saturation and light generated current.

In the above equation, I_L and I_o represent the light-generated and dark saturation current, respectively. Light-generated current is the current achieved based on the generation and collection of light-generated carriers, mentioned previously. As for dark saturation current, this is the measure of the recombination in a PV device. Thus, as light-generated current increases via the creation of electron-hole pairs or the collection of carriers at the p-n junction, the open-circuit voltage increases. However, as more recombination takes place, the open-circuit voltage decreases.

Breaking this down to other terminology introduced in this section, the open-circuit voltage of a PV device increases with increasing band gap.[44] This is because recombination is less frequent in devices with larger band gaps, and thus the saturation current decreases. Accordingly, open-circuit voltage increases with increasing carrier mobility and lifetime.

---

[43] Honsberg, C. and Bowden, S., "Open-Circuit Voltage", (PVEducation, 18 September, 2017).
[44] Ibid.

2.4 Promising Trends in Solar Cell Efficiency

Like any manufactured products, the scientific community is interested in increasing the efficiency of photovoltaics. The National Renewable Energy Laboratory has compiled extensive data that shows while some types of solar cells have leveled off with regard to efficiency, newer types indicate a significant increase in efficiency over a short period of time.[45] Therefore, a closer look at each type of solar cell is important in understanding where future research could be effective and meaningful to the advancement of photovoltaics as a means for energy production.

2.4.1 Generations of Solar Cells: Comparing Cost and Efficiency

Solar cells are generally classified into three generations.[46] The first generation encompasses crystalline silicon cells, which currently dominate the solar panel market due to their high stability and achieved efficiency of 20%. One major drawback to this generation of solar cells is the high energy required in production. First generation solar cells, such as silicon, must be manufactured at very high temperatures (~1500℃) which equates to a high cost and energy demand. Conversely, second generation solar cells can be manufactured in room temperature conditions, greatly reducing the energy demand during production. First generation solar cells have reached costs of about $0.30/Watt, which is an incredible improvement from the initial cost of $76/Watt in 1977.[47] More information on the price of silicon solar cells over the past four decades can be seen below in Figure 12.

---

[45] "Cost of Solar Panels Over Time", (2017, May 31).

[46] Green, Martin A. *Third Generation Photovoltaics Advanced Solar Energy Conversion*, (Springer, 2006).

[47] *Solar Cell* (Wikipedia, 2017).
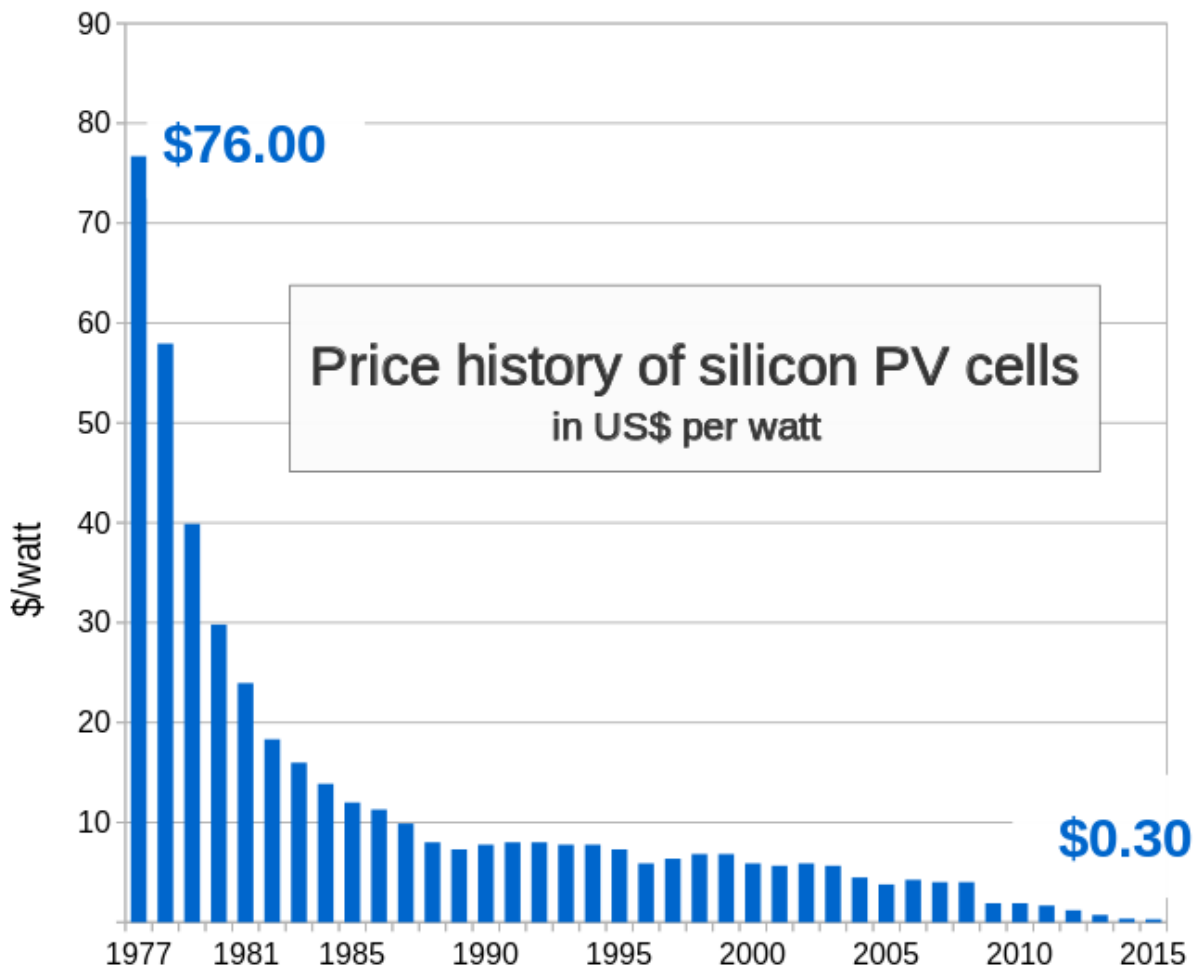
Figure 12. Shows the trend in cost for silicon solar cells from 1977-2015. The cost of silicon solar cells has dropped from $76/Watt to $0.30/Watt over this period of time.[48]

Although the cost has significantly decreased to its current value of $260/m^2, the cost is still a barrier preventing solar cells from being more widely used across the globe. Therefore, a material with similar efficiencies to silicon, but at a lower price, would be a pivotal factor in solar cell development. This gap in solar cell advancement brought about second generation solar cells called thin-film solar cells. Amorphous silicon, CIGS, and CdTe are thin film solar cells and make up the second generation of solar cells. Thin film solar cells have a higher absorption coefficient

---

[48] *Solar Cell* (Wikipedia, 2017).

than first generation solar cells. This allows them to be thinner than crystalline silicon solar cells, and can be created with less material. Additionally, thin film cells can be manufactured at a much lower cost than crystalline silicon due to the fact that they are deposited on a substrate at low temperatures,[49] unlike crystalline silicon, which is manufactured at high temperatures (>1500 °C).[50] However, the commercialization of the second generation of solar cells is limited by the scarcity and toxicity of the elements required for production (Cd, Te, Ga). While second generation solar cells were meant to have a lower cost of manufacturing than first generation solar cells, the scarcity of elements such as cadmium, tellurium, and gallium used in thin film cells keeps their cost high. [associated with energy consumption.] Finally, the third generation is characterized by multijunction solar cells. Multijunction solar cells have two or more absorbing semiconductors in order to combat the loss of energy as heat associated with photons that have an energy greater than the band gap, as well as the loss of low-energy photons with energies below the band gap. By having both a high-energy and low-energy band gap in the same solar cell, the overall efficiency can be increased beyond that of just one band gap energy-level.[51]

As seen in Figure 13, silicon solar cells require a large increase in cost in order to obtain incremental increases in efficiency. Solar cells made from amorphous silicon, CIGs, and CdTe have yet to reach an efficiency greater than silicon. Alternatively, third generation solar cells have the potential to greatly increase their efficiency with only a small increase in their cost per square meter, based on the fact that they have more than one junction.[52] Third generation solar cells include tandem and multijunction units. These types of photovoltaics can overcome the limitations of a single layer by increasing the utilization of each solar photons.[53]

---

[49] Dirjish, Mat, "What's The Difference Between Thin-Film And Crystalline-Silicon Solar Panels?", (May 16, 2012).
[50] Ibid.
[51] "Photovoltaic Research", (National Renewable Energy Laboratory, n.d.).
[52] Madsen, M. V. "Solar Cells – The Three Generations", (DTU Energy, n.d.).
[53] Esfandyarpour, Rahim. *Multi-Junction Solar Cells*, (Stanford University, 12 Dec. 2012).
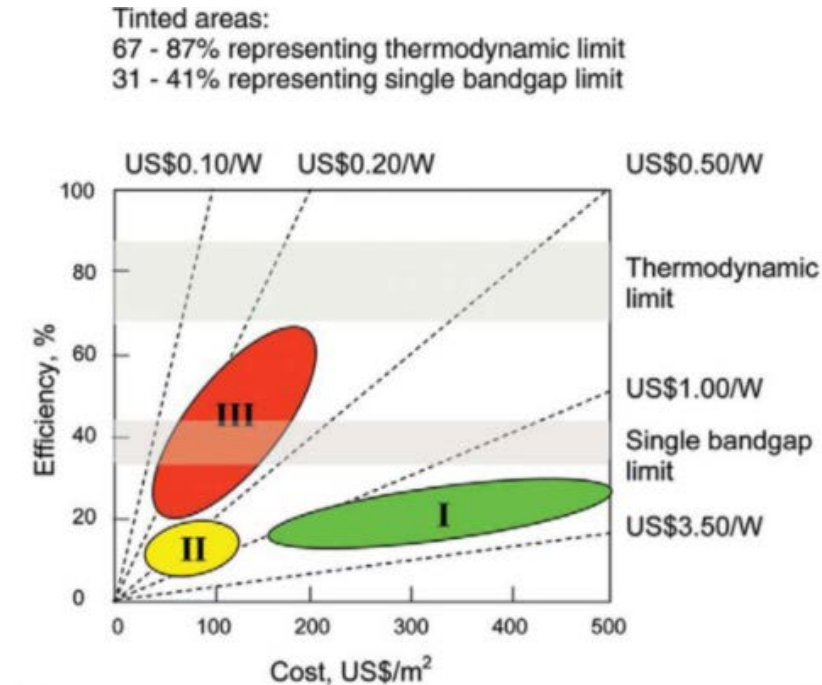
Figure 13. Multi-generational comparison of theoretical solar cell efficiency and cost. Predictions of second and third generation efficiencies.[54]

2.4.2 Efficiency Over the Years

The National Renewable Energy Laboratory has compiled efficiency data for all generations dating from 1975 to the present. Shown in Figure 14, it becomes clear that the rate of improvement in silicon efficiency (blue lines in the plot) has essentially been zero since the turn of the century.

---

[54] Sohrabi, Foozieh, et. al, "Optimization of Third Generation Nanostructured Silicon- Based Solar Cells", *Solar Cells: Research and Application Perspectives,* (6 March, 2013).
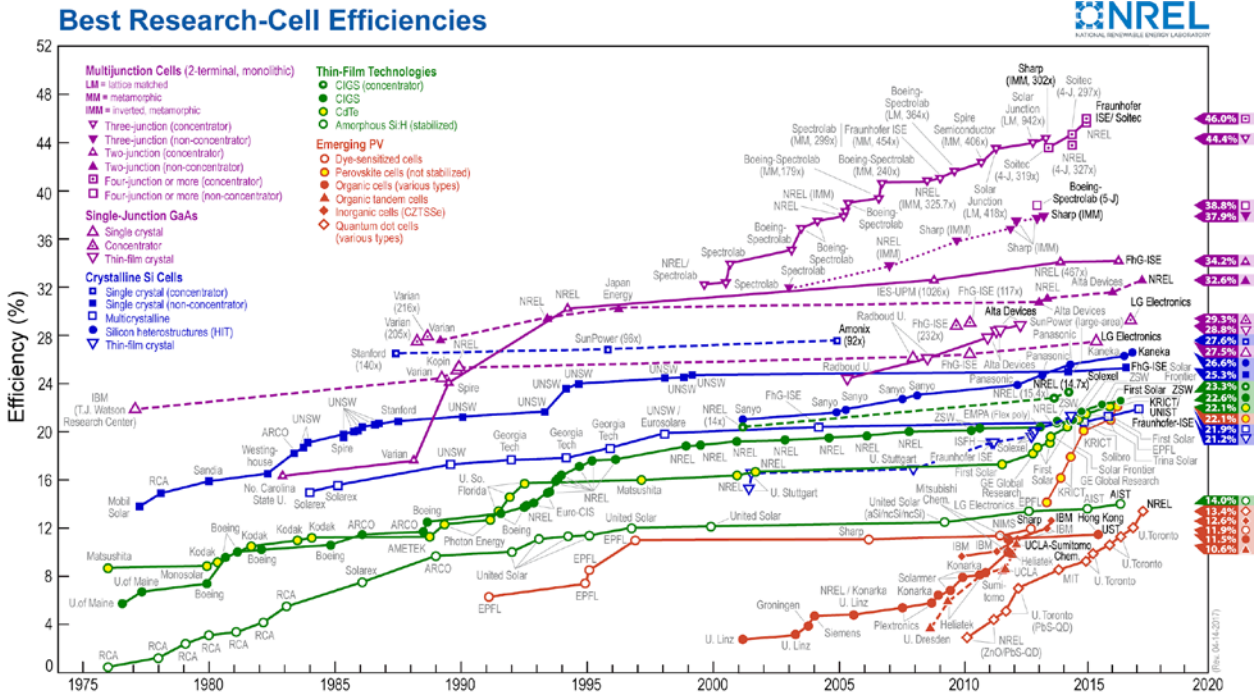
Figure 14. NREL graph depicting efficiency of different types of solar cells from 1975 to the present. Steeper slopes represent rapid rates of increase in efficiency.

Looking at generation two solar cells represented by the green lines, it is apparent that they closely follow the same trend as silicon solar cells. However, perovskites, represented by the orange lines, show tremendous increases in efficiency in just two decades. This rate of improvement is extremely promising. However, their toxicity and poor stability limits their practical use in commercial solar cells. Multijunction solar cells, shown in purple, display the highest achieved efficiency, approaching 30% for a two-junction solar cell, and 40% for a three-junction solar cell. However, continuing research on thin-film solar cells such as BiI_3 will allow for additions to the NREL chart that can be used to direct future research. Based on these concepts, it is of interest to compare the material properties of BiI_3 to the widely used semiconductor, silicon, and to the material of much interest, methylammonium lead iodide. To narrow these concepts down to the focus of this project, specific semiconductor materials were reviewed.

31

2.5 The Current State of Knowledge on Relevant Semiconductor Materials

As a means to gain insight on the current materials used in the application of photovoltaic solar cells, the following section discusses three different semiconductor materials: first generation silicon (Si), second generation methylammonium lead iodide ($CH_3NH_3PbI_3$)--a type of perovskite--, and second generation bismuth triiodide (BiI_3). Each were selected to elaborate on as they are each representative of a different generation in the types of solar cells. Furthermore, to put the materials in perspective with one another, their optical and optoelectronic properties will be discussed. The comparison and contrast of three semiconductor materials consequently creates a greater context to consider upon analysis of each semiconductor material individually.

Considering the abundance of it in the earth's surface, silicon is a readily available semiconductor material. Silicon is the second most abundant material in the earth's surface. However, in order to manufacture the element into wafers for solar energy applications, the element has to be treated and deposited at higher temperatures. This further implies that a greater amount of energy is needed to produce silicon solar cells than with bismuth triiodide. Since there are some properties of silicon that are not as optimal, this further indicates the need to look towards other materials as alternatives.

The perovskite methylammonium lead iodide, as stated previously, has shown a similar efficiency to silicon but at a faster rate of improvement. That is, in just 17 years, the power conversion efficiency of methylammonium lead iodide increased from approximately 4% to almost 15% efficiency. Considering the classification of the two semiconductor materials to be the same, and the research of methylammonium lead iodide being successful over the past 17 years, it was deemed a good comparison to understand the favorability of the optical and optoelectronic properties of bismuth triiodide.

Furthermore, research has been conducted on methylammonium lead iodide which yielded promising results that indicate the material has optimal characteristics regarding its quantum mechanics. For example, there have been studies which have resulted in the perovskite having long charge carrier diffusion lengths. It was proposed that the long diffusion lengths were most likely due to a low recombination efficiency of the electrons and holes in the material.

The found increase in efficiency for methylammonium lead iodide is what establishes bismuth triiodide as a suitable semiconductor as well. Methylammonium lead iodide has been found to have efficient transport properties even in the presence of defects (e.g. dislocations,

interfaces, volume defects, etc.). Accordingly, methylammonium lead iodide is currently being considered as a viable option to improve solar cells. The transport properties of methylammonium lead iodide have been previously attributed to the partially oxidized Pb^{2+} cation.[55]

Bismuth triiodide also has a partially oxidized p block cation which keeps a lone pair of electrons. This lone pair creates an ionic radius which facilitates the maximum s orbital character for the valence band of the material.[56] Therefore, BiI_3 was chosen to be investigated for this project due to its relative characteristics and lack of toxicity in contrast to the lead cation in methylammonium lead iodide. Additionally, to differentiate BiI_3 from silicon, it has been found that BiI_3 can be produced as a "thin-film" semiconductor at a lower cost than silicon because of deposition at lower temperatures. To investigate relationships like this, the optical and optoelectronic properties of the three materials from literature were compared quantitatively.[57]

2.5.1 BiI_3 and its Application in Multijunction Cells

Perovskites, such as methylammonium lead iodide, have achieved a PCE of over 22%,[58] which is similar to the achieved efficiency of single crystal silicon solar cells.[59] However, perovskites show an increased rate of improvement over single crystal silicon solar cells.[60] Advanced processing development has led to this increased efficiency, however, there are still concerns regarding the commercialization of methylammonium lead iodide. The toxicity of lead is a major reservation with using these solar cells on a large scale. BiI_3, the nontoxic alternative, has shown promising results for a second generation photovoltaic with a measured band gap of 1.8 eV as a spin-coated thin film.[61] More information about the material structure of BiI_3 can be found in Appendix A.

Bismuth triiodide has potential applications as a third generation photovoltaic when used in a tandem or multijunction cell. These types of solar cells increase efficiency because they have

[55] Brandt, Riley E., et. al, "Investigation of Bismuth Triodide (BiI_3) for Photovoltaic Applications", *The Journal of Physical Chemistry Letters*

[56] Ibid.

[57] Ibid.

[58] Hamdeh, U. H., Nelson, R. D., Ryan, B. J., Bhattacharjee, U., Petrich, J. W., & Panthani, M. G. (2016). Solution-Processed BiI_3 Thin Films for Photovoltaic Applications: Improved Carrier Collection via Solvent Annealing. *Chemistry of Materials, 28*(18), 6567-6574. doi:10.1021/acs.chemmater.6b02347

[59] "Photovoltaic Research", (National Renewable Energy Laboratory, n.d.).

[60] Ibid.

[61] Hamdeh, U. H., Nelson, R. D., Ryan, B. J., Bhattacharjee, U., Petrich, J. W., & Panthani, M. G. (2016). Solution-Processed BiI_3 Thin Films for Photovoltaic Applications: Improved Carrier Collection via Solvent Annealing. *Chemistry of Materials, 28*(18), 6567-6574. doi:10.1021/acs.chemmater.6b02347

two or more materials with different band gaps in order to cover a wider range of the spectrum.[62] Tandem solar cells are constructed by having two or more cells connected in series, while multijunction solar cells have more than one junction within the cell.[63] The band gap of silicon is reported to be 1.12 eV, whereas the band gap of BiI$_3$ is approximately 1.8 eV. Therefore, if these two photovoltaic materials were combined in either a tandem or multijunction solar cell, the absorption of solar photons would increase due to the decrease in losses associated with photon energies too high or too low from the band gap. A theoretical plot of solar cell efficiency for two materials in tandem can be seen in Figure 15 below.
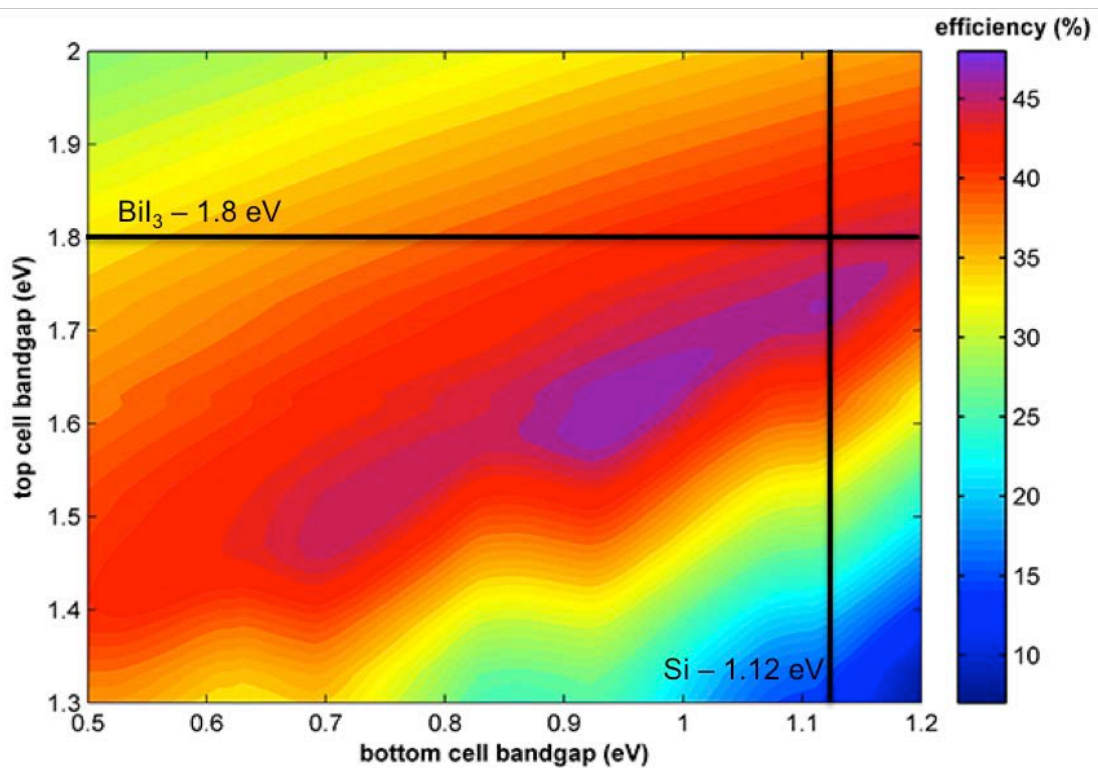
Figure 15. Theoretical efficiency plot of BiI$_3$ in tandem with a silicon solar cell based on experimentally found band gaps of BiI$_3$ and the accepted band gap of silicon.[64]

[62] Esfandyarpour, R., "Multi-Junction Solar Cells", (2012, December 12).

[63] Bremner, S. P., Levy, M. Y., and Honsberg, C. B., "Analysis of tandem solar cell efficiencies under {AM1.5G} spectrum using a rapid flux calculation method", *Progress in Photovoltaics: Research and Applications*, vol. 16, pp. 225–233, 2008.

[64] Adapted from Honsberg C. and Bowden S., *Tandem Cells* (PVEducation, 2016).

Using the band gaps of silicon and BiI$_3$ previously stated, silicon would ideally be the bottom cell material, and BiI$_3$ would be the top cell material. This would result in a theoretical efficiency ~44%, which is nearly double the current efficiency of crystalline silicon on its own.

2.5.2. Quantitative Comparison of Silicon, Methylammonium lead iodide, and bismuth triiodide's Optical and Optoelectronic Properties

To develop more context for the comparison of the three materials, the qualitative relationships are represented by numerical quantities in this subsection. A comprehensive table can be found below in Table 1 that outlines previously obtained quantitative data for the three materials. Additionally, an extensive version of the table, including qualitative information, can be found in Appendix B.

Table 1. Quantitative Comparison of the Properties of Silicon, BiI$_3$, and CH$_3$NH$_3$PbI$_3$.

COMPARISON OF SILICON, BII3, AND PEROVSKITE PROPERTIES			
Property	Silicon	BiI3	Methylammonium Lead Iodide
Band gap	1.18 +/- 0.03 eV	1) 1.67 (optimal- 1.8 eV) 2) 1.79 +/- 0.05 and 1.80 +/- 0.05 3) 1.82eV	indirect bandgap of 60meV and direct bandgap of 1.51 eV
Thickness	0.5 micrometers	100nm/ 1 micrometer (BiI3, HTL, ETL)	200nm- efficiency= 31% at this thickness
Electron Mobility	1400 cm^2/ (V*s)	260 +/- 50 or 1000 +/- 200 cm^2/(V*s)	~66cm^2/(V*s)
Hole Mobility	450 cm^2/ (V*s)	260+/- 50 cm^2/Vs	~322 cm^2/V*s
Hole Effective Mass	0.57/0.81 (m(h,dos)/m(0))	10.39	mh* = 0.29m0
Electron Effective Mass	1.08	1.85	me* = 0.23m0
Electron Diffusion Lengths	100-300 micrometers	1.9 or 4.9 micrometers	>1000nm or 1micrometer
Light Absorption Coefficient	For wavelength 800nm, apsorption depth=1.0x10^-3 cm^-1	16900 and 20,000 cm^-1 absorption doublet other absorption bands C and D at ca. 23500 and 27500 cm^-1	at 550nm, 1.5e+4 cm^-1, at 700nm, 0.5e+4 cm^-1 absorption coefficient= ~10^4 (600nm)
Lifetime	recombination of first surface=1000cm/s... **Ts= 1.49e-5 s and Teff=1.46e-5 s** 1ns to 1ms	180-230 ps for PVT films 190-240 ps- solution processed films 160-260 ps for single-crystal sample	~ 1 microsecond

As stated in Section 2.3.2, the charge carrier mobility also contributes to the diffusion length of the charge carriers. The three semiconductor materials (i.e. silicon, $CH_3NH_3PbI_3$, and BiI_3) discussed previously have carrier mobilities that differ. The electron and hole mobility for silicon is greater than those of methylammonium lead iodide and bismuth triiodide. This further implies that silicon has a greater diffusion length than methylammonium lead iodide and bismuth triiodide. Therefore, there is potential for additional research in optimizing the materials, especially BiI_3 as it has a substantially lower diffusion length.

In addition to the mobilities, the carrier lifetimes of the materials contribute to the determination of the material diffusion lengths. Carrier lifetimes vary greatly depending on the methods used to produce solar cells. For silicon solar cells the carrier lifetime can range anywhere from 1 nanosecond to 1 microsecond.[65] Methylammonium lead iodide has an average carrier lifetime of 1 microsecond. [66] This comparison establishes methylammonium lead iodide as a promising material for photovoltaic applications as it is comparable to the carrier lifetime of a material that has been used in industry for decades. In regards to bismuth triiodide, it has been found experimentally that it has carrier lifetimes of 160-260 picoseconds for single-crystal samples. [67] Although the carrier lifetime for bismuth triiodide is about six orders of magnitude less than that of silicon and methylammonium lead iodide, the values are still promising considering how much less it has been researched than silicon.

Different experimental data proves this implication true. The diffusion length of methylammonium lead iodide has been found to be >1000nm or 1$\square$m.[68] The diffusion length for BiI_3 has been determined to be 1.9 or 4.9$\square$m[69]; and Silicon has been found to have a diffusion length of 100 to 300$\square$m[70]. That is, the diffusion length of Silicon can be over 100 times the length of that for methylammonium lead iodide and bismuth triiodide.

[65] Meroli, Stefano, "The Minority Carrier Lifetime in Silicon Wafer. Bulk and Surface Recombination Process.", (n.d.).

[66] Ibid.

[67] Brandt, Riley E., et. al., *Investigation of Bismuth Triiodide (BiI₃) for Photovoltaic Applications* (American Chemical Society, 2015), 4299.

[68] Caraballo, F., Kumano, M., Saeki, A., *Spatial Inhomogeneity of Methylammonium Lead-Mixed Halide Pervoskite Examined by Space-and Time-Resolved Microwave Conductivity.* (American Chemical Society, 2017).

[69] Brandt, Riley E., et. al., *Investigation of Bismuth Triiodide (BiI₃) for Photovoltaic Applications* (American Chemical Society, 2015), 4297.

[70] Honsberg, C. and Bowden, S., "Diffusion Length", (PVEducation, September 2017).

The band gaps for silicon, methylammonium lead iodide, and bismuth triiodide all vary. Silicon has the lowest band gap with a value of 1.18 +/- 0.03 eV.[71] Methylammonium lead iodide ($CH_3NH_3PbI_3$) and bismuth triiodide have band gaps of 1.51 eV and approximately 1.82 eV, respectively.[72] These band gap values indicate that there is more energy necessary for an electron to be sent from the conduction band to the valence band for methylammonium lead iodide and bismuth triiodide than for silicon. Defects can be employed to optimize different optical, electronic, or optoelectronic properties. [73]

Currently, methylammonium lead iodide has a greater absorption coefficient than silicon which implies it isn't as strong at absorbing photons and thus exciting electrons into the conduction band. These values can also be found in Appendix B. As a result of methylammonium lead iodide's higher absorption coefficient, the semiconductor layer doesn't have to be as thick due to a smaller absorption depth.[74] Bismuth triiodide has been proven to have an even larger absorption coefficient in the visible region of the solar spectrum.[75] This indicates the necessary thickness of bismuth triiodide as the semi-conductive layer in a solar cell could be less than both silicon and methylammonium lead iodide.

These discussed quantities put in perspective the current status of bismuth triiodide in comparison to other semiconductive materials. They highlight the material's potential applications and improvements, which will be discussed in the following sections.

2.5.3 The Need for Research and Development

There has been minimal research and published material regarding the photo-optical properties of BiI_3. As a result, our own efforts will be used to better understand the functional nature of this semiconductor material. This serves as the basis of our research project -- much of the data and knowledge attained through this research project will build on what little contemporary understanding there is of BiI_3.

---

[71] Low, Jeremy J., et. al. "Band Gap Energy in Silicon", *American Journal of Undergraduate Research*, vol. 7 no. 1 (Millersville University, April 16 2008).

[72] Garg, A., Tomar, M., Gupta, V., "Synthesis of Characterisation of Thin Films of Bismuth Triiodide for Semiconductor Radiation Detectors" in *Conference Papers in Science*, ed. P Mandal, R. K. Shivpuri, and G.N. Tiwari vol. 2014 (Hindawi, 2014).

[73] Rudolph, Peter, *Fundamentals of Defects in Crystals*, vol. 916, Issue 1 (AIP Conference Proceedings, June 2007).

[74] Honsberg, C. and Bowden, S., "Band Gap", (PVEducation, September 2017).

[75] Brandt, Riley E., et. al., *Investigation of Bismuth Triiodide (BiI_3) for Photovoltaic Applications* (American Chemical Society, 2015), 4299.

A 2015 study of BiI$_3$ from Brandt, et al., *Investigation of Bismuth Triiodide (BiI$_3$) for Photovoltaic Applications*, showed some promising results regarding the future use of this material. In the study, the researchers grew thin films of phase-pure BiI$_3$ using a sublimation furnace over a range of temperatures and then spin-coated the material. They found some of the most useful properties of BiI$_3$ to be room temperature photoluminescence, its near-ideal band gap of 1.8 eV, and its absorption coefficient of $>10^5$ cm^{-1}, which indicates that it can achieve high photocurrents at a very low thickness (<1 µm).[76] Each of these properties demonstrate potential for the material in terms of photovoltaic application.

The research study also articulated some areas of improvement for BiI$_3$ - these areas will serve as the basis of our own research study. For instance, the carrier lifetime must be improved for this thin-film material in order for it to produce effective and high-performing PV devices.[77] BiI$_3$ intrinsically has a high resistivity and thus requires a longer lifetime to yield a better fill factor; the series resistance is governed by photoexcited carrier concentration, a value proportional to carrier lifetime.[78] The researchers assert that "improved controls of phase purity, elemental purity, and intragranular structural defect density will prove essential to increasing lifetime."[79]

In order to improve phase purity, it may be useful to explore annealing temperatures that are cooler and do not approach the BiI$_3$ sublimation point (250 - 300°C). At these higher temperatures, the material will begin to dissociate and evaporate, which hinders the natural stoichiometry of BiI$_3$.[80] Additionally, researchers have suggested that the physical structure of BiI$_3$ may be a factor that actually influences structural defects and decreases lifetime.

2.6 Influence of Thermal and Chemical Treatments on Photovoltaic Properties

A number of different thermal and chemical treatments could be used to enhance and modulate the electrical properties of semiconductor materials such as BiI$_3$. These treatments have the capability of improving the band gap, diffusion length, carrier lifetime, and other material properties. This section explains the role of defects as well as different techniques which will likely play a role in our research project methodology.

---

[76] Brandt, Riley E., et. al., *Investigation of Bismuth Triiodide (BiI$_3$) for Photovoltaic Applications* (American Chemical Society, 2015), 4299.
[77] Ibid.
[78] Ibid.
[79] Ibid.
[80] Ibid.

2.6.1 Defects of n-type doping

Given that there are a number of intrinsic material defects that are present in n-type photovoltaics, it is ultimately important to understand these very defects in BiI_3. There are several different conditions of defects required in effective n-type semiconductors. The first -- the concentration of donors must be high, meaning that dopant formation must have a low formation enthalpy.[81] In terms of BiI_3, the formation enthalpy is low for both Bi-rich and I-rich conditions, and therefore the defect is abundant.[82] Another intrinsic condition for n-type doping is that the donors must have shallow levels, meaning that they are easily and readily ionizable.[83] This phenomenon is illustrated in Figure 16, which depicts a conceptual electron energy diagram. Upon excitation, electrons ideally obtain enough energy to move from the valence band to the conduction band. However, in n-type semiconductors, donors will lie closely (a shallow level) to the conduction band, where room temperature thermal energy is sufficient to free an electron to the conduction band.
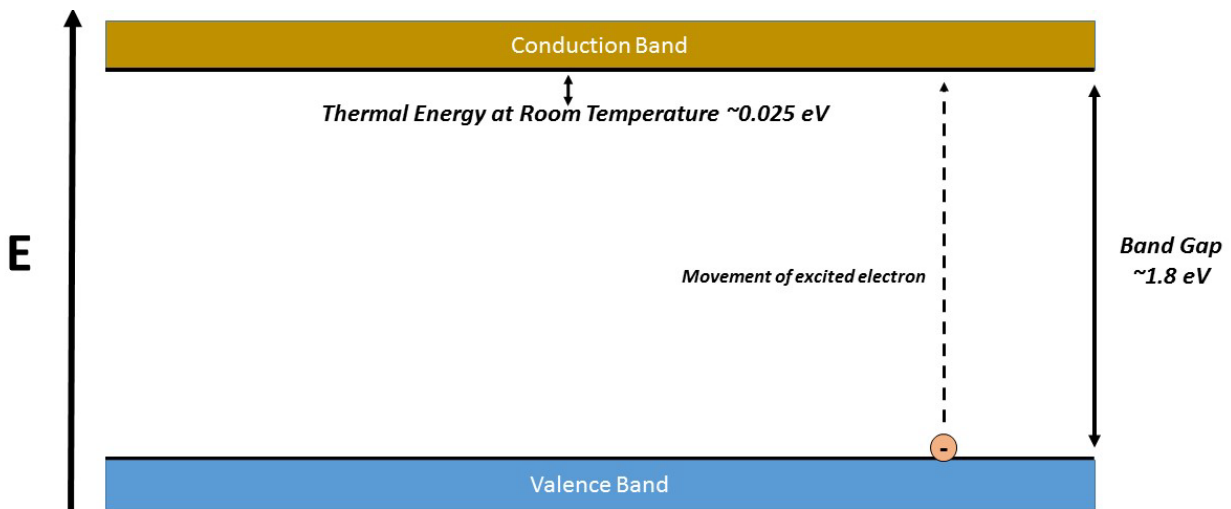
Figure 16. Conceptual energy diagram of electron movement from valence to conduction band.

Thus, BiI_3 is n-type at Bi-rich conditions because the Bi interstitial, Bi_i (donor), is supplying the electrons. A final rule or condition for n-type doping is that a material's electron affinity cannot

---

[81] Zunger, A., Killic, C., Wang, L., *Defects in Photovoltaic Materials and the Origins of Failure to Dope Them* (National Renewable Energy Laboratory, 2002).
[82] Ibid.
[83] Ibid.

be too small. If this is the case, the electron-killer defects will be generated and replace the electron-producing agent.[84]

2.6.2 Extrinsic Doping

Extrinsic doping is the process of introducing an outside chemical material as treatment to enhance electrical properties. One modern method of extrinsic material doping is ion implantation. Through this technique, the dopant materials are ionized, brought to high energy, and then fired at the material. After this, the material surface is heated quickly and then cooled slowly, or annealed, to rectify the damage caused by the ion implantation.[85] This method is common and useful as it provides the advantage of precision.

In terms of our study of BiI_3, previous research has suggested that extrinsic doping with antimony (Sb) has potential to enhance PV properties.[86] This is surprising because antimony is in the same group as bismuth, where usually materials are doped with elements that are in the group before or after it, as discussed in Section 2.2.1. Antimony has potential to be a successful dopant in this case because Sb^{3+} has shown to be soluble in in BiI_3. In a study testing Sb doped BiI_3, a 5% doping level resulted in optimal properties.[87] It was shown that doping with antimony increased the electron mobility by about 70%, increased the resistivity of the material, and reduced the formation and the migration of iodine vacancies.[88]

2.6.3 Thermal Annealing

Thermal annealing, as mentioned previously, is a heat treatment in which a material is heated rapidly and then cooled gradually to enhance its chemical properties. People use thermal annealing because it is a simple yet effective procedure that enhances properties such as grain size and thus facilitates electron and hole diffusion. In a previous research study of bismuth (III) sulfide (Bi_2S_3), researchers examined a similar nontoxic n-type semiconductor material with the objective of optimizing its efficiency through different annealing methods. According to the researchers, by

---

[84] Zhang, S.B., Wei, S.H., Zunger, A., *Intrinsic n-type versus p-type doping asymmetry and the defect physics of ZnO* (National Renewable Energy Laboratory, 2000).

[85] Parthavi, Uma M., *Doping by Diffusion and Implantation* (Indian Institute of Technology Delhi, n.d.).

[86] Brandt, Riley E., et. al., *Investigation of Bismuth Triiodide (BiI₃) for Photovoltaic Applications* (American Chemical Society, 2015), 4299.

[87] HyukSu, H., et. al., *Defect Engineering of BiI₃ single crystals: enhanced electrical and radiation performance for room temperature gamma-ray detection. The Journal of Physical Chemistry C* 118, no. 6 (2014): 3244-3250.

[88] Ibid.

sulfur annealing solution-deposited Bi_2S_3 at 445°C, they were able to increase grain size, and thus carrier lifetime, internal quantum efficiency, among other features.[89] This method also enabled them to achieve carrier diffusion lengths similar to the light absorption depth, "which makes it promising for photovoltaic and petrochemical energy conversion applications."[90]

In another study, it was found that annealing BiI_3 in solvent vapor, especially dimethylformamide (DMF) vapor, increased the grain sizes of the material. This thermal annealing was performed at 100 °C for 10 minutes.[91] When BiI_3 is annealed the temperature of the material increases. This increase in temperature causes the grains that make up the BiI_3 to increase in size. This is shown in Figure 17 below.

Figure 17. When BiI₃ is annealed though solvent vapor annealing, the increase in temperature increases the size of the grains.

The larger grains result in less grain boundaries, which make less obstacles for electrons and holes to move across while diffusing through the BiI_3 layer. More grain boundaries would increase the carriers' chances of getting trapped in the semiconductor layer thus decreasing the carrier's lifetime and mobility. Decreasing the lifetime and mobility will inhibit carriers from reaching their respective layers. This is essential to the operation of the solar cell, so decreased

[89] Zhehao Zhu, et al. *Enhancing the Solar Energy Conversion Efficiency of Solution-Deposited Bi₂S₃ Thin Films by Annealing in Sulfur Vapor at Elevated Temperature*. (*Sustainable Energy Fuels*, 2017, 1, 2134).
[90] Ibid.
[91] Hamdeh, U. H., Nelson, R. D., Ryan, B. J., Bhattacharjee, U., Petrich, J. W., & Panthani, M. G. (2016). Solution-Processed BiI₃ Thin Films for Photovoltaic Applications: Improved Carrier Collection via Solvent Annealing. *Chemistry of Materials, 28*(18), 6567-6574. doi:10.1021/acs.chemmater.6b02347

boundaries should increase the efficiency of the cells. This was confirmed in the study that tested DMF as the vapor solvent while annealing. They were able to make cells that had a power conversion efficiency of 1%, which is the highest reported efficiency for BiI_3 cells.[92]

2.6.4 Intrinsic Composition Tuning

A final procedure that may be used to modulate and enhance the chemical properties of a semiconductor material, such as BiI_3, is composition tuning. This technique can be used to generate a more p-type or n-type material composition of a thin film semiconductor material, such as BiI_3. With BiI_3, this will likely be done through intrinsic doping with bismuth or the removal of iodine. Explained previously in Sections 2.2.2 and 2.2.3, the process begins via a concentration gradient between electrons and holes, subsequent diffusion to respective layers, and a resultant electric field generated through this diffusion process.

There are positive and negative consequences of creating a more n-type or p-type material. For BiI_3, if iodine atoms are removed, the electric field at the interface (in the BiI_3) will become stronger, which will effectively result in a weaker electric field at the ETL. This may either facilitate the diffusion of electrons or hinder the process completely because holes are still the minority carrier. Conversely, if the material is made more p-type, it is possible that recombination will occur more frequently because the concentration gradient is reduced, and thus the material will become more neutral. If there is no concentration gradient, there is no net motion of carriers, and similarly, if there is a small concentration gradient, the movement of carriers is increasingly hindered.[93] This would ultimately depend upon how p-type the material becomes - if hole diffusion is facilitated while maintaining a substantial concentration gradient, then this may prove to be a useful technique for our project methodology.

While outside research has determined BiI_3 to be a promising PV material, there are also a number of areas needing improvement, such as carrier lifetime and phase purity. Our research study serves to examine and rectify these areas needing improvement via some or all of the techniques mentioned throughout this section.

---

[92] Hamdeh, U. H., Nelson, R. D., Ryan, B. J., Bhattacharjee, U., Petrich, J. W., & Panthani, M. G. (2016). Solution-Processed BiI_3 Thin Films for Photovoltaic Applications: Improved Carrier Collection via Solvent Annealing. *Chemistry of Materials, 28*(18), 6567-6574.
doi:10.1021/acs.chemmater.6b02347doi:10.1021/acs.chemmater.6b02347
[93] Honsberg, C. and Bowden, S., "Movement of Carriers in Semiconductors," (PVEducation, Dec. 2017).

3.0 Design of Experiments and Modeling

This section first outlines our methodology for synthesizing and characterizing BiI_3 solar cells. Then, a discussion follows which details possible procedural modifications that can be made to enhance the photovoltaic properties of the benchmark cell. Finally, these experimental modifications are examined in conjunction with computational modeling to better assess the validity of our hypotheses, outlined in Section 3.2.3.3.

3.1 Synthesizing and Characterizing Benchmark BiI₃ Solar Cells

There are five primary steps in the synthesis of a benchmark BiI_3 cell, each corresponding to depositing the different layers: glass and FTO etching, TiO_2, BiI_3, P3HT, and gold evaporation. The following subsections outline the procedures used to create or deposit each layer of the benchmark solar cell. The benchmark cell is that which corresponds to the unmodified standardized synthesis procedure outlined from laboratory training sessions for a BiI_3 thin-film solar cell.

Steps

1. Etch and Clean FTO:

2. Deposit TiO₂ Electron Transport Layer:

3. Deposit BiI₃ Semiconductor Layer:

4. Deposit P3HT Hole Transport Layer:

5. Evaporate Gold Layer:
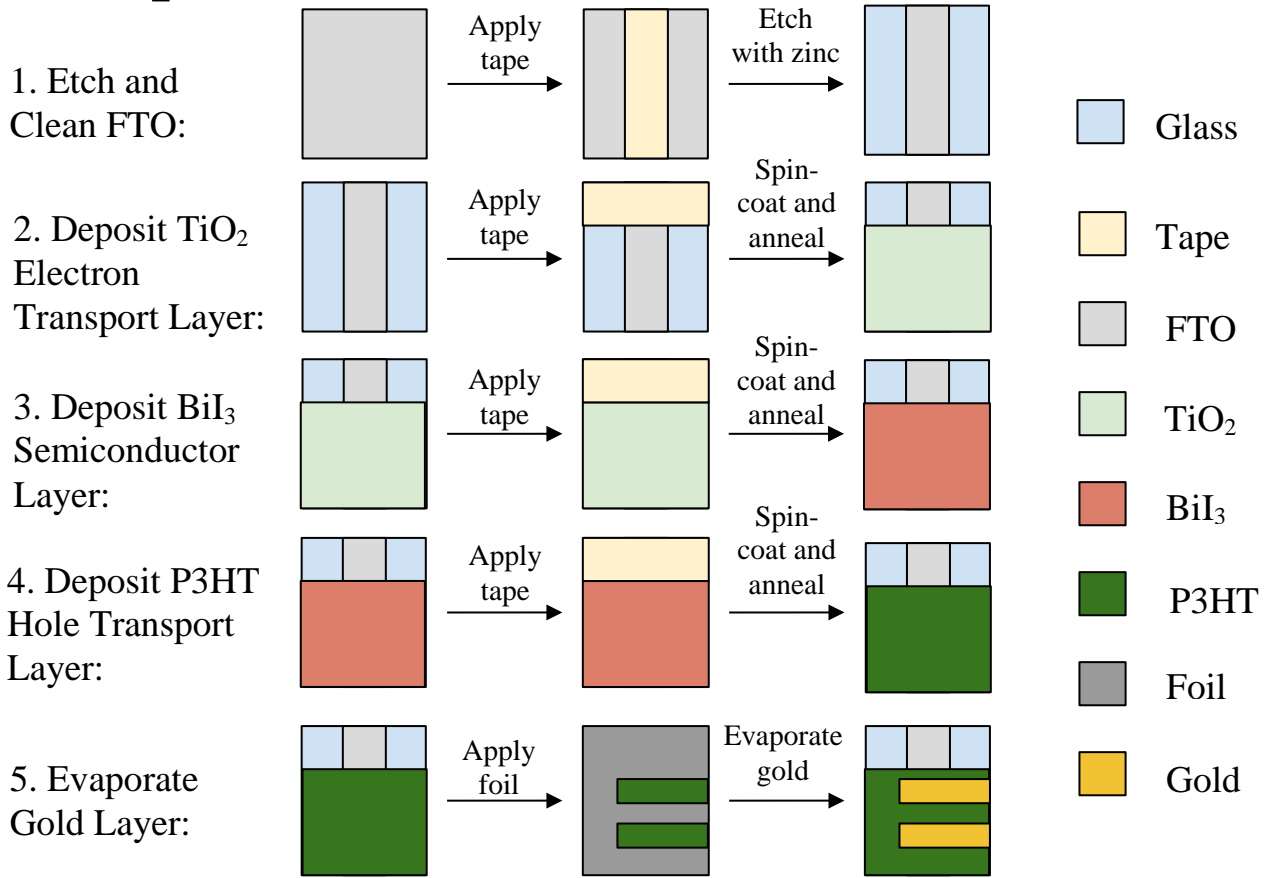
Figure 18. Diagram showing the top view of the cell during BiI₃ synthesis. The detailed procedures for each step are found in Sections 3.1.1-3.1.5.

3.1.1 Glass and FTO Etching

The first step in synthesizing a solar cell was to create a designated area for the electron transport layer (ETL). This step began by cutting fluorine doped tin oxide (FTO)-glass sheets into 2 cm x 2.5 cm rectangles. Only one side of the glass contained a layer of FTO, therefore only one side of the sample was conductive. Once the desired amount of samples were cut out, the conductive sides were identified using a multimeter. The next step was to etch enough of the FTO off of the sample in order to leave a 0.8 centimeter strip left in the middle of the rectangle. In order to do this a 0.8 centimeter wide piece of tape must be put on top of the FTO, shown above in step 1 of Figure 18. Tape is placed on the FTO sample before etching to protect the FTO during the etching process. The tape is used to ensure that the FTO under the tape is not etched away.

The FTO was etched using zinc powder and 6M hydrochloric acid (HCl). The zinc powder was placed via spatula on the two outside strips of the glass sample that were not covered by tape. The strip in the middle covered by the tape was the section of FTO that remained on the glass. After the reaction occurs between the zinc and HCl, and the FTO is effectively etched, the residual zinc was cleaned off with DI water. The tape was then removed, revealing an 0.8 cm strip of FTO. Next, the samples undergo three more cleaning procedures including a soap and water rinse, a boiling water rinse, and finally a rinse in a 1:1:1 solution of isopropyl alcohol, acetone, and DI water. Once the samples were cleaned and dried they were ready for the next stage. A detailed procedure for cutting, etching FTO, and cleaning the samples can be found in Appendix C1.

3.1.2 Compact TiO$_2$ Electron Transport Layer

The next component vital to the operation of a solar cell is synthesizing solutions of titanium oxide (TiO$_2$) to apply to the sample. Two solutions of different molar concentrations were used in the construction of the compact TiO$_2$ layer and were both applied directly to the now-etched FTO-glass of each sample. A 0.15M solution as well as a 0.3M solution were created. These solutions were made from diisopropyl titanium oxide and 1-butanol. Through the techniques of spin-coating and annealing the layer is effectively deposited, as shown above in step 2 of Figure 18. One strip of the sample was covered in tape to prevent the solution from covering all of the FTO and glass during the spin-coating process. A small part of the FTO must be exposed to be used as a conductive contact in the testing procedure once the sample was completed. The application of a TiO$_2$ layer on top of the etched glass was necessary as it served as the electron transport layer (ETL) explained previously in Section 2.2.3.2. The specifications involved in the application procedure can be found in Appendix C2.

3.1.3 BiI$_3$ Semiconductor Layer

The next step in order to build this solar cell was to create a semiconductor layer, that is, the BiI$_3$ layer. This layer was vital because it is the layer that absorbs the light and where the operation of the solar cell begins. This stage started with making a 300 mg/mL solution of BiI$_3$ solution in dimethylformamide (DMF). This solution needed to be stirred for 2-3 hours before it could be deposited onto the sample. Once the solution was mixed, it was deposited onto the sample through spin-coating and annealing. Tape was used again to ensure exposure of the FTO contact.

Step 3 in Figure 18 details the top view of the deposition of the BiI$_3$ layer. A more detailed procedure for synthesizing the BiI$_3$ layer can be found in Appendix C3.

3.1.4 P3HT Hole Transport Layer

The next layer when creating the solar cell was the hole transport layer. For this layer, we used poly(3-hexylthiophene-2,5-diyl), or P3HT. 15 mg of P3HT was weighed out and placed into a vial. Next, 1 mL of 1,2-dichlorobenzene was added to the vial using a syringe. The vial was then stirred with a stir bar for 30 minutes. The next step in establishing the P3HT layer was spin-coating, which adds a thin layer of P3HT atop the surface of the sample. After the spin-coating process, the sample was annealed for 20 minutes and then allowed to cool. Again, tape was used to maintain the exposed FTO contact. This process is diagrammed in step 4 of Figure 18. More detailed instructions for creating this layer can be found in Appendix C4.

3.1.5 Gold Current Collector Layer

The final layer of the solar cell was the gold layer, which is known as a current collector layer. Upon deposition of the P3HT layer, the samples were covered in aluminum foil and two small rectangular strips of aluminum foil were cut out, exposing the P3HT. This is shown in step 5 of Figure 18 below. The entire layer of P3HT was not covered in gold in order to ensure defined cells and gold contacts and to allow area for more than one cell on each sample. Once the two strips of P3HT were exposed, gold was deposited onto the surface of the aluminum foil using a gold evaporator. Following this step, the aluminum foil was removed and the cells were ready for testing.

This setup allowed for only the areas with exposed P3HT to be evaporated with gold, creating two separate cells per sample. These cells should theoretically have the same optoelectronic properties since they are part of the same sample. The areas that were covered in gold and intersected the 0.8 centimeter FTO strip in the middle were considered the solar cell. The gold strip was used as a contact for testing the cells.
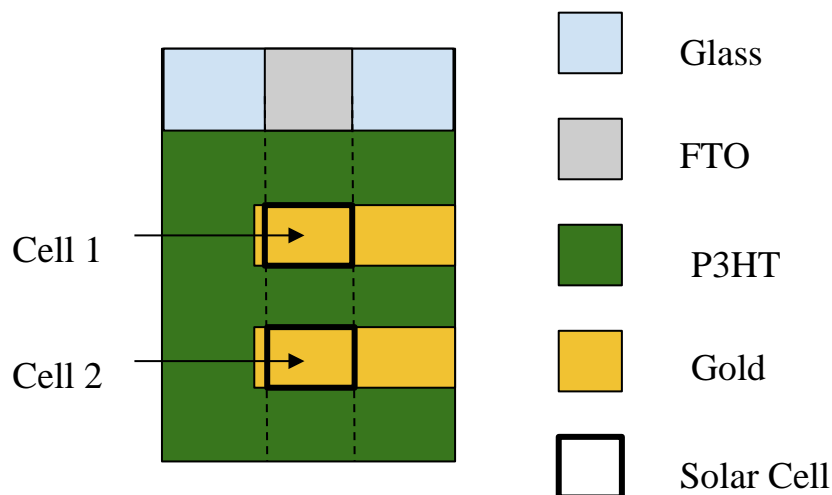
Figure 19. This diagram shows a top view of a finished sample. The top section of glass and FTO have been preserved by placing tape over the section during all rounds of spin-coating. The cells that are tested are at the intersection of the gold and FTO strips, as designated by the bolded solar cell boundaries. The cell closest to the exposed glass and FTO was designated as cell 1, and the cell farthest from the exposed glass and FTO was designated as cell 2.

Figure 19 shows what the sample looks like after the gold evaporation step. The diagram also outlines the cell boundaries. The cell areas were measured with a ruler and reported in square centimeters.

3.1.6 Solar Cell Performance Testing

Once the samples were completely synthesized, they were ready to be tested for their optoelectronic performance. This was measured by testing each cell's open circuit voltage, short circuit current, and then calculating the resultant cell efficiency. This data was gathered using an EC Lab program[94]. The first step in obtaining these results was to suspend and position the sample 13 centimeters away from the lamp using the clamp and ring stand setup pictured in Figure 20 below. This distance ensured the light intensity of one sun.

---

[94] "Electrochemistry: EC-Lab", (Bio-Logic Science Instruments, 2016).

Potentiostat

Computer
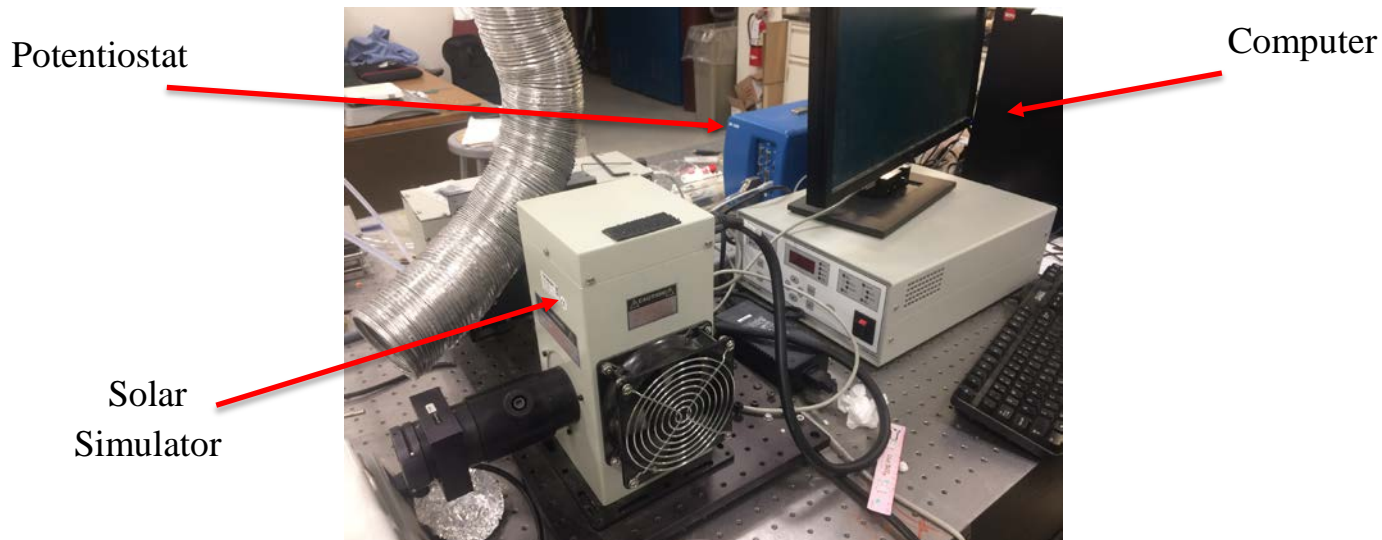
Solar
Simulator

(a)
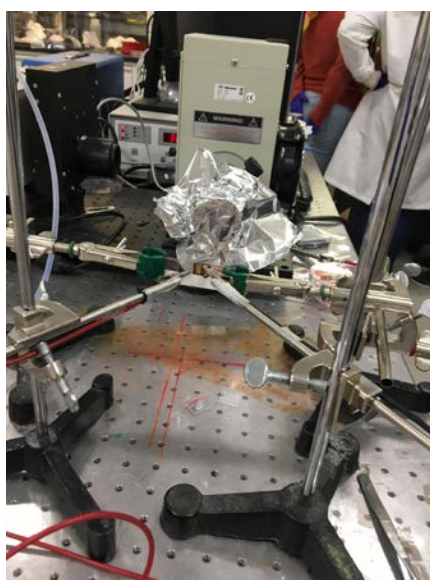
(b)
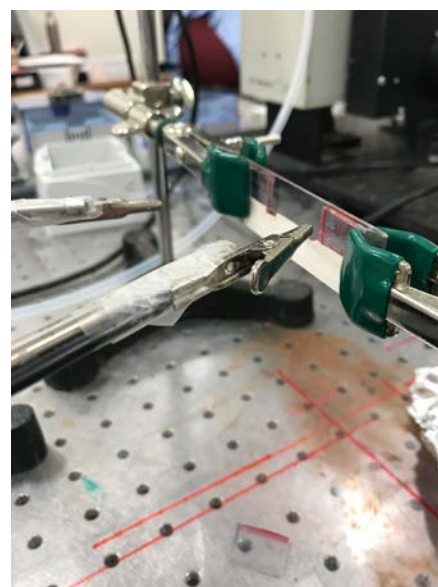
(c)

Figure 20. These image show the equipment necessary for testing samples. Image (a) shows the solar simulator, potentiostat, and the computer where the results are sent to. Image (b) shows the sample setup for testing and image (c) is a closer up shot of the apparatus that is built to ensure that the sample is secured in place for testing. Images (b) and (c) also show the probes that are used to touch the FTO and gold contact, which are connected to the potentiostat to collect the data.

In this setup, one end of the red probe had to touch the FTO contact and one end of the black probe had to touch the gold contact. The other ends of the probes had to be clamped to the

contacts that are connected to the potentiostat which writes data to the computer program. Next, the computer program had to be open and the lamp had to be turned on. When the cell was ready to test, the lamp cover was opened up to allow light to shine on the cell and the data collection to start. When the test was finished, the data was saved and the test was repeated for the next cell. The data collected here makes a graph, more specifically a J-V curve as explained in Section 2.3.7. The x-intercept of the graph was the open circuit voltage, the y-intercept was the short circuit current, and using these numbers the efficiency could be calculated. A more detailed procedure on how to set up and run these tests can be found in Appendix C5.

3.1.7 Scanning Electron Microscope (SEM)

After the solar cells were tested for open-circuit voltage (V_{OC}), short-circuit current density (J_{SC}) and power conversion efficiency (PCE) using the EC-lab software and the lamp, select samples were cut for examination of both the top layer and cross-sectional views of the cells under the scanning electron microscope (SEM). This allowed for the composition of the solar cell, namely layer thicknesses and grain boundaries, to be investigated. The images allowed for correlations between the composition of the solar cells and their performance to be inferred. This was done by adhering the samples into the bracket designated for SEM imaging. A diagram of this setup is pictured below in Figure 21.
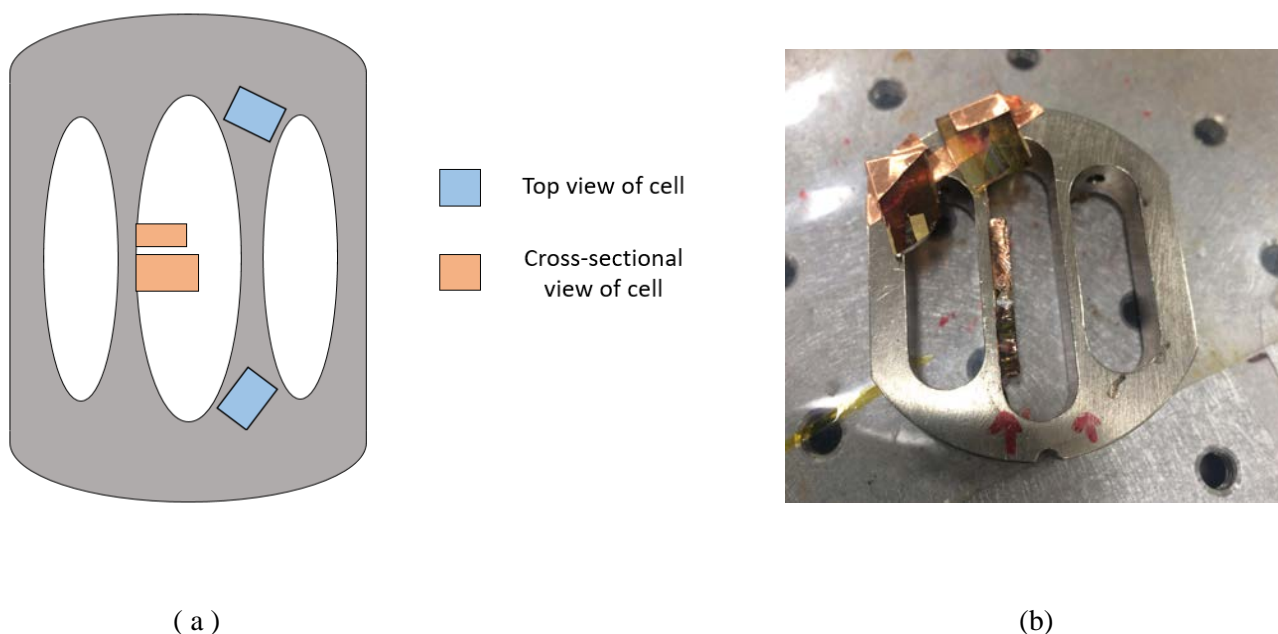
Figure 21. These images show (a) a diagram of samples that are cut out and then secured to the metal bracket and (b) and a picture of an example setup of samples to be examined through scanning electron microscopy.

3.2 Investigation of potential modifications for optimizing BiI₃ photovoltaic cells

Given the procedures outlined for the synthesis of a benchmark BiI_3 cell, there were several possible procedural modifications that could be made to optimize the J_{SC}, V_{OC}, and the resultant efficiency of the cell. In this section, we discuss potential modifications that we used to change and assess the photovoltaic properties of the BiI_3 cell. The purpose of this section is to examine these ideas more closely and discern which of these methods could have the largest effect on the performance of our cells.

3.2.1 Compact and Mesoporous combinations of TiO₂

As a means to optimize the surface area of the BiI_3 layer, various combinations of compact and mesoporous layers of TiO_2 were applied.[95] The combinations of compact and mesoporous layers of TiO_2 in this research project include samples with one layer of compact TiO_2, samples with one compact layer and one mesoporous layer of TiO_2, and samples with one layer of compact and two layers of mesoporous TiO_2. Therefore, all samples included one run through of the process

---

[95] Kovalsky, A. and Burda, C., "Optical and Electronic Loss Analysis of Mesoporous Solar Cells" (IOP Publishing, 2016).

corresponding to the application of a compact layer, which was outlined previously in Section 3.1.2.

For the samples designated to have mesoporous layers in addition, a separate process was conducted which called for different components for the solution, different parameters for sonicating and spin-coating, as well as only calling for one temperature and a different time to anneal the samples at. The samples which needed two layers of mesoporous TiO_2 were left to cool prior to conducting the process again. The specifications for this procedure can also be found in Appendix C2.

3.2.2 Altering the frequency of rotation of spin-coat instrument

Spin-coating is a technique commonly used for the application of thin-films. It involves the deposition of fluid onto some surface or substrate followed by the spinning of the substrate at very high speeds. Through centripetal acceleration, the applied fluid was spread uniformly across the surface of the substrate, creating a thin-film.[96] In this study, the frequency of rotation (in rpm) of the spin-coat instrument was altered for the BiI_3 layer to examine the effect on the PV properties of our cells. We hypothesized that a decreased frequency of rotation would create a thicker BiI_3 layer giving the absorption length and charge collection the potential to be improved, thus improving the resultant J_{SC}.

To assess this, we examined different BiI_3 sample cells spin-coated at 500, 1000, and 1500 rpm. The spin-coating was conducted at the three different speeds for each type of TiO_2 layer synthesized. By discerning the rpm and TiO_2 layer combination that corresponds with the top performing samples, we were better able to optimize our benchmark cell. Table 2 outlines the specifics of this assessment.

---

[96] "Spin Coating Theory", (University of Louisville: Micro/Nano Technology Center, Oct. 2013).

Table 2. This table gives the sample combinations synthesized to optimize TiO$_2$ layer combination and spin-coating speed. c indicates compact TiO2 and m indicates mesoporous TiO2.

TiO$_2$ Layers	Spin-coating Speed (rpm)
c-TiO$_2$	500
c-TiO$_2$	1000
c-TiO$_2$	1500
c-m-TiO$_2$	500
c-m-TiO$_2$	1000
c-m-TiO$_2$	1500
c-m-m-TiO$_2$	500
c-m-m-TiO$_2$	1000
c-m-m-TiO$_2$	1500

3.2.3 Intentional Oxidation and Additional Modifications

Following the application of the BiI$_3$ layer, intentional oxidation was executed via multiple annealing methods in air. A variety of annealing procedures and parameters were tested in order to determine which method would yield the best performance.

3.2.3.1 Box Furnace Annealing

One annealing method that was investigated was annealing in the box furnace. Select samples were annealed in the box furnace in air at 250ºC, 200ºC, 150ºC, or 100ºC. At each temperature, the time in which the samples were in the box furnace was also varied, exposed to these temperatures for 10, 15, or 20 minutes. This experimental procedure is outlined in Table 3 below.

Table 3. This table gives the combinations of samples heated in the box furnace at different temperatures and durations of time.

Box Furnace Temperature (°C)	Duration (min)
100	10 15 20
150	10 15 20
200	10 15 20
250	10 15 20

After investigating the effects of the three different temperatures mentioned above, we found the optimal time duration to be 10 minutes. We believe that time durations above 10 minutes caused sample overexposure to the heat treatment, especially at the higher temperatures. Accordingly, we continued to investigate alternative temperatures of 40°C to 110°C at increments of 10°C for 10 minutes each. This experimental setup is detailed in Table 4 below.

Table 4. This table gives the combinations of samples heated in the box furnace at an additional set of temperatures for 10 minutes.

Box Furnace Temperature (°C)	Duration (min)
40	10
50	10
60	10
70	10
80	10
90	10
100	10
110	10

Overall, the purpose of the box furnace approach was determine an optimal annealing temperature for the samples.

3.2.3.2 Dimethylformamide (DMF) Solvent-Vapor Annealing

One deviation from the benchmark annealing procedure is the method of solvent vapor annealing (SVA). The advantage of the SVA approach, as demonstrated in Section 2.6.3, is that it has the capability of increasing grain sizes and therefore the mobility and lifetime of charge carriers.

Procedurally, SVA annealing is relatively simple, illustrated in Figure 22 below. A hot plate was first preheated to 100°C and then two samples were placed onto the surface of the hot plate. The sample on the right, illustrated below, is the sample of interest, with layers deposited up to the BiI_3 semiconductor layer. The sample on the left is FTO-glass with 20 µL of dimethylformamide (DMF) solvent deposited onto the surface. Following the placement of these two samples onto the hot plate, an inverted petri dish was carefully placed on top of the samples so that the samples were located on opposite ends of the petri dish. The inverted petri dish allows for the DMF to stay as a vapor in that closed system while the sample of interest is annealing. Finally, the samples were removed from the hot plate after ten minutes.
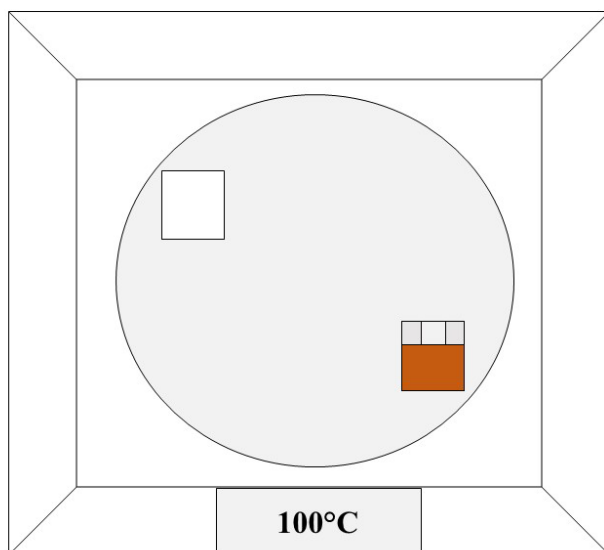
Figure 22. Top view of solvent vapor annealing (SVA) procedure, where the BiI₃ sample (right) and DMF solvent sample (left) are placed atop a hot plate with a petri dish covering both samples on opposite ends for ten minutes at 100°C.

Using the approach described, we tested different samples to determine if SVA heat treatment helped or hindered the synthesis process.

3.2.3.3 Additional Post-Annealing

A final alteration to our benchmark annealing procedure was an additional anneal after all layers were deposited. Essentially, after the final gold evaporation procedure, we tested our benchmark samples for J_{SC}, V_{OC}, and PCE. Then, we annealed the completed samples for an additional ten minute "post-anneal" at 100°C on a hot plate to discern if this would improve the cell performance. We hypothesized that the additional anneal would improve overall interlayer contact and therefore the J_{SC} and resultant PCE. This was also a suggested procedure from prior literature.[97]

---

[97]Hamdeh, U. H., Nelson, R. D., Ryan, B. J., Bhattacharjee, U., Petrich, J. W., & Panthani, M. G. (2016). Solution-Processed BiI₃ Thin Films for Photovoltaic Applications: Improved Carrier Collection via Solvent Annealing. *Chemistry of Materials, 28*(18), 6567-6574. doi:10.1021/acs.chemmater.6b02347

3.2.3.4 Experimental Hypotheses

The methodologies described in the previous subsection were used to assess four different hypotheses detailed below in Figure 23. These assessments were crucial to characterizing the nature and optimizing the optoelectronic properties of the BiI$_3$ cell.
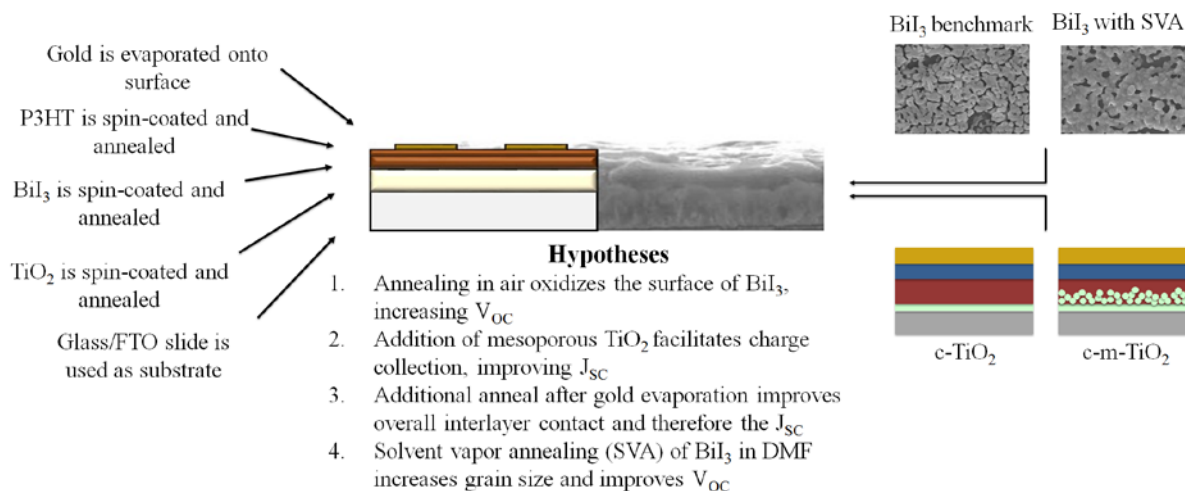
Figure 23. Potential synthesis and optimization approaches used to enhance the properties of a BiI$_3$ cell. Hypotheses 1-4 guided our research. The left portion of the schematic outlines the different layers of the solar cell and how they were deposited. The right portion of the schematic shows how two of the methods (adding mesoporous TiO$_2$ and SVA) in our hypotheses changed the composition of the solar cell.

We also examined hypothesis 1 more thoroughly by performing computational molecular modeling procedures, which will be discussed in the next section.

3.3 Molecular Modeling of BiI$_3$

This section outlines the procedure for modeling BiI$_3$ with and without oxidation. All of the calculations were performed on Vienna Ab initio Simulation Package (VASP)[98] using density functional theory on a linux operating system. After optimizing the lattice constants for BiI$_3$, we added defects to BiI$_3$, and then created density of states plots for each system. The following sections will explain how we ran these calculations. The calculations were performed using the following command lines on WPI's ACE computer system:

---

[98] VASP, "What is VASP?" (RocketTheme, LLC., 2009).

```
module load vasp/5.3
svasp -N 1 -n 18 -t 24:00 -I INCAR
```

The time argument (-t 24:00) can be changed depending on the calculation being done, although the maximum time is shown here as 24 hours. Additionally, a memory argument (-m 128000) can be added for larger calculations.

3.3.1 Modeling bulk BiI₃ without atomic level defects

BiI_3 is a layered, hexagonal structure, as shown in Figure 24a. The unit cell contains 6 bismuth atoms and 18 iodine atoms, shown in Figure 24b. The Perdew-Burke-Ernzerhof (PBE) exchange and correlation functionals were used in these calculations.[99] Additionally, the electron-ion interactions were modeled with the projector augmented-wave (PAW) method.[100] Dispersion interactions between the BiI_3 layers were modeled with the Grimme D3 dispersion correction.[101]

[99] Ernzerhof, M. and Scuseria, G., *Assessment of the Perdew-Burke-Ernzerhof exchange-correlation functional*, (Journal of Chemical Physics, vol. 110, no. 11, 15 March, 1999).

[100] Blochl, Peter, et. al., *Projector augmented wave method: ab initio molecular dynamics with full wave functions,* (Indian Academy of Sciences, vol. 26, no. 1, Jan. 2003), pp. 33-41.

[101] Caldeweyher, E., et. al., *Extension of the D3 dispersion coefficient model*, (The Journal of Chemical Physics, July 2017).

(a)   *(b)*
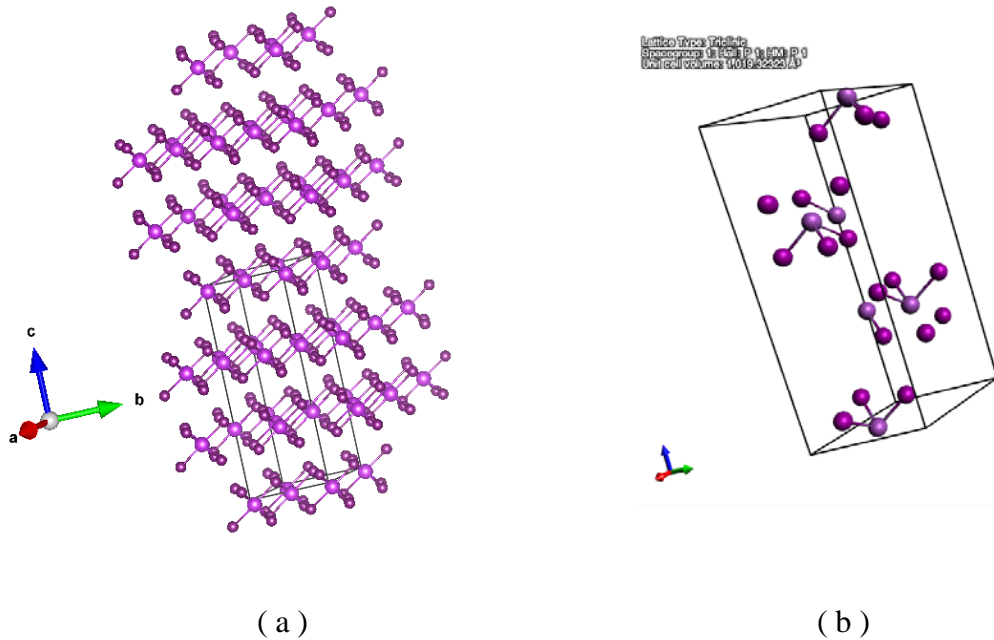
Figure 24. Illustration of BiI₃ that we modeled, where (a) shows the layered structure of BiI₃ and (b) Shows the unit cell of BiI₃, containing 6 bismuth atoms and 18 iodine atoms. In both images, bismuth atoms are shown as light purple atoms where iodine atoms are shown as a darker purple.

When modeling BiI_3, the ENCUT was first optimized by testing values of 200, 300, 400, 500, and 600 eV for bulk BiI_3. The ENCUT value determines how big the basis set is and therefore determines how long each calculation could take. A graph was made with the calculated energy at each ENCUT value, and the point where the energy began to level off or reach a constant value was the ENCUT value we used in the project. This graph is given in Figure 25 below, which shows the optimal ENCUT as 300 eV. We used a k-point mesh of 331 for these calculations.

ENCUT Optimization
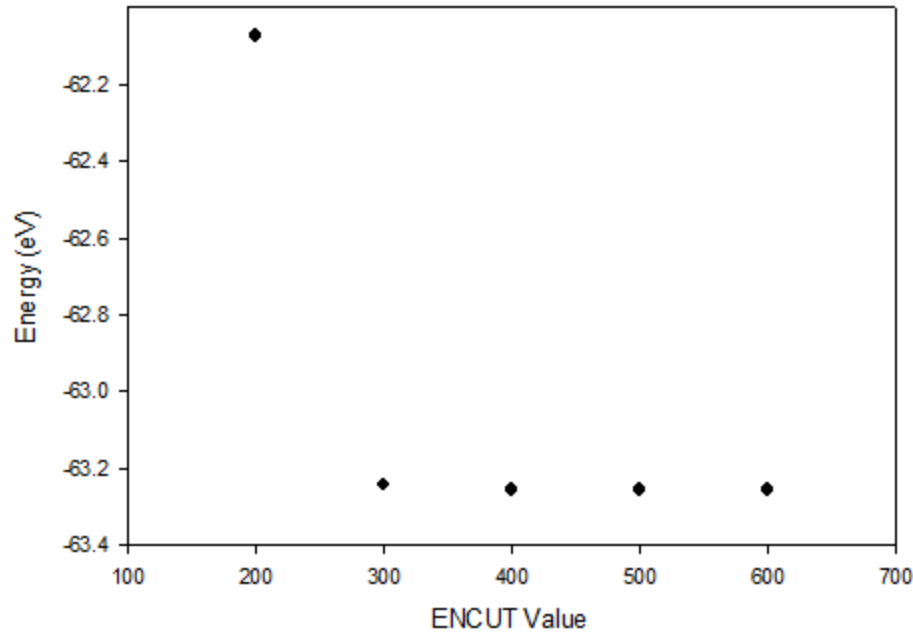
Figure 25. ENCUT values versus total calculated energy for bulk BiI₃. This graph is used to find the optimal value of ENCUT. An ENCUT value of 300 eV shows little change in energy compared to higher ENCUT values and was used for this project.

The next step in the modeling was optimizing the KPOINTS. This calculation was carried out using the obtained ENCUT from the previous step (300 eV). The KPOINTS we tested were as follows: 221, 222, 331, 441, 442, 444, 664, 666, 884, 888. Similar to the ENCUT procedure, a graph was made with the obtained energy and tested KPOINTS. The corresponding KPOINTS when the energy leveled off was used as the optimal values. The graph and the optimal set of KPOINTS, 331, is shown below in Figure 26.

KPOINTS OPtimization
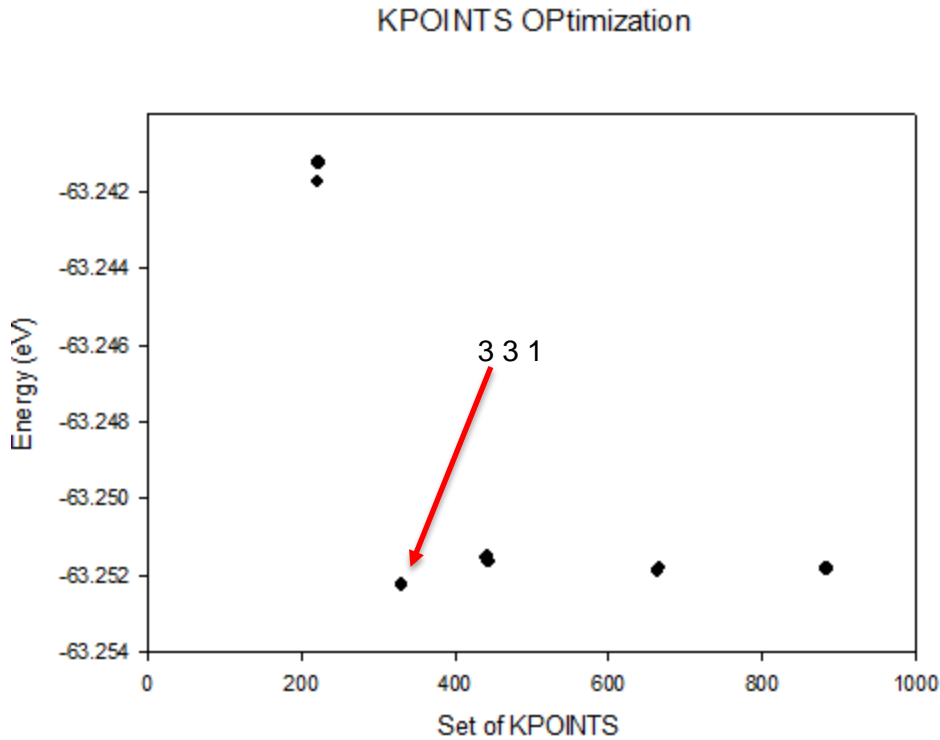
Figure 26. Energy of bulk BiI₃ compared to the k-point values. This graph is used to find the optimal sent of KPOINTS which is found at the minimum value or where the line starts to level off. The k-point set of (3 3 1) is indicated.

The final step in modeling bulk BiI₃ was optimizing the lattice parameters of the unit cell. The unit cell has two lattice parameters that can change, a and c-values. The lattice parameter b was equal to the a-value. All the calculations performed in this step used the optimal values of ENCUT and the optimal set of KPOINTS. A variety of lattice parameters were tested and these parameters were changed for each calculation in the POSCAR file. The first range we used were a-values 7.03 - 8.13 Å with a/c ratios of 0.31 - 0.37. Calculations were run at each of these combinations and a graph was made of the energy versus the corresponding a-value at each ratio, shown in Figure 27 below.
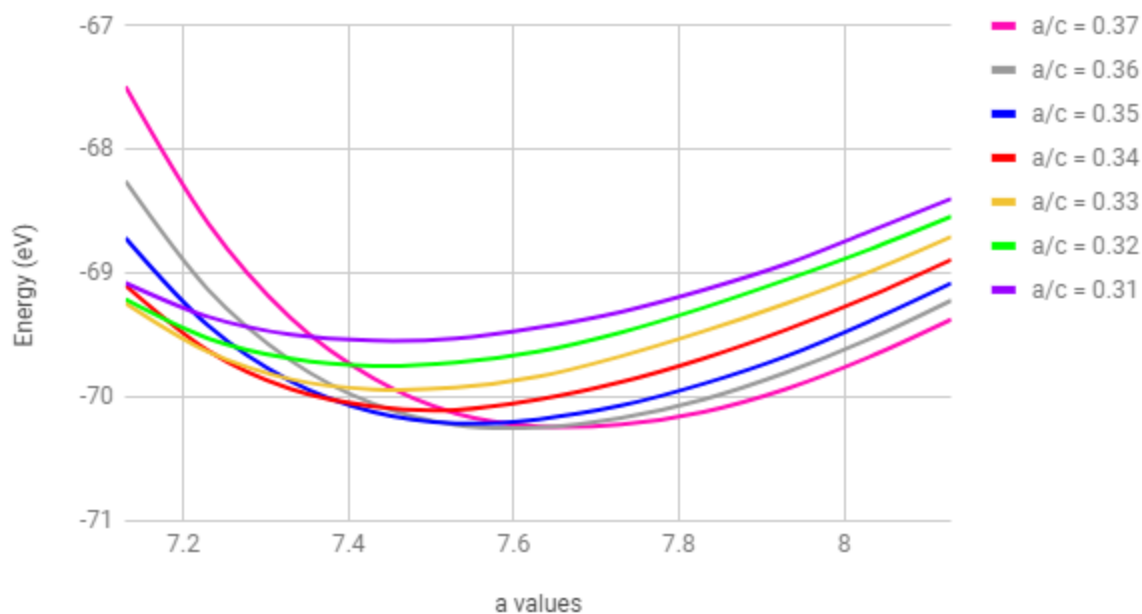
Figure 27. The total energy of bulk BiI₃ compared to different a values and a/c ratios. This graph is used in finding the optimal lattice parameters for BiI₃ at different ratios of a/c. The minimal value was explored further to find the global minimum of lattice parameters.

This graph was used to determine the minimum energy, or optimal ratio of a/c, which we found to be about 0.36. In order to further refine our results around the minimum point and ensure that the global minimum was found a new set of parameters were tested. These parameters were in an a-value range of 7.50 - 7.58 Å and a c-value range of 20.60 - 20.90 Å. A graph was made showing the energy versus the corresponding a-value at each c-value.

Lattice Optimization
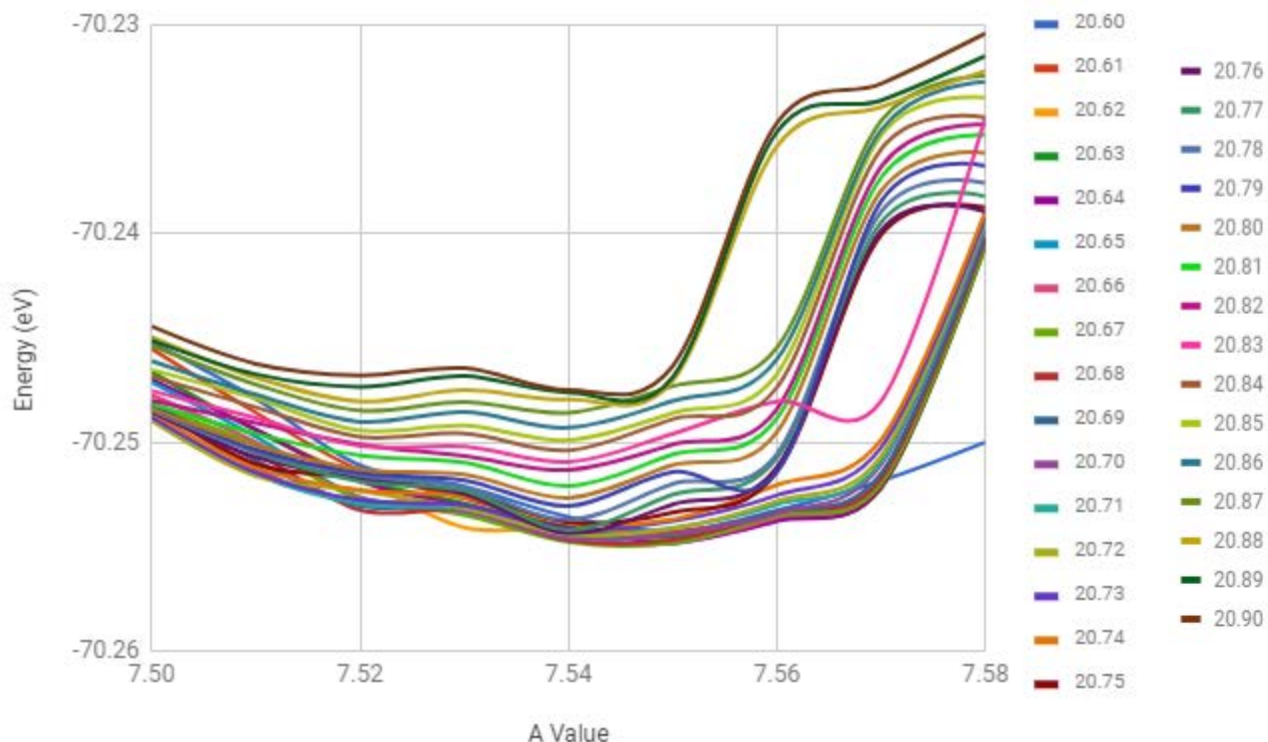
Figure 28. This graph is used to find the optimal lattice parameters of bulk BiI₃ based on the minimum energy for the corresponding a and c value.

Using Figure 28, a global minimum was determined at an a-value of 7.55 Å and a c-value of 20.65 Å so therefore the optimal lattice parameters were found. After finding the optimal ENCUT value, set of KPOINTS, and lattice parameters, the files containing all of these optimal parameters were saved for use in further calculations. The files we used in modeling BiI₃ are given in Appendix D1.

3.3.2 Modeling BiI₃ with Substituted and Interstitial Oxygen Atoms

As discussed in Section 3.2.3, we worked to understand how oxidation affected BiI₃. In order to better explain the experimental results we modeled the oxidation of BiI₃. Three different types of oxidation were modeled, including substituting one oxygen for two iodines, substituting one oxygen for one iodine and adding in an interstitial oxygen. These resulted in unit cells containing $Bi_6I_{16}O$, $Bi_6I_{17}O$, and $Bi_6I_{18}O$ respectively. The first step in modeling these oxidized systems was to introduce the oxygen atom into the unit cell. This was done using the POSCAR

file from the perfect BiI_3 calculations and a modeling software called Avogadro[102]. For each type of oxidation, the appropriate amount of iodine atoms were deleted and an oxygen atom was added in. This new geometry was exported into a POSCAR file and used in the calculations for each oxidized system. The calculation run for this step was done using the same command lines in Section 3.3 above with the input files INCAR, KPOINTS, POSCAR, and POTCAR. These files can be found in Appendix D2.

3.3.3 Analyzing Modeling Data through Density of States Graphs and Reaction Energies

In order to understand and compare the modeled perfect BiI_3 to the oxidized BiI_3 we created density of states (DOS) graphs and calculated energies of the oxidation reactions. DOS graphs are made by running a DOS calculation (using the lorbit = 10 keyword) and then using a script to create the graph. This script is given in Appendix D3. This script uses pymatgen which is an open-source Python library for material analysis.[103] DOS calculations were run with the same type of input files as mentioned in Section 3.3.2 and commands as described in Section 3.3 although additionally the file CHGCAR from the geometry optimization calculation was used for this computation along with the INCAR keyword ICHARG = 11. A few lines of the INCAR file were altered to ensure a DOS calculation rather than the geometry optimization calculations discussed previously. These lines are indicated below.

ISMEAR = -5
NSW = 0
IBRION = -1
EMIN = E-Fermi - 6
EMAX = E-Fermi + 6
NEDOS = 1200
LORBIT = 10
ICHARG = 11

---

[102] Hanwell, M., et. al., "Avogadro: An advanced semantic chemical editor, visualization, and analysis platform", (Journal of Cheminformatics, 2012).
[103] "Pymatgen", (The MIT License, 2011 – 2012).

The E-Fermi value is necessary to determining the EMIN and EMAX values above. This value can be found in the OUTCAR file of the geometry optimization calculation. Once the DOS calculation was completed, the script was used to generate the graphs. This was done for each of the different oxidation substitutions and interstitials and compared to the perfect BiI_3. The other way to assess the oxidation is the energy of reaction. This is determined using the computed energy from a geometry optimization calculations. Using these energies and the stoichiometric coefficients in the reactions below, the energy of each type of reaction was determined, outlined in Figure 29.

$$(a) \ Bi_6I_{18} + \frac{1}{2}O_2 \rightarrow Bi_6I_{16}O + I_2$$
$$(b) \ Bi_6I_{18} + \frac{1}{2}O_2 \rightarrow Bi_6I_{17}O + \frac{1}{2}I_2$$
$$(c) \ Bi_6I_{18} + \frac{1}{2}O_2 \rightarrow Bi_6I_{18}O$$
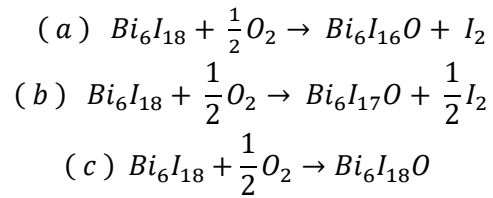
Figure 29. Reactions representing the (a) substituting one oxygen for two iodines (b) substituting one oxygen for one iodine and (c) addition of an interstitial oxygen.

The reaction energy indicates how likely each defect is to occur.

4.0 Results and Discussion

This section reports and explains the results obtained using the experimental and theoretical procedures described in the methodology.

4.1 Experimental Results

This section describes the experimental results that were obtained throughout the timeline of our project. It starts with the original benchmark cell, and then shows how the procedural modifications enhanced the performance of our cells. Appendix E contains a table outlining all raw data pertaining to all samples, including the benchmark samples.

4.1.1 Benchmark BiI₃ Cell

In order to complete our first objective, which was to synthesize BiI_3 solar cells using a reproducible method, the procedures outlined in Section 3.1 were used. After synthesizing approximately 25 samples using these procedures, we determined that the best performing sample was Sample 22 Cell 2 with the benchmark BiI_3 setup. Some of the other benchmark cells failed or did not perform as well. Prior to modifying the procedure several samples were synthesized and tested to practice the procedures as well as to ensure we could consistently synthesize working cells. The benchmark BiI_3 cell derives from the standardized synthesis procedure for a BiI_3 thin-film solar cell. The sample achieved a short circuit current (J_{SC}) of 0.14 mA/cm², an open circuit voltage (V_{OC}) of 0.0066 V, and a resultant efficiency of 0.0021%. Although this is a low efficiency, it was used as a basis for improvement throughout the next steps of our experimental procedures. The efficiency of this sample, along with subsequent samples, was measured to address our second objective which sought to benchmark the solar cell layers.

4.1.2 Optimized BiI₃ Cell

Based on our results from the benchmark BiI_3 cell, we made several procedural modifications to develop an "optimized" BiI_3 cell. The main procedural modifications we made, as described in Section 3.2, were altering the composition of the TiO_2 layers, the spin-coating speeds of BiI_3, and the BiI_3 annealing procedures. The results from each of these modifications are discussed in the following sections and the compiled data set for all modifications can be found in Appendix F1.

4.1.2.1 Investigation of Alternative TiO$_2$ Layer Combinations

We investigated different combinations of TiO$_2$ to observe the effect on sample PCE. Accordingly, the compact (c) TiO$_2$ layer was assessed in combination with mesoporous (m) TiO$_2$. Mesoporous was investigated specifically because according to previous research, the increase in surface area would increase the contact between the BiI$_3$ layer and the TiO$_2$ layer, which would facilitate the transfer of electrons.[104] The mesoporous layer may be more effective due to the reduced recombination of charges within the BiI$_3$ layer. This combination allows for improved charge collection prior to charge carrier recombination.

The results of our investigation of compact only (c-TiO$_2$), compact with one layer of mesoporous (c-m-TiO$_2$), and compact with two layers of mesoporous (c-m-m-TiO$_2$) are shown below in Figure 30. The graph shows that c-m-TiO$_2$ gives the top performing combination of TiO$_2$ layers at a spin-coating speed of 1000 rpm.

---

[104] Kovalsky, A. and Burda, C., "Optical and Electronic Loss Analysis of Mesoporous Solar Cells" (IOP Publishing, 2016).
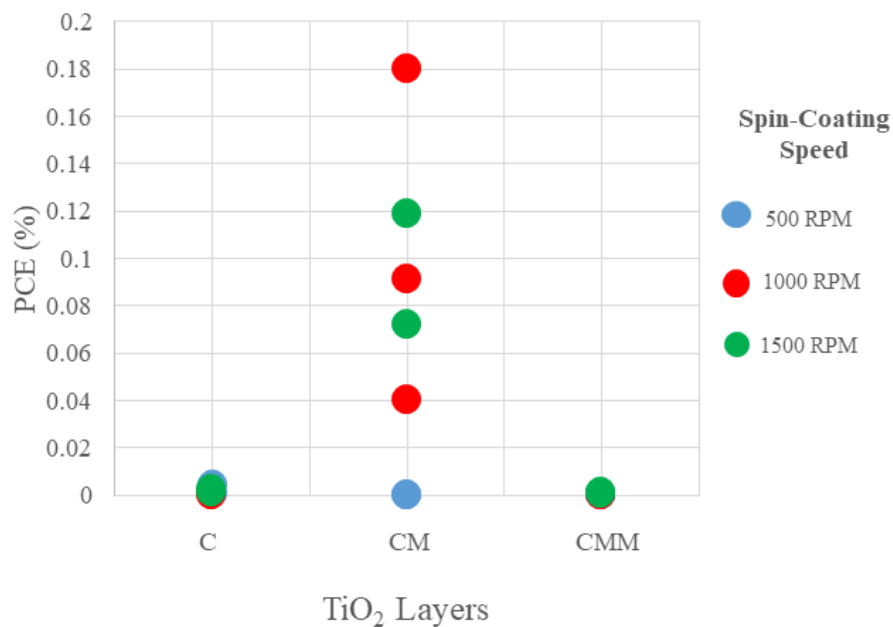
Figure 30. This graph represents the set of samples that were used to optimize the combination of TiO_2 layers as well as the spin-coating speed of the BiI_3 layer. It clearly shows that compact and one layer of mesoporous TiO_2 obtained the best results.

This figure shows that the combination of compact and mesoporous TiO_2 layers improved the performance of the cells. We believe this is due to the porous material increasing layer contact between the TiO_2 and the BiI_3, and therefore increasing carrier extraction which increases V_{OC}, proving our second hypothesis. We believe that two layers of mesoporous was less effective because it caused too substantial of a distance between the TiO_2 and BiI_3 layer, reducing carrier transport. Carrier transport may have decreased due to there being greater probability of charge carrier recombination at the interface between the mesoporous layer and the BiI_3 layer. As for c-TiO_2, previous research indicated that it is much more effective when treated via solvent vapor annealing, so we proceeded with testing c-TiO_2 with SVA only.[105] The data for these tests can be found in Section 4.1.2.2.2.

---

[105]Hamdeh, U. H., Nelson, R. D., Ryan, B. J., Bhattacharjee, U., Petrich, J. W., & Panthani, M. G. (2016). Solution-Processed BiI3Thin Films for Photovoltaic Applications: Improved Carrier Collection via Solvent Annealing. *Chemistry of Materials, 28*(18), 6567-6574. doi:10.1021/acs.chemmater.6b02347

4.1.2.2 Modified BiI₃ Annealing Procedures

We hypothesized that annealing samples in air led to an oxidized film on top of the BiI_3 layer. Hamdeh et al confirmed the presence of oxidized Bi on the surface of the semiconductor layer using XRD.[106] The oxidized layer facilitates hole extraction because BiOI is a p-type semiconductor that increases the valence band maximum, thus decreasing the band gap.[107] Since the measured band gap of BiI_3 is 1.8 eV, a slightly shorter band gap would increase the potential efficiency according to the Shockley-Queisser Limit discussed in Section 2.3.1. Although, this layer of oxidized BiI_3 may be too thin to absorb enough light to make this the reason for increased cell performance. To investigate this further, oxidized BiI_3 was modeled and analyzed in Section 4.2 to come. This increased performance from oxidation could also be caused by the oxidized 6p cation, Bi^{3+}. This compound has a lone pair of electrons around the cation, thus increasing the ionic radius. The increased ionic radius leads to a more disperse valence band which increases the valence band maximum.[108]

4.1.2.2.1 Box Furnace Annealing Temperature versus Efficiency

The annealing temperature of each sample on the hot plate, particularly during the BiI_3 layer annealing procedure, could affect the sample's performance. We predicted that, due to heat loss via conduction, the surface of the sample would be substantially less than the surface of the hot plate. To assess this, we conducted a simple experiment in which we set a hot plate to 100℃, the desired annealing temperature of BiI_3, and then placed a thermocouple in contact with the surface of an FTO-glass sample atop the hot plate. We found that, although the surface of the hot plate was approximately 100℃, the surface of the sample achieved a maximum temperature of only 77℃ during the annealing procedure.

---

[106] Ibid.

[107] Liu, Guigao, et al. "Band-Structure-Controlled BiO(ClBr)(1â^˙x)/2Ix Solid Solutions for Visible-Light Photocatalysis." *Journal of Materials Chemistry A*, vol. 3, no. 15, 2015, pp. 8123–8132., doi:10.1039/c4ta07128j.

[108] Brandt, Riley E., et al. "Investigation of Bismuth Triiodide (BiI₃) for Photovoltaic Applications." *The Journal of Physical Chemistry Letters*, vol. 6, no. 21, 2015, pp. 4297–4302., doi:10.1021/acs.jpclett.5b02022.

This prompted us to begin annealing samples in a box furnace, where the temperature reading of the box furnace was accurate because the sample was exposed to the temperature displayed in a closed environment as opposed to that of the surface of the hot plate in an open system. Essentially, convection is the more prominent mode of heat transfer in the box furnace whereas conduction is more prominent on the hot plate, where the material dictates the degree of conduction. We examined the effect of annealing the BiI_3 samples at different box furnace temperatures, ranging from 40°C to 250°C. The efficiency graph for this temperature range is pictured below in Figure 31.
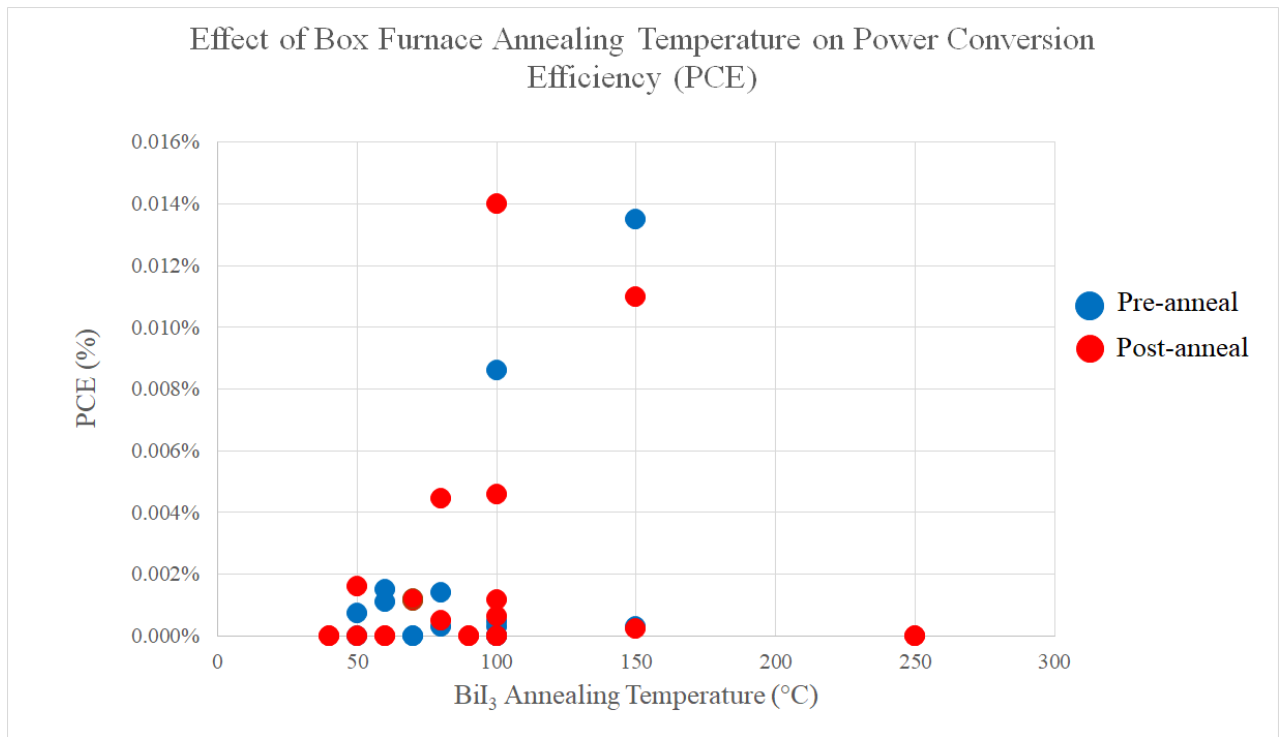
Figure 31. Power conversion efficiency for samples annealed in box furnace, demonstrating that 100°C is the likely optimal annealing temperature.

Based on the above graph, we see that samples performed poorly on the extreme ends of the temperature range (40°C and 250°C). For the case of 40°C, we believe that this can be attributed to insufficient annealing of the BiI_3 atop the surface of the TiO_2 layer, rendering its semiconductor properties ineffective. If the temperature was not high enough, then the material will not solidify and expand, which limits interlayer contact of the cell. As for annealing at 250°C, we believe that

69

the poor PCE is a product of overexposure to temperatures that cause sublimation of BiI_3. We also observed discoloration of the BiI_3 solution at higher temperatures, and in some cases little or no visible solution upon removing the sample from the box furnace. Because of the poor performance of most samples in the Box Furnace, this modification proved to be ineffective in increasing the performance of our cells. This is shown in the statistical analysis graph in Appendix F2. Narrowing in on the graph from the outer temperature ranges toward 100°C, we see that sample efficiencies began to improve. Figure 31 indicates that the optimal annealing temperature of BiI_3 was near 100°C, with the four best samples outperforming samples at all other temperatures. Figure 30 also indicates whether each data point was tested before or after the anneal once all of the samples were deposited (i.e. pre-anneal and post-anneal). As shown in this graph, generally the post-anneal data points outperform the pre-anneal data points. We believe this is due to the increase in interlayer contact that the additional anneal allows for between all of the samples layers. The increased interlayer contact would then increase the diffusion of charges through the cell which increases the J_{SC}, therefore proving our third hypothesis. Adding a post-anneal step was one of the most impactful modifications made in our research, and this can be shown in the statistical analysis graph in Appendix F.

4.1.2.2.2 Solvent Vapor Annealing

The SVA experimental results are illustrated below in Figure 32. Overall, we found that SVA annealing of BiI_3 in DMF improved the optoelectronic performance of the samples compared to the benchmark samples. We predicted that this was the result of increased grain sizes and therefore a decrease of grain boundaries within the BiI_3 layer. This enhanced carrier mobility and lifetime because grain boundaries are a recombination site for holes and electrons, so having fewer grain boundaries results in a longer carrier lifetime. As was described in Section 2.3.7.2 increasing carrier mobility and lifetime also increases the V_{OC}. Additionally, the graph indicates that SVA is better-suited for c-TiO_2 than c-m-TiO_2.
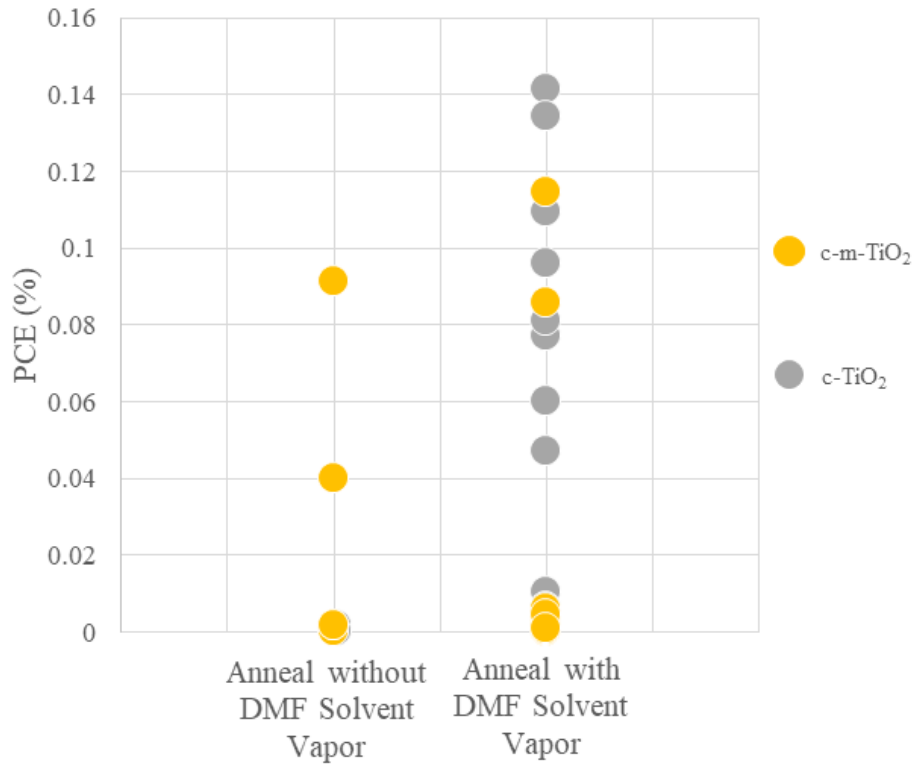
Figure 32. Power conversion efficiency for samples annealed with and without SVA, demonstrating that SVA is a better method for improving PCE.

To affirm this prediction, we observed the top view BiI_3 layer under a SEM with and without SVA. The photos are illustrated in Figure 33, with the benchmark BiI_3 synthesis on the left and the SVA sample on the right. In the SVA photo, the grain sizes are visibly larger and there is better interconnection of grains within the layer.
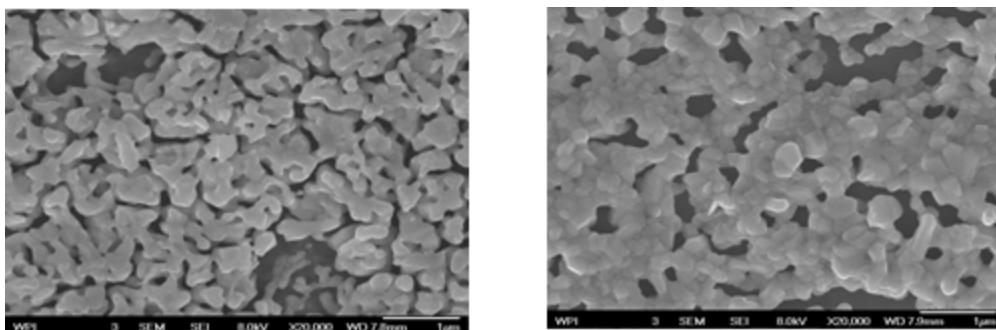
Figure 33. SEM photos of BiI$_3$ benchmark layer (left) and BiI$_3$ with SVA heat treatment (right), showing increased grain size in the SVA sample.

The quantitative and qualitative data found and observed regarding SVA reflects the effectiveness of the modification, proving our fourth hypothesis, which is that solvent vapor annealing of BiI$_3$ in DMF increases grain size and improves V$_{OC}$. This result was also found in previous literature.[109] For example, our best performing cell was made when BiI$_3$ was treated with SVA and these results are shown in the J-V curve below.

---

[109]Hamdeh, U. H., Nelson, R. D., Ryan, B. J., Bhattacharjee, U., Petrich, J. W., & Panthani, M. G. (2016). Solution-Processed BiI$_3$ Thin Films for Photovoltaic Applications: Improved Carrier Collection via Solvent Annealing. *Chemistry of Materials, 28*(18), 6567-6574. doi:10.1021/acs.chemmater.6b02347
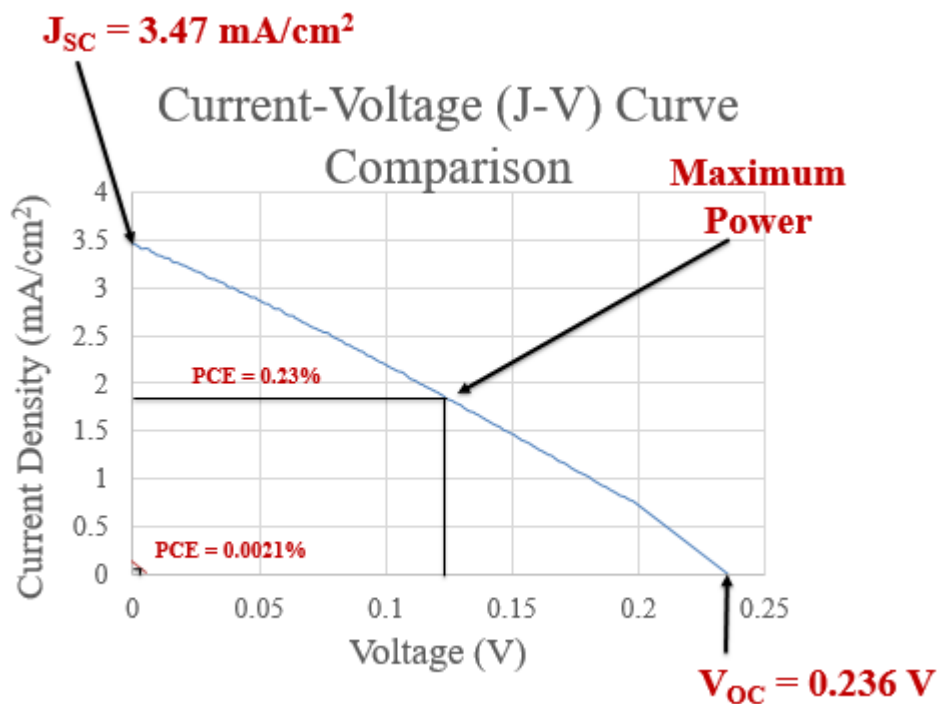
Figure 34. Current-voltage curve for our best performing sample with modifications compared to our best performing benchmark cell. This figure indicates the power conversion efficiency (PCE) of each of the samples and the J_{SC} and V_{OC} for the overall best performing cell with modifications.

Additionally, this sample was post-annealed, which was found to be optimal in Section 4.1.2.2.1, had a BiI$_3$ spin-coating speed of 1000 rpm, which was found to be optimal in Section 4.1.2.1, and a TiO$_2$ layer of just c-TiO$_2$. Although in Section 4.1.2.1, Figure 30 indicates that the c-m-TiO$_2$ was the optimal combination, yet Figure 32 indicates that SVA helped samples with just c-TiO$_2$ and did not help samples with c-m-TiO$_2$. We believe that the mesoporous layer of TiO$_2$ originally improved performance of the samples when annealed on the hotplate. This could be attributed to the thinner BiI$_3$ layer created when using mesoporous TiO$_2$ which provided less BiI$_3$ for the charges to travel through. Although, the interface between the mesoporous layer and the BiI$_3$ is also a site for potential charge recombination. The physical results that SVA caused in BiI$_3$ (i.e. increasing grain size) helped even more than the mesoporous layer did, which means that the combination of SVA and c-m-TiO$_2$ most likely had a greater probability of charge recombination at the TiO$_2$ and BiI$_3$ interface, rendering the mesoporous layer unnecessary when annealing with solvent vapor. Solvent vapor annealing was one of the most impactful modifications made in our

research, and this can be shown in the statistical analysis graph in Appendix F2. All of these optimal procedural modifications are recommended to be used to improve the performance of BiI_3 solar cells which completes our third objective, which stated to use experimental data to provide a basis on improving the material and optimizing its production process.

4.2 Theoretical Modeling of Bulk BiI₃ and Oxidized BiI₃

In order to determine whether or not oxidizing BiI_3 is beneficial to the solar cell's performance we modeled bulk BiI_3 and oxidized BiI_3 using the density functional theory, which addressed our fourth objective. Two methods were used to assess the effect of oxidation: density of states (DOS) and energy of reactions, as described in Section 3.3.3. The three types of oxidation that we explored were substituting one oxygen for two iodine atoms, one oxygen for one iodine atom, and adding in an interstitial oxygen atom. For each of these substitutions/additions, we tried three different initial geometries. This means that we added the oxygen in different layers and positions within the unit cell, to see how the different geometries affect the DOS and the energy of reaction. Each of these geometries correspond to its own calculation and are outlined in Table 5 below.

Table 5. Summary of the modeling calculations with substitution or addition of oxygen atoms for each calculation

Calculation #	Type of Substitution/Addition of Oxygen
1	One oxygen atom for two iodine atoms
2	One oxygen atom for two iodine atoms
3	One oxygen atom for two iodine atoms
4	One oxygen atom for one iodine atom
5	One oxygen atom for one iodine atom
6	One oxygen atom for one iodine atom
7	Interstitial oxygen atom
8	Interstitial oxygen atom
9	Interstitial oxygen atom
10	No substitution/addition; unoxidized BiI_3

The following sections show the results from the two methods of analysis, and how these results can help explain the experimental results that we obtained and described in Section 4.1 above.

4.2.1 Analyzing and Comparing Modeled BiI_3 and Oxidized BiI_3 Density of States Graphs

We first analyzed the density of states for the oxidized structures. Once each of the graphs were generated using the procedure in Section 3.3.3, they were compared to the density of states graph of unaltered BiI_3. Three calculations were run for each type of oxidation, and therefore a total of nine graphs were created for oxidized BiI_3. Additionally a graph was made for normal BiI_3 as a basis for comparison. These ten graphs along with images of their corresponding optimized geometries are shown in Figures 34-43 below. Appendix G contains additional geometric views of these unit cells.
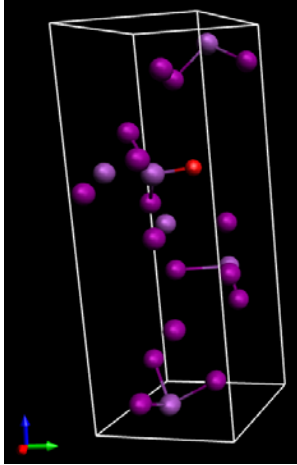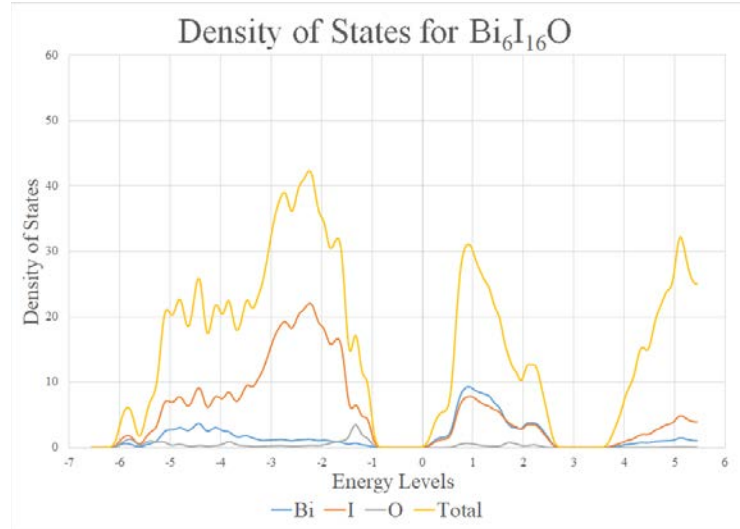
Figure 35. Results from Calculation 1 (O substitution of two I) including (a) Optimized Geometry and (b) DOS Graph for Bi₆I₁₆O. Light purple spheres represent bismuth atoms, dark purple spheres represent iodine atoms, and the red sphere represents the oxygen atom. The zero energy level has been set to the conduction band edge.
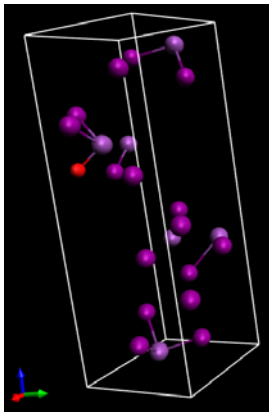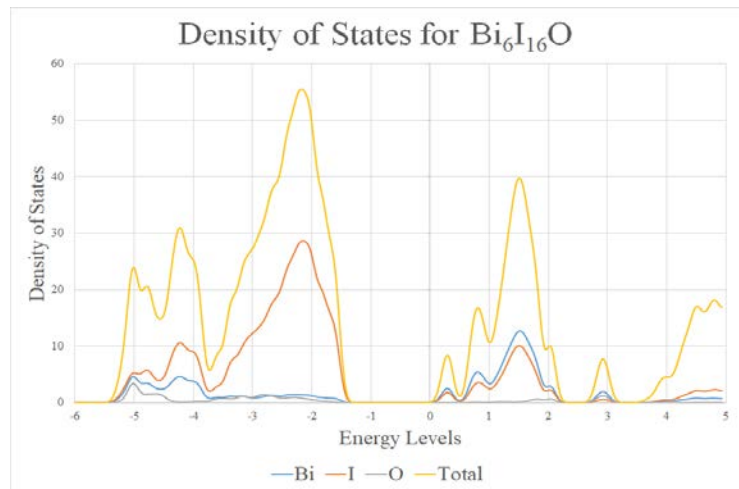
Figure 36. Results from Calculation 2 (O substitution of for two I) including (a) Optimized Geometry and (b) DOS Graph for Bi₆I₁₆O.
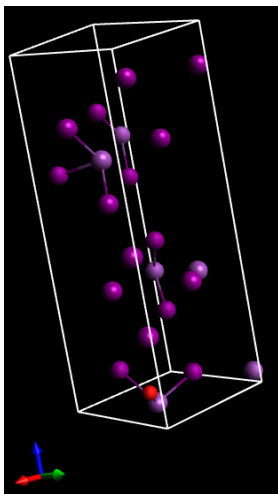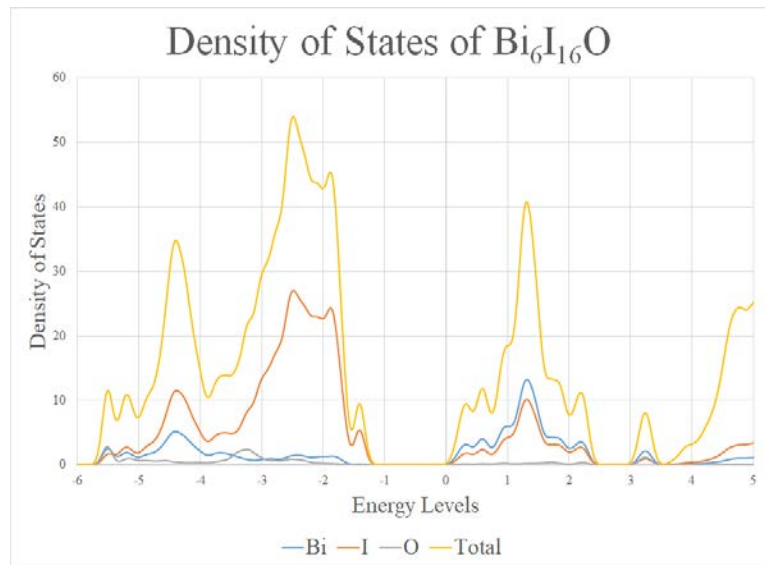
Figure 37. Results from Calculation 3 (O substitution of two I) including (a) Optimized Geometry and (b) DOS Graph for Bi₆I₁₆O.
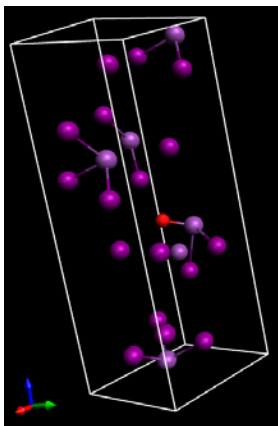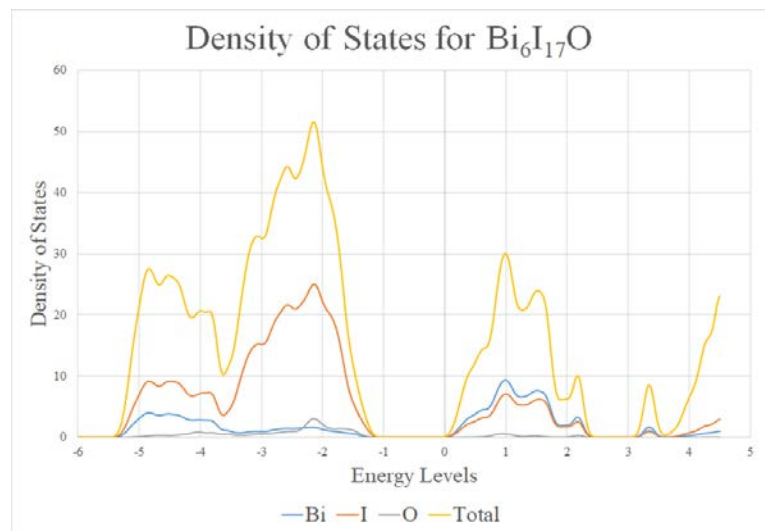
Figure 38. Results from Calculation 4 (O substitution of I) including (a) Optimized Geometry and (b) DOS Graph for Bi₆I₁₇O.
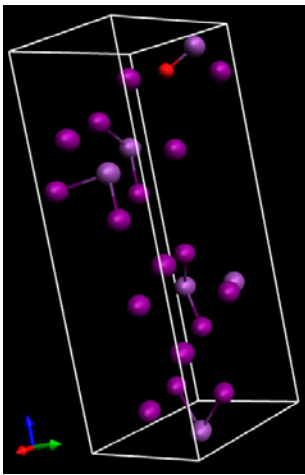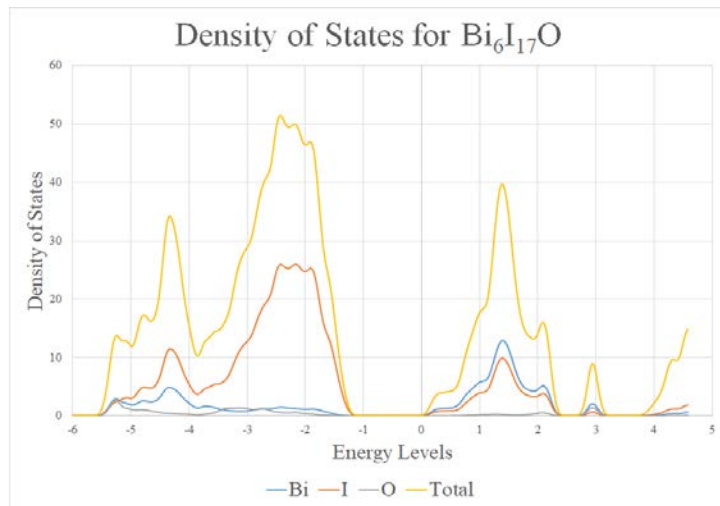
(a)   (b)

Figure 39. Results from Calculation 5 (O substitution of I) including (a) Optimized Geometry and (b) DOS Graph for $Bi_6I_{17}O$.
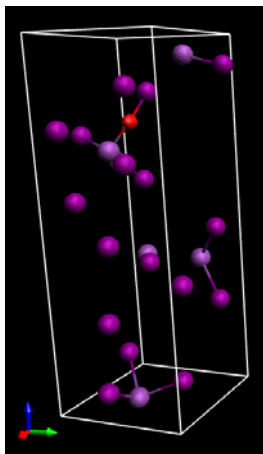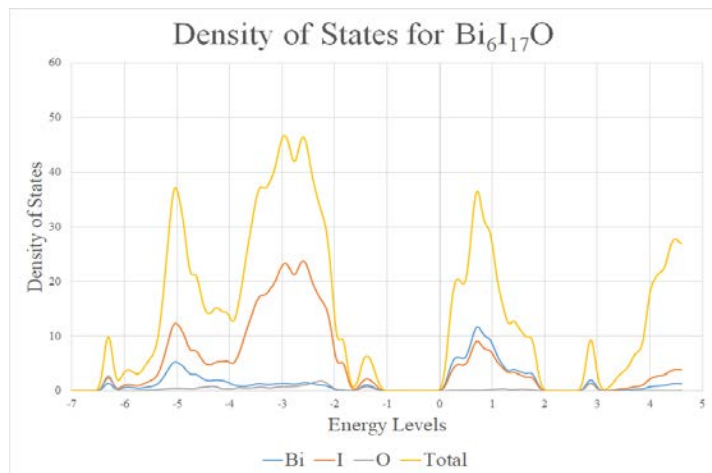
(a)   (b)

Figure 40. Results from Calculation 6 (O substitution of I) including (a) Optimized Geometry and (b) DOS Graph for $Bi_6I_{17}O$.
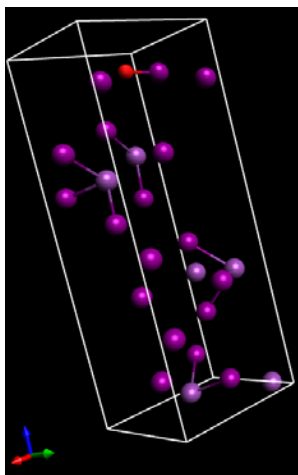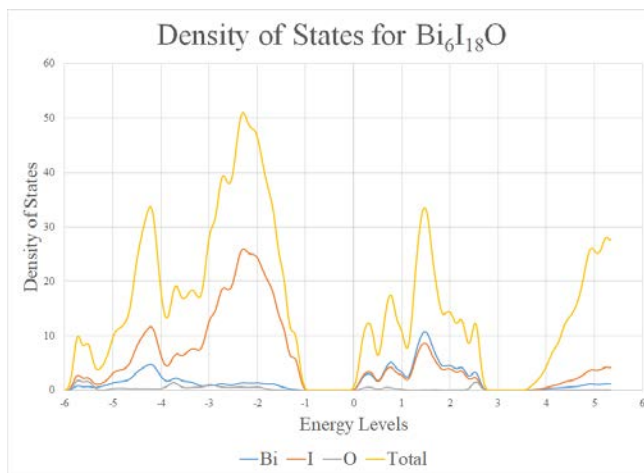
(a)   (b)

Figure 41. Results from Calculation 7 (O interstitial) including (a) Optimized Geometry and (b) DOS Graph for Bi₆I₁₈O.
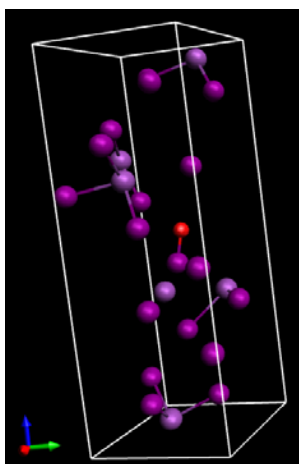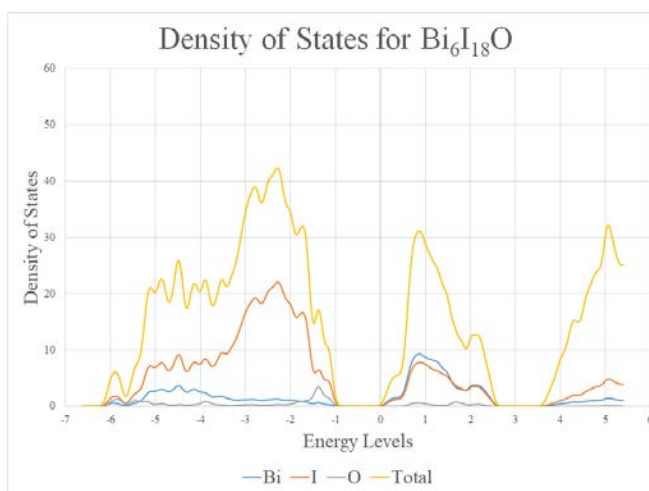
(a)   (b)

Figure 42. Results from Calculation 8 (O interstitial) including (a) Optimized Geometry and (b) DOS Graph for Bi₆I₁₈O.
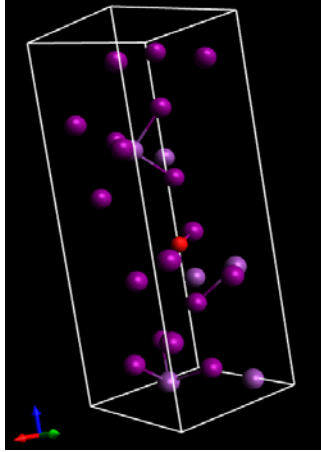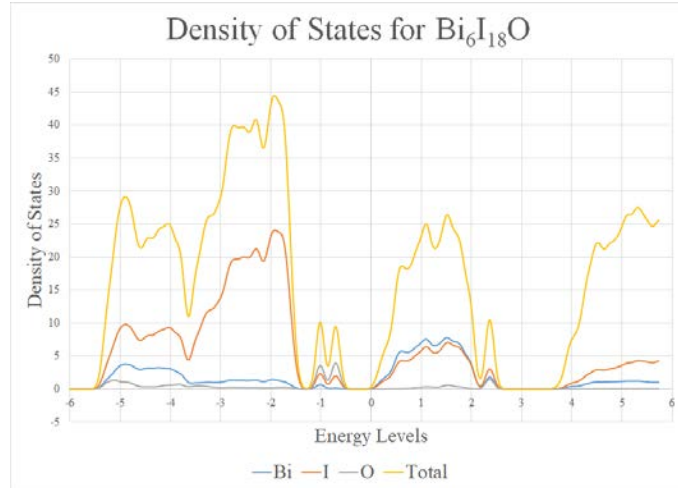
(a)   (b)

Figure 43. Results from Calculation 9 (O interstitial) including (a) Optimized Geometry and (b) DOS Graph for Bi$_6$I$_{18}$O.
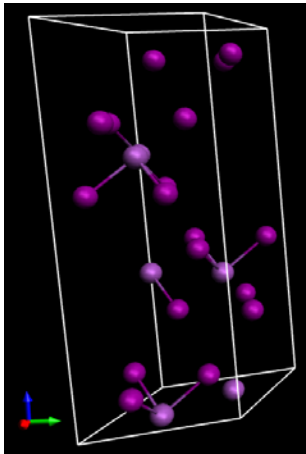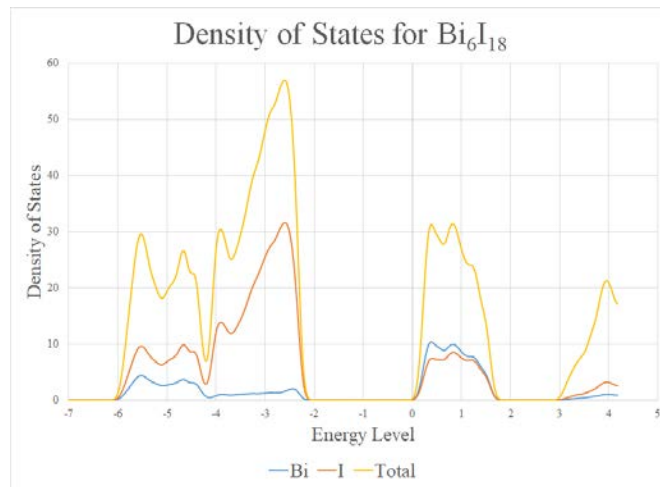
(a)   (b)

Figure 44. Results from Calculation 10 (unoxidized BiI$_3$) including (a) Optimized Geometry and (b) DOS Graph for Bi$_6$I$_{18}$.

The band gaps on all of the oxidized graphs (Figures 35-43) are smaller than that of the Bi$_6$I$_{18}$ (Figure 44), although this may not have much of an effect in the real sample since the layer

of oxidized BiI_3 was so thin in the synthesized cell. Additionally, BiI_3 is n-type and BiOI, an oxidized form of BiI_3, was determined to be p-type by previous research.[110] Oxidized BiI_3 is also likely p-type, so a layer of oxidized BiI_3 on the surface of the BiI_3 would create a stronger electric field and more efficient extraction of charges at the interface, improving V_{OC} and the overall performance of the cell, proving our first hypothesis theoretically. There are gap states on the graphs from Figures 36, 40 and 43. If these gap states were in the middle of the band gap, then recombination of holes and electrons would be much more likely to occur, which would negatively impact the performance of the solar cell. Since they are just at the end of the conduction band for the graph in Figure 36 and valence band for the graphs in Figures 40 and 43, all they really do is make the band gap smaller, which as was just mentioned is beneficial. This analysis addressed our fifth objective, which was to use theoretical data to explain important features of experimental data.

4.2.2 Analyzing and Comparing Types of BiI₃ Oxidation through Energy of Reaction Calculations

We calculated the energy of reaction for each oxidation type, as discussed in 3.3.3 Similar to the DOS calculations, an energy of reaction was calculated for each of the different geometries for each of the different types of oxidation. The resulting energy of reaction from each of these computations can be found in Table 6 below. In order to understand the differences in energy of reaction from each calculation, the coordination number and bond lengths of each of the oxygen atom's bonds were also noted in Table 6 below. The coordination number of oxygen represents how many atoms it is bonded to, and relates to the stability of the structure. The coordination number of the oxygen atom was found by counting how many atoms it was bonded to in the modeling software VESTA. The bond lengths shown below were measured for each structure in VESTA.[111] The lower the bond length typically the stronger the bonds are, but all bonds under 2.5 Å are considered strong bonds.[112] Each of the energies pertain to geometries from calculations 1-9 above.

[110]Hamdeh, U. H., Nelson, R. D., Ryan, B. J., Bhattacharjee, U., Petrich, J. W., & Panthani, M. G. (2016). Solution-Processed BiI3Thin Films for Photovoltaic Applications: Improved Carrier Collection via Solvent Annealing. *Chemistry of Materials, 28*(18), 6567-6574. doi:10.1021/acs.chemmater.6b02347

[111] Momma, Koichi, "Vesta", (JP-Minerals, 2004 – 2018).

[112] Martz, E. and Ditmore, D., "PE's Reference Manual", (UMass, April 2001).

Table 6. Summary of energy of reactions, coordination numbers and bond lengths of all the optimized geometries of oxidized BiI_3. N/A indicates that the oxygen was bonded to only one atom.

Calculation #	Calculation Type	Molecular Formula	Energy of Reaction (eV)	Oxygen Coordination #	Bond Length 1 (Å)	Bond Length 2 (Å)
1	O substituting two I	$Bi_6I_{16}O$	1.52	2	2.07728 (O-Bi)	2.10552 (O-Bi)
2	O substituting two I	$Bi_6I_{16}O$	1.08	1	2.07314 (O-Bi)	N/A
3	O substituting two I	$Bi_6I_{16}O$	1.81	2	2.09888 (O-Bi)	2.12386 (O-Bi)
4	O substituting one I	$Bi_6I_{17}O$	1.79	1	1.96521 (O-Bi)	N/A
5	O substituting one	$Bi_6I_{17}O$	1.91	2	2.08664 (O-Bi)	2.09334 (O-Bi)
6	O substituting one	$Bi_6I_{17}O$	3.27	2	2.06976 (O-Bi)	2.16394 (O-I)
7	O interstitial	$Bi_6I_{18}O$	2.16	2	1.97205 (O-I)	2.14553 (O-Bi)
8	O interstitial	$Bi_6I_{18}O$	0.06	1	1.86293 (O-I)	N/A
9	O interstitial	$Bi_6I_{18}O$	2.24	1	1.88812 (O-I)	N/A

As seen in Table 6, the type of oxidation that had the lowest energy of reaction was calculation 8, which was an interstitial oxidation resulting in $Bi_6I_{18}O$. This low energy of reaction of 0.06 eV is substantially less than the rest of the other interstitial reaction energies as well as all of the other substitutions. This means out of all of the geometries we modeled, this is the one most likely to form experimentally. In order to explain this, we first found coordination number and bond lengths to determine the stability of the structure and therefore make conclusions on why

some had lower reaction energies than others. Because oxygen is a group 16 element, it is most stable when bonded to two atoms. With this reasoning, geometries with a coordination number of 2 should have the lower energy of reactions and be more likely to form. However, with calculation 8, this is not the case. To understand this better, a closer look was taken at calculation h and i, since h had a coordination number of 2 but had a much more endothermic reaction energy compared to 8. The interstitial oxygen atom in calculation h actually induced structural distortions around itself. For example, one of the Bi-I bonds near the oxygen increased by ~0.5 Å in the geometry for calculation 7 when compared to the defect-free Bi_6I_{18} unit cell geometry. Therefore, the distortion that the oxygen atom causes in calculation h outweighs the stability that the coordination number of 2 offers this structure. This distortion does not occur in the geometry for calculation 8, and that in combination with the low bond length makes geometry 8 more stable. Overall, the resulting reaction energies show that BiI_3 is easily oxidized, particularly when one oxygen atom was substituted for two iodine atoms, and when oxygen was placed interstitially in the BiI_3 structure.

5.0 Conclusion and Recommendations

The collective experimental and theoretical results obtained from this research project show evidence that suggests the validity of the four main hypotheses. The first hypothesis regarding additional oxidation of the solar cell at the stage of the BiI_3 layer had some supporting evidence of improved V_{OC}, J_{SC}, and PCE. Three different methods were executed to introduce oxygen to the semiconductor layer as a means to investigate their effects on the cells' optoelectronic properties. These methods included annealing the samples in air via solvent vapor annealing, a hot plate, and a box furnace at varied temperatures and times. The evidence of poor V_{OC}, J_{SC}, and PCE from samples annealed at lower temperatures suggest inadequate oxidization. In contrast, samples annealed at too high of temperatures cause sublimation of BiI_3 also yielding poor $V_{OC,}$ J_{SC}, and PCE. Therefore, these results lead us to believe that the temperature of $100^{\circ}C$ yielded the optimal amount of oxidation of the BiI_3 layer. Experiments were not conducted with an inert gas, therefore, we were not able to prove that oxidation alone is the reason for the improvement. In order to understand this hypothesis more, we conducted theoretical modeling.

The DOS graphs obtained through VASP modeling demonstrated that oxidized BiI_3 has a smaller band gap than the standard BiI_3. Although, the oxidized layer of BiI_3 is very thin so the main argument for oxidized BiI_3 being beneficial is that this layer that gets oxidized is p-type and the unoxidized BiI_3 is n-type. This difference in charge concentration causes a stronger electric field which in turn increases charge separation. This provides evidence that suggests validity to our first hypothesis, which was that oxidized BiI_3 improves optoelectronic properties. Additionally, gap states attached to the conduction or valence band are ideal because if they were in the middle of the gaps in the DOS graphs, recombination within the band gap would be more likely.

The second hypothesis proposing the effectiveness of a compact-mesoporous TiO_2 layer also provided results that showed increased J_{SC} and PCE. The compact-mesoporous TiO_2 layer consistently resulted in producing the most efficient BiI_3 thin-film solar cells until the modification of solvent vapor annealing was applied. The success of compact-mesoporous TiO_2 can be attributed to the increased surface area contact between the TiO_2 and BiI_3 layers. This facilitated better carrier transport for the cells, further improving optoelectronic results. Interestingly, samples

with just compact-TiO$_2$ performed better than samples with a compact-mesoporous TiO$_2$ layer only when the BiI$_3$ was annealed via solvent vapor annealing.

The third hypothesis regarding the additional annealing of the solar cell after all layers have been deposited also improved the cells' J$_{SC}$, and PCE after analyzing our experimental results. The improved optoelectronic performance can be attributed to improved interlayer contact within the cell. Increased annealing has the potential to expand the material and eliminate any gaps within the layers, therefore, improving carrier transport through the cell.

Lastly, the fourth hypothesis proposing the effectiveness of solvent vapor annealing in DMF proved to be impactful on the optoelectronic properties of the cells. SVA was selective in the cells it improved the performance of. SVA suggests that it is helpful with cells composed of solely compact-TiO$_2$, whereas, it was detrimental for cells with a compact and a mesoporous TiO$_2$ layer. The mesoporous layer of TiO$_2$, as mentioned above, improved the performance of the cells, and it is believed this is because it created a thinner BiI$_3$ layer for the charges to travel through the cell with a lesser chance of recombining. Although, there is greater potential for charge recombination at the interface of the TiO$_2$ layer and the BiI$_3$ layer. Since SVA increased grain size of the BiI$_3$ layer, it helped facilitate more efficient carrier transport, which aided in the performance of the cell more than the introduced mesoporous layer. From this, we concluded that the mesoporous layer is unnecessary if SVA is applied.

Separate from the four main hypotheses, it was also found that a spin-coating speed of 1000 rpm optimized the performance of the BiI$_3$ solar cell. Spin-coating speeds of 500 rpm, and 1500 rpm were either too slow or too fast to yield the best results. This implies that 500 rpm deposited a TiO$_2$ layer too thick, and a speed of 1500 rpm deposited a layer too thin to yield optimal optoelectronic results.

Post-annealing a BiI$_3$ thin-film solar cell with a compact TiO$_2$ layer after gold evaporation, and a BiI$_3$ layer deposited at 1000 rpm and annealed through SVA at 100°C yielded the best results with a short circuit density of 3.46 mA/cm^2, an open-circuit voltage of 0.247 V, and a PCE of 0.23%.

Given these conclusions, it is recommended to continue to research BiI$_3$ as a semiconductor material for thin-film solar cells. More specifically, the effect of SVA on cell performance should be further investigated both for optimization purposes and to understand the relationship between both a c-TiO$_2$ and cm-TiO$_2$ layer. Coinciding with further investigation of SVA, it is recommended

to synthesize more cells annealed in an inert gas for more distinct comparison. Different theoretical principles have proved to be effective, therefore, with sufficient research, optimization of the impactful modifications found in this research project could be valuable.

It is also recommended to utilize X-ray diffraction (XRD) to characterize the cell as a means to explain optoelectronic performance. This technology could pinpoint what else in a BiI_3 thin-film solar cell should be optimized and/or which layer in the cell needs to be focused on.

If these modifications are perfected and the optoelectronic properties are optimized enough to commercialize the BiI_3 thin-film solar cell, the demand for solar cells may increase due to the existence of a more economical alternative to the current, standard silicon solar cell.

5.1 Transition to Professional Writing Chapter

Along with the conclusions and recommendations drawn from the chemical engineering MQP, a more broadly-focused professional writing MQP component begins in Section 6.0. This section aims to fulfill the requirements for a professional writing double major. Written by teammate Andrew Callahan, the scope of this project is more abstract and is intended to focus on photovoltaics, in the coming decades, when second generation solar materials become more efficient and marketable.

6.0 A Technology Acceptance Model for Solar Adoption

6.1 Introduction

This study develops and proposes a technology acceptance model (TAM) to identify how users come to accept and use solar technologies in the United States. With the solar industry growing and installation prices decreasing, photovoltaic technologies have potential to contend with legacy sources such as fossil fuels. Achieving large scale effective implementation requires a systematic strategy suitable to American cultural and political contexts.

6.1.1 The Status of Solar Energy in the United States

The Office of Energy Efficiency and Renewable Energy affirms that solar power in the United States is more affordable, accessible, and widespread than ever before.[113] Their studies indicate that installations in the U.S. have expanded seventeen-fold since 2008, with power usage increasing from 1.2 gigawatts (GW) to approximately 30 GW today. This, combined with a decrease in the cost of solar PV panels by 60% since 2010, renders the future of the industry promising and bright. Research also suggests that Americans wish to expand renewable energy production, recognizing a consistent increase in energy consumption each year.[114]

Although much progress has been made toward advancing solar energy in the United States, there is still work be done before solar becomes a household energy source. The most evident problem is with pricing - solar is not as affordable as conventional energy sources.[115] As mentioned previously, the manufacturing cost of perfected silicon wafers is much too high to be sold at an affordable American price. Many efforts towards lowering the cost of PV materials take the form of research and development studies, such as that of the primary focus of this project (BiI_3). However, the best recorded efficiencies on second generation solar cells have been too low for them to be marketed at the moment. Even so, once the desired efficiencies are achieved, there lies more barriers with the implementation of these technologies.

---

[113] "Solar Energy in the United States", (Office of Energy Efficiency and Renewable Energy, n.d.).
[114] Funk, C., Kennedy, B., "Public opinion of renewables and other energy sources", (Pew Research Center, October 2016).
[115] "Solar Energy in the United States", (Office of Energy Efficiency and Renewable Energy, n.d.).

6.1.2 The Challenge of Technology Implementation

The most difficult component of technology design is the implementation of it; integrating new and potentially innovative technologies in the context of a society is challenging and unpredictable. We see how things can go wrong (Section 6.3.2) or incredibly right (Section 6.3.2) when new technologies are introduced. Thus, technology implementation is seldom a simple process – it most often requires several working parts to come together in a favorable way. There is no clear recipe for success in this genre because human activity is dynamic and continually shaping the way people interpret the value of different technologies. In an age where people's eyes are glued to their phones, information spreads very quickly and discourse is fast and continuous. Contemporary technology simplifies human interaction while simultaneously creating new avenues for communication, thus complicating it all the same.

There are many external variables that create the need for a given technology and also shape the way people perceive it. With the media, for instance, an applauding review from a notable figure may influence the perceived value of a new device favorably. However, a negative rumor about the same device may dissuade public adoption. It becomes increasingly interesting when the rate at which information spreads is factored in as well. This is just one external variable that people fundamentally cannot control. Inventors in the past, such as Thomas Edison, would embrace the media to create an image and persona for himself, which effectively added value to his inventions.

From Bazerman's *The Languages of Edison's Light*, we see how Edison was able to manufacture an opening in the organizational system surrounding gas lighting to introduce electric lighting into society.[116] Along with the persona that Edison created for himself, he was also about to disrupt the network of lighting technologies, emphasizing the needs of families, to implement a new and innovative opportunity. Any technology implementation requires careful predictive planning. Some researchers have created models for the purpose of understanding how people come to accept technologies–these models are referred to as technology acceptance models.

---

[116] Bazerman, Charles, *The Languages of Edison's Light*, (MIT Press, 2002).

6.1.3 The Technology Acceptance Model

The technology acceptance model (TAM) assesses and examines end-user acceptance of a new technology based on the end-users perceived usefulness and perceived ease-of-use of the technology introduced.[117] TAM was developed based on the Theory of Reasoned Action (TRA), which explains that a person's actual behavior could be predicted or determined based on his or her prior intentions - essentially, behavioral intention affects actual behavior. Additionally, it emphasizes that an individual's intention toward a particular behavior is affected by his or her attitude and subjective norms. TRA has been used to study a number of different subjects, including health behavior and consumer attitudes towards renewable energy.[118] Some studies for instance, used this theory to discern that positive views of renewable energy yields a stronger likelihood of spending the money needed to obtain this energy source for consumer homes.

The first technology acceptance model (TAM 1) was developed by Fred Davis in 1989 (Figure 45). This model served as a foundation or outline to later models, and attempts to identify meaningful factors which influence user technology adoption.
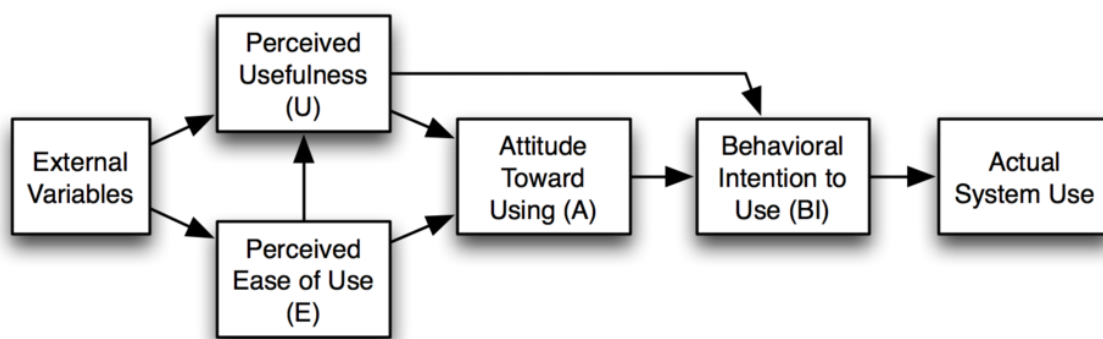
Figure 45. Fred Davis' 1989 technology acceptance model (TAM 1)[119]

TAM 1 begins with external variables, such as the media, that dictate whether or not a new technology achieves public interest. Then, these external variables are followed with the four major TAM components:

---

[117] "Technology Acceptance Model (Perceived Usefulness and Perceived Ease of Use)", (Consumer Health Informatics Research Resource, n.d.).

[118] "Theory of Reasoned Action", (Communication Institute for Online Scholarship, n.d.).

[119] Davis, F., *Perceived Usefulness, Perceived Ease of Use, and User Acceptance of Information Technology*, (Management Information Systems Research Center, September 1989) vol. 13, no. 3, pp. 319-340.

(1) **Perceived Usefulness (U)** depicts the degree to which an individual believes that using a particular technology enhances job performance.

(2) **Perceived Ease of Use (E)** depicts the degree to which an individual believes that a particular technology is easy to operate.

(3) **Attitude Toward Using (A)** depicts an individual's attitude toward a particular technology, influenced by U and E.

(4) **Behavioral Intention to Use (BI)** depicts the degree to which an individual intends to use a particular technology, influenced by U, E, and A.

If each of the above components are variables are regarded as favorable or positive, then a user is expected to make use of a technology.

The problem with the original TAM 1 is that, although it focuses on user perception, it fails to define the external variables which heavily influence technology adoption. The model overlooks the connections between people or users, both the interpersonal and social relations in which they act, and the broader social structures which strongly influence social practice.[120] Thus, some question its practical predictive effectiveness. Especially with modern information dissemination, these external variables are crucial in understanding the resultant user attitude toward a technology. For instance, a technology may seem worthwhile on the whole, but if its perceived cost does not align favorably with its perceived benefits, then a user is much less likely to adopt.

In 2000, TAM 2 was created to better discern external variables, previously undefined by TAM 1, which strongly influence user's perception of a new technology, both in terms of usefulness and ease of use (Figure 46).

---

[120] Terry, Deborah J. et. al., *The Theory of Reasoned Action: Its Application to Aids-preventive Behavior*, (January 1993).
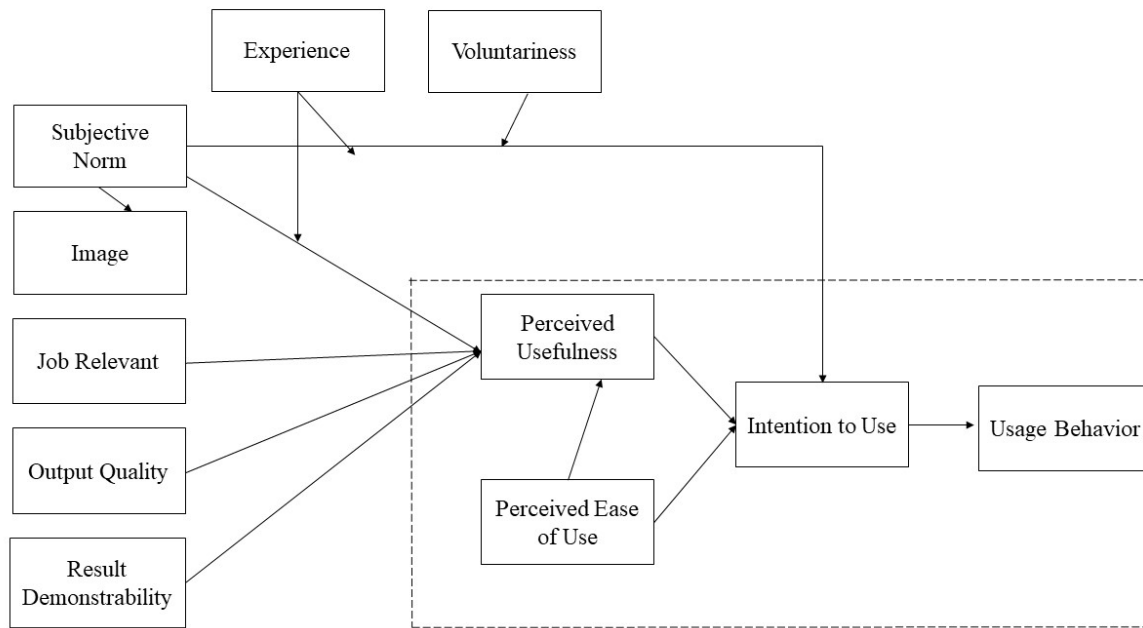
Figure 46. Venkatesh and Davis' 2000 technology acceptance model (TAM 2).[121]

Based on the model, we see that it considers external variables that ultimately influence technology adoption such as output quality, image, and result demonstrability. The inclusion of these variables yields a more meaningful model because the external factors of the model are the most dynamic and are constantly changing based on what people value. In particular, subjective norm as an external factor represents what a group perceives as normal or accepted. This can be a very challenging barrier to overcome especially when new and foreign technologies are introduced to markets. Overall, the inclusion of these external variables shares more of the larger picture of technology implementation. The complexity with these, as mentioned, is that they can vary by culture.

---

[121] Adapted from Sullivan, M., "Extended Technology Acceptance Model (TAM 2)", (Real KM, August 2016).

6.2 Literature Review of Relevant Works

The following section incorporates a literature review examining works relevant to technology adoption. From examining how people interpret and respond to messages to Edison's implementation of the electric light bulb, four different themes were derived which are applicable to technology implementation and adoption. The four themes are: human behavior, message, dynamism, and kairos. Each of these themes were common, yet interrelated concepts drawn from the related texts and are divided into respective subsections. Additionally, the works examined in this section are primarily of the 2000s with the aim to remain contemporary. Each review is broken into a descriptive portion and is then followed by a translative portion, which explains the piece's applicability to the larger research project—the technological implementation of solar energy.

6.2.1 Human Behavior

Intrinsic human behavior and inclinations influence the way we respond to messages. In order to achieve effective persuasion, it is essential to consider the values of those whom you are selling an idea to. This section includes a literature review of chapters and journal articles relevant to the human behavior theme.

Thomas Frank's "What's the Matter with America?" [122]

Descriptive:

The author of this piece, Thomas Frank, found himself perplexed as to why an American county of "struggling ranchers and dying farm towns" was so strongly in favor of the Republican presidential candidate, George W. Bush. This county, the poorest of all in the United States, voted against its own economic interests for a conservative candidate. The author argues that conservatives won the hearts of many Americans by playing a "trick" that "never ages," by creating an "illusion" that "never wears off" (7). Called The Great Backlash, this phenomena is a style of conservatism that mobilizes voters with "explosive political issues" and causes "public outrage" (5). It emphasizes individual values that define the human character beyond one's socioeconomic status or political position. Items such as abortion rights and gay marriage are brought to the forefront of conservative campaigns to sway voters into calling forth their traditional values. These

---

[122] Frank, Thomas, *What's the Matter with Kansas? How Conservatives Won the Heart of America*, (2004).

values are ultimately more significant when deciding upon one's beliefs toward a political candidate, or any belief, for that matter.

In effect, the Republicans always win, Frank argues. They mask their political campaigns with these items that draw upon moral values, and once elected, they revert back to their typical regimes, such as bringing about tax breaks for the wealthy, among others. Liberals, in comparison, are always one step behind – they have good intentions and are clear and genuine about their campaign objectives, but fall for the same trick each election season. They are left defending themselves and their own beliefs and fail to achieve the same sort of rhetoric that conservatives have mastered.

Translative:

The idea behind this Great Backlash is applicable to new and rising technologies such as solar cells. Scientists and engineers have demonstrated the growth and capability of solar power and photovoltaics on a global scale. They have informed the public with scientific data and cold facts, increased public awareness of climate change and global warming, and have engineered increasingly inexpensive designs on an annual basis. The public, however, needs more to be swayed. What professionals have failed to draw upon are the people's values and mindsets regarding energy use. On the whole, first world markets perceive the usefulness of energy based on the cost of it and how easy it is to harness. If people are unable to get their energy on demand and at a low cost, then they seldom choose to adopt solar derived technologies. While many are aware of climate change, few are passionate enough about it to move away from fossil fuel energy sources. In order to effectively persuade people into going solar, either a technology must be engineered that connects and meets the demands of human values and needs or such values must be redefined. However, the latter of the two is more difficult to achieve.

Kahan, Smith, and Braman's "Cultural Cognition of Scientific Consensus" [123]

Descriptive:

The three authors who composed this piece call to attention a common phenomenon within public discourse – despite scientific consensus, the public is often in disagreement about topics such as climate change and the safety of nuclear power, among others. The authors affirm that this sense of disagreement is not a result of people being unexposed or indifferent to scientific consensus, but rather that people disagree with what scientists tell them. The reasoning behind this, and the theme of the journal article, is cultural cognition; this concept is defined as the "tendency of individuals to fit their perceptions of risk and related factual beliefs to their stored moral evaluations of putatively dangerous activities" (148). Thus, the corresponding thesis of cultural cognition to explain this behavior is that humans are psychologically drawn to believe that behavior they find honorable is socially beneficial to them and the reverse of that socially detrimental to them. In essence, people will more readily recall expert opinions that are consistent with their cultural predispositions and likewise will often reject information that does not align with their worldviews (149). They will use phrases such as "This is what the science really shows…" even if their viewpoint is in line with an overwhelming minority of experts.

The authors conduct a study on two different parties they refer to as "egalitarian communitarians" and "hierarchical individualists." Communitarians tend to develop opinions and make decisions based on the group as a whole. For instance, if there is a known intersection that causes a substantial number of car accidents, the communitarian would more likely argue the need for added or improved road signs or signals. As for individualists, they would argue for the need for more comprehensive driver education to improve motor skills because they are more focused on individual decision-making and responsibility. Additionally, in terms of egalitarians, they emphasize equal rights and opportunities, whereas those deemed as "hierarchical" believe that the top performers deserve the most in all aspects of life. By piecing these concepts together, we see that the hierarchical individualist is generally more conservative in his or beliefs, whereas the egalitarian communitarian is generally more liberal and equality-oriented in his or her beliefs. In this piece, the highlight of what the researchers discovered is that egalitarian communitarians are much more inclined to deem an expert as trustworthy and knowledgeable when the expert is in support of a "high risk position" (162) than are hierarchical individualists. Inversely, if an opinion

---

[123] Kahan, D., et. al., *Cultural Cognition of Scientific* Consensus, (Journal of Risk Research, 2010).

is depicted as "low risk," then hierarchical individualists tend to trust expert opinions more than egalitarian communitarians.

Translative:

This piece, similar to the previous, focuses on the ideas of human behavior and human inclinations; the difference is that these behaviors are explained in association with scientific consensus. The researchers assert that you can, with 80-90% confidence, predict people's stances on different issues, such as climate change and nuclear power, based on their predispositions (such as, if they are labeled as an egalitarian communitarian or hierarchical individualist). The reality of it, according to Kahan, Smith, and Braman, is that culturally-speaking, the science matters not. People will rely on their own predispositions when forming opinions, and will hold onto those opinions so long as there is an individual they deem as professional and qualified, who has the same opinion. With things like global warming, most scientists affirm that climate change is real and is happening every day, yet the minority of scientists who consider it bogus is enough for the predisposed people to reject it completely. As for those who trust the scientific consensus, the vast majority are unwilling to make inconvenient changes to their daily lives to help protect the environment. Instead, they excuse their harmful practices by pointing at the oil and gas industry and other larger contributors to the problem. Cultural cognition would predict that, until the egalitarian individualist and the hierarchical individualist have the same stance on climate change, solar energy will stand little chance in the energy market. That is, unless it becomes as easy and inexpensive to harness as fossil fuel energy.

Clay Spinuzzi's "Who Killed Rex? Tracing a Message through Three Kinds of Networks" [124]

Descriptive:

In "Who Killed Rex? Tracing a Message through Three Kinds of Networks," Spinuzzi shares an anecdote of a family in Texas who calls a telephone company, called Telecorp, to fix an issue with the family's telephone service. Upon the serviceman's arrival, he opens a gate that the family's dog, Rex, bolts out of and then Rex is hit by a car several blocks down the road. From the naïve eye, it may appear that it is the Telecorp employee's fault because he opened the gate which resulted in the death of poor Rex. However, Spinuzzi analyzes three entangled networks which make up Telecorp to assign blame for the death of Rex: telecommunications, the actor-network, and the activity network. The reality is that the homeowners informed Telecorp that they owned a high energy dog, but this piece of information was not shared with the serviceman. Another question posed by the author – can we blame an individual for the failure of a company's self-regulative practices?

As mentioned, the three networks involved in the story of Rex are telecommunications, the actor-network, and the activity network. By analyzing the telecommunications network, we find that Telecorp is actually the middleman between the homeowner and a service provider known as BigTel. By isolating the actor-network, we learn that actants – both human and nonhuman – must be re-enrolled or added into play constantly so that Telecorp can continue to appear as a unitary and stable company. Finally, by focusing on the activity network, we understand that there is a much larger network to consider in this seemingly simple scenario – BigTel, Texas and United States legislatures, contractors, costumers, and the like. As Spinuzzi brings these isolated networks together, it becomes evident how non-unified the "telephone company" is. The investigation persists and eventually Spinuzzi assigns blame to the activity group at the narrowest part of the network – the NCC employee who first picked up the call to hear about the homeowners' complaint.

Translative:

This study highlights certain aspects of human behavior – in particular, the inclination to assign blame to a given party despite ignorance to the magnitude of a problem. Similarly, there are many pieces which, layered together, amount to the presence of the solar industry. These pieces,

---

[124] Spinuzzi, C., "Who Killed Rex? Tracing a Message through Three Kinds of Networks" (2007).

in the form of groups or parties, influence the way the public perceives the need for renewable energy. For instance, people may feel strongly about climate change – some believe it exists while others view it as a ploy to persuade people into being more conscious of their environmental pollution. Who do we trust and who is to blame for the division of opinion? It is not so simple as to blame one individual for this problem.

6.2.2. Message

Finding the activity or central purpose of a form is crucial. To sell an idea effectively, the associated message needs to be clear and contextualized. This section includes a literature review of a book and chapter relevant to the message theme.

Chip and Dan Heath's *Made to Stick* [125]

Descriptive:

In Chip and Dan Heath's *Made to Stick*, they provide the reader with strategies to help make their ideas "stick" more effectively. By "stick," they mean to generate a lasting and memorable impact on an audience that truly resonates with them. If we recall slogans from commercials that we find memorable or brilliant, they all likely have some common attributes. The Heath brothers explain that sticky ideas tend to have six common traits: simplicity, unexpectedness, concreteness, credibility, emotions, and stories (SUCCESs). They argue that the most successful ideas are actually more ordinary than the least successful ones, which fail in their own unique ways. Throughout the piece, the authors share relevant anecdotes which they use to help make their own ideas stick.

The main problem expressed in the book is the "Curse of Knowledge," where an individual sharing a piece of information (who possesses the knowledge) to an audience often has difficulty enabling their audience to understand it. This person already understands the relevance of the topic as well as the minor details, and thus they will likely neglect the core of what they are trying to convey because they do not realize that it is not exactly obvious. The authors use a "tappers and listeners" anecdote to describe this phenomena; people would be assigned a song to tap their feet to for another individual to decipher. When tapping, the tapper can easily hear the song in their

---

[125] Heath, C. and Heath, D., *Made to Stick: Why Some Ideas Survive and Others Die*, (Random House, 2007).

heads and it seems obvious to them. However, for the listener, all they can hear is a monotone spacing of foot taps that is very unclear and difficult to connect with.

Translative:

The techniques that humans use to sell their ideas, however elaborate, are often ineffective and overthought. We sometimes get caught up in the *what* and not the *why*. Some ideas we have may be interesting but few sensational, truthful but seldom mind-blowing, or important but not life-or-death (8). When advocating for solar energy, the arguments made for it are bland and ordinary; some arguments are surprising, but few astonish people enough to make a difference. Solar energy is not a hot topic – which leads to the question – how may educators make it more of a hot topic? The Heath brothers would argue that educators could scrutinize their rhetoric and determine if it is simple, unexpected, concrete, credible (likely), emotional, and anecdotal. There is likely work to be done.

Berkenkotter and Huckin's "You Are What You Cite: Novelty and Intertextuality in a Biologist's Experimental Article" [126]

Descriptive:

In this chapter of *Genre Knowledge in Disciplinary Communication*, the authors emphasize the importance of contextualizing research into a larger realm of thought. They argue that contextualizing material helps to enhance its relevance to a reader or audience. As evidence, they use an anecdote of a biologist, Davis, submitting drafts of her experimental results to a reviewer. Davis' objective with her writing was to show a link between *C. albicans* (a pathogenic yeast) and Tumor Necrosis Factor (TNF). Davis saw the significance of her own results, but based on initial drafts, reviewers did not understand what differentiated her work from others. As a result, Davis began to synthesize sources and reference them in her drafts, which effectively transformed both her writing and her message. It encouraged her to find connections that she had not even thought of beforehand and thus paint a more meaningful picture with her writing.

By contextualizing her work, Davis found clarity in her message – she found the *core* of it as the Heath brothers would call it in *Made to Stick*. Not until her final draft submission was Davis able to put down into words the evidence that completely solidified her argument. It was as simple

---

[126] Berkenkotter, C., *Genre Knowledge in Disciplinary Communication*, (1995).

and concise as "If *a* produces *b* in vitro, then it is reasonable to suppose that *a* will produce *b* in vivo." The anecdote of this chapter highlights the same message in the *Made to Stick*. For one, there is the Curse of Knowledge, where Davis was baffled as to why her message was unclear since she understood it so well. Fortunately, she was able to overcome this curse by contextualizing her work and finding the core of her selling point.

Translative:

It is possible that this chapter highlights fundamental miscommunication between scientists and the general public. We know what global warming is, but do we really know what is at stake? Have scientists done an adequate job articulating their concerns and contextualizing them with relevant discourse? From my perspective, the public is provided little relevant context in regards to global warming. Many people do not recognize how climate change will affect them in the future if it remains as uncontrolled as it currently is. By better contextualizing this sort of discourse, I believe that scientists will be able to paint a better picture for the public on what is truly at stake and why it is so vital that we take action.

6.2.3 Kairos

Humans influence and take advantage of, but do not determine, an opportune moment in time. With origins from the Ancient Greeks, kairos depicts the need to consider the timing of a technological implementation. This section includes a literature review of chapters and journal articles relevant to the kairos theme.

R. John Brockmann's *Exploding Steamboats, Senate Debates, and Technical Reports* [127]

Descriptive:

In *Exploding Steamboats, Senate Debates, and Technical Reports*, Brockmann writes of the 19th century problem of steamboat explosions and four subsequent bills submitted before Congress to be voted on. This problem was very substantial – thousands of people were killed because of technical issues with the boat design, negligent operators, and genuine accidents and mess-ups. At the same time, technology was developing and expanding more rapidly than America had ever seen before. The book highlights a conflict of the era – steamboat designs were evolving rapidly, but there were fundamental problems with the designs that were neglected for far too long. For instance, one bill, brought before Congress by Wickliffe, was not passed, in part, because Congress was worried about "impinging upon the improvements of the new age" (37). Where do we draw the line between creating problems and making progress? The first three bills submitted to Congress, designed to help rectify the problems with steamboat design, failed to pass.

In the final chapter of this book, the year 1852 was labeled as the year of *kairos*. The ancient Greeks define this term as "the exact or critical time, season or opportunity" (128). This was the year which marked the first time that a steamboat bill was passed; interestingly, the subsequent law was very similar to the former bills submitted in the late 1830s. This bill became a law not because it was written with stronger technical verbiage or more powerful rhetoric, but rather because the timing of it was perfect and opportune. Instead of pointing fingers at different probable contributors to the steamboat explosions, Americans understood that something had to be done about it. The value or priority behind these incidents was no longer being the people or machinery at fault, but rather about protecting the lives that were at stake.

---

[127] Brockmann, J., *Exploding Steamboats, Senate Debates, and Technical Reports*, (Baywood Publishing Company, Inc., June 2002).

Translative:

Kairos carries a very large connotation – an opportune or "right" moment of time is not predetermined or set in nature. It is created gradually through the efforts of many. In the case of steamboats, the problem with steamboats was called to attention by lawmakers, among many others. Some may have considered their efforts toward passing restrictive laws to be unsuccessful because they did not generate the sort of impact they intended, but these efforts certainly helped to expedite the moment of *kairos*. This same concept applies to the implementation of any new or up-and-coming technology into society. With solar energy, a moment of kairos will likely require many years before it is ever seen. However, current efforts of raising awareness about climate change, drawing attention to the benefits of solar power, and using other rhetorical tools to persuade people, will help in the long run. Technologies affect culture in an "ambivalent manner" (130) and thus it is very difficult to predict the path that a society will take.

Bazerman's *The Languages of Edison's Light* [128]

Descriptive:

In Bazerman's *The Languages of Edison's Light*, he writes of the rhetorical brilliance of Thomas Edison in his rise to fame through the introduction and integration of electric lighting (the incandescent lamp) into American society. Edison's fame was no accident – he strategically used the resources and information outlets at his disposal, which he learned to gratefully appreciate. Beyond his marvel inventions, Edison created a personality for himself in the media, used his fame and influence to gain public trust, and strategically "with[held] information until an opportune moment" (29). Edison was the master of kairos; he used his own power and influence to create symbolic material value. He expedited and manipulated this opportune moment in time – his inventions became a waiting game, an everyday awe. Let's take a chandelier for instance – 19th century families would envy over their neighbors who owned these wonderful illuminating pieces of art. Edison's magic was not the creation of chandeliers – he created the transformation from gas to electric lighting, which in turn yielded items such as these. Homeowners *had* to own these novel creations, and Edison created the conditions that sparked homeowner interest.

Heterogeneous symbolic engineering, as detailed by Bazerman, follows the idea that "as technologies and societies become more complex, so do the symbolic accompaniments of the

---

[128] Bazerman, Charles, *The Languages of Edison's Light*, (MIT Press, 2002).

material technology" (336). As an example, Bazerman argues that in financial and commercial markets, gas lighting was already established as a valuable and profitable commodity, so incandescent lighting and central power "piggybacked" on that established value (337). However, as time evolves, it becomes less obvious and straightforward the meaning systems for technological development, appreciation, production, funding, and the like.

Translative:

This very idea is applicable in the solar industry. In order for solar energy to have a chance of effective societal integration, those with strong influence must engage in systemic rhetoric to create the need and drive toward renewable energy. However, because the development of solar energy stemmed from dozens to hundreds of previous or benchmark inventions, it is unlikely that another Thomas Edison would interact with the public. It is possible, however, for a group of influential individuals to come together and advocate for solar. Another likely issue is that solar energy falls under so many different discursive topics, and thus it is difficult to connect all of it in an effective and concrete manner. This is a challenge – a path must be created for people to follow (just as Edison did) before solar PV kairos is ever seen.

6.2.4 Dynamism

Genres are fluid and change over time in response to sociocognitive needs. This section includes a literature review of chapters and journal articles relevant to the dynamism theme.

Berkenkotter and Huckin's "New Value in Scientific Journal Articles" [129]

Descriptive:

In this chapter of *Genre Knowledge in Disciplinary Communication*, the authors examine the dynamism of scientific journal articles. They explain that many different physical qualities of them have changed because the meaning and value of these articles have shifted over time and are continuously evolving. For instance, the titles are more narrative and informational, the abstracts more essential and standardized, the introduction more results-driven, the subheadings more informative, the methodology less emphasized, and the raw data omitted. This shift in the way that these articles are constructed reflects the way scientists go about interpreting the work of others in the professional field. They are more interested in how scientific data and results fall into the greater picture or realm of thought than understanding the methodology of a research project.

The purpose of this piece is to demonstrate that both genres and activity are dynamic and constantly changing over time. They are heavily interrelated – activity helps to modify the purpose of a form; when the purpose changes, a new meaning is created. In the example provided in this chapter, the dynamic activity of scientists is analyzed. The methodology of laboratory research has become fairly standardized and regulated – scientists now scrutinize the works of others primarily to gain a stronger understanding of the status of a given field and the direction that it is taking. Accordingly, the structure of these pieces has been modified to accommodate for the needs and interests of scientists. The same idea is applicable in other seemingly bland or stationary genres such as PowerPoints (from "The PowerPoint Presentation and its Corollaries: How Genres Shape Communicative Action in Organizations") as well as RFQs and labor contractions (from "Using Text to Manage Continuity and Change in an Active System"). Each of these are as alive as ever and are constantly changing to accommodate for the needs of businesses and professionals.

---

[129] Berkenkotter, C., *Genre Knowledge in Disciplinary Communication*, (1995).

Translative:

Just as the genres in this chapter are proven to be dynamic and evolving, so too are many other genres that we often do not consider. For instance, e-communication has grown and evolved substantially based on constant redefinition of its purpose and the activity around it. Contemporary first world societies are invested in receiving information and communicating to one another as rapidly as possible. Thus, instant messaging services have thrived while genres such as email have been left almost strictly for professional business communication. Bringing together the dynamic nature of communication and information spread and the concept of human behavior, the meaningful selling points of messages, and the opportunity of karios, I believe that there has never been a more opportune time for technology implementation.

Codding and Faber's "Popularizing Synthetic Biology: The Public Rhetoric of Synthetic Biology 2006 – 2015" [130]

Descriptive:

In "Popularizing Synthetic Biology: The Public Rhetoric of Synthetic Biology 2006 – 2015," Codding and Faber write of their study to determine if the field of synthetic biology is instantiated or if it is still emerging into a publicly recognized science. They perform this study by examining several different factors which contribute to instantiation: media perception of value and representations. This study is conducted based on literature from 2006 – 2015 because this timeframe represents "a critical period in synthetic biology's contemporary popular emergence and instantiation as academic practice" (6). Their study consisted of 162 articles from national and localized media sources which collectively had 24 recurring representations.

Based on their study, Codding and Faber first found that "the value of synthetic biology had yet to be fully stabilized in the popular science media" (8). There was no consistent trend of perceived positive value in articles from the latter years of the timeframe, 2012 – 2015. As for their representation study, the two found that high occurring representations were persistent but average and low occurring representations were generally sporadic in articles. Due to the "multiplicity of representations", Codding and Faber ultimately concluded that synthetic biology had not yet been fully instantiated. Finally, upon completing this study, they discerned a coming

---

[130] Codding, K., Faber, B., "Popularizing Synthetic Biology: The Public Rhetoric of Synthetic Biology 2006 – 2015", (2018).

together or practical alignment of biology and engineering consistently portrayed throughout the readings (16). Though Faber is not convinced that instantiation of synthetic biology will occur in the near future, Codding is more hopeful.

Translative:

  This piece demonstrates the process of instantiation within a given genre– in this case, synthetic biology. There is an element of dynamism that always persists, perhaps even when a genre is deemed as "instantiated." However, when a genre is still emerging, it tends to be more sporadic in terms of its perceived value by the public. This same problem could be applicable in regards to solar renewable energy. There are, for instance, very sporadic opinions of the legitimacy of global warming and thus inconsistent viewpoints on the need for renewable energy technologies. As a result, I would affirm that the solar energy genre must be instantiated before PV technologies are adopted widely.

6.2.5 Literature Review Conclusions

  Drawing from the dynamism theme, we understand that genres are fluid and constantly changing in response to sociocognitive needs. In relation to technology implementation, the external variables that influence our perceptions and attitudes toward new technologies are dynamic. From the message theme, we understand that solar energy needs to be established and substantiated as meaningful and promising by crafting the message at hand. This can be done by better contextualizing the benefits environmentally while also emphasizing what is at stake. Finding the meaning or central purpose of a form or genre is crucial.

  As for human behavior, users are much more likely to accept and make use of a new technology that carries a message or purpose aligning with their values. Finally, from kairos, we see that those who are seeking to implement technology must consider the timing of their introduction to gauge whether or not general public response will be favorable. Overall, if the message for the implementation of new solar technologies is created appropriately and at the right time, with attention to the dynamic nature of human behavior, solar technologies will continue to grow in the coming decades.

6.3 Case Studies of Technology Implementation

The following section consists of three case studies applicable to solar technology implementation. It begins with a case study of an integrated solar technology acceptance model in South Korea similar to this research study. Then, it continues with two case studies of successful (6.3.2) and unsuccessful (6.3.3) technology implementation. The first of these two details the successful attributes of Tesla's electric car and the latter addresses Steve Jobs' NeXT computer. Through these case studies, a more holistic understanding of factors which influence technology implementation was obtained.

6.3.1 Integrated Solar TAM in South Korea

A 2013 research study, similar to this one, was conducted by five members of the Graduate School of Innovation and Technology Management and the Korea Advanced Institute of Science and Technology. Their aim was to propose a solar TAM specifically for South Korea and gather data, through surveying and interviewing, to assess its validity. As the authors affirm, a systematic approach to solar energy should be established before actual system use in the industry.[131]

The authors begin their study with a general assessment of the current status of solar energy in South Korea. They recognize a heightened public interest in protecting and preserving the environment, but tangibly-speaking the development of these technologies is described as "weak" in comparison to many other nations. In effect, there is pressure to develop advanced clean energy technologies focused on customer-oriented strategies.[132] These advanced technologies would take the form of solar photovoltaics due to their efficient energy conversion capabilities. Finally, the authors remark on increased government incentive to improve research and development studies toward the improvement of PV technologies.

With the South Korean energy status outlined, the authors introduce the proposed research model (Figure 46).

---

[131] Kim, H., et. al., "An integrated adoption model of solar energy technologies in South Korea", (Science Direct, 2014).
[132] Ibid.

106
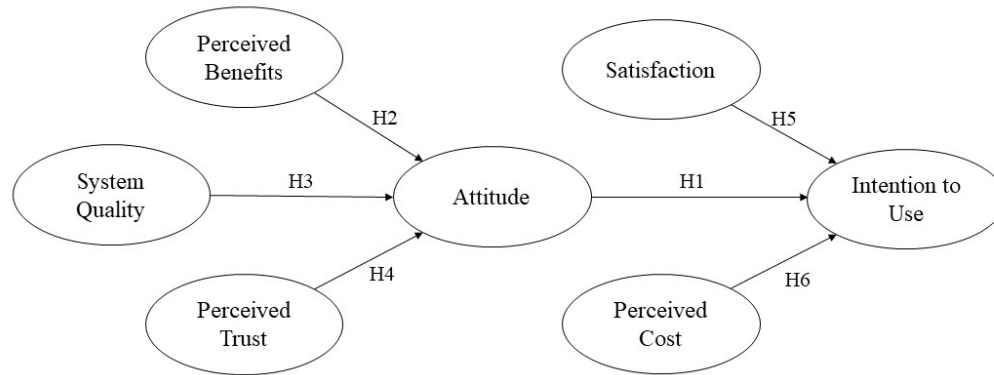
Figure 47. South Korea integrated solar TAM.[133]

From the above figure, we see that the authors hypothesized perceived benefits, system quality, and perceived trust as external variables influencing user attitude and satisfaction and perceived cost influencing the user's intention to use.

To assess the validity of the proposed model, the researchers administered a survey to approximately 1,700 people and conducted interviews. The majority of the survey questions were likert (1 = Definitely disagree, 7 = Definitely agree, etc.), allowing the researchers to understand quantitatively the degree to which users are influenced by the proposed factors. Their results indicated that user satisfaction and attitude had positive effects on the user's intention to use while the perceived cost yielded a negative correlation. Their hypothesized model was supported and confirmed through this study, though they recognized several limitations to their research. For instance, they understand that their model would likely have structural differences when applied to other nations. Additionally, they did not factor in demographics, which can strongly influence survey responses. Finally, the five researchers articulate that there are other potential variables which may substantially influence the user's intention to use. Accordingly, this research model served as a framework and inspiration to many components of the proposed model in the coming section.

6.3.2 Tesla, Inc. and the Electric Car

Tesla, Inc.'s mission is to "accelerat[e] the world's transition to sustainable energy, offering the safest, quickest electric cars on the road and integrated energy solutions. Tesla products work

---

[133] Adapted from Kim, H., et. al., "An integrated adoption model of solar energy technologies in South Korea", (Science Direct, 2014).

together to power your home and charge your electric car with clean energy, day and night."[134] This company's message is meaningful and reflects a global effort toward clean, sustainable energy use. Although largely an automotive business, Tesla, Inc. shares its business endeavors while also paying close attention to the underlying message. Thus, Elon Musk and Tesla, Inc. are representative of a successful case of clean energy technology implementation.

The purpose of this case study is that it showcases certain external factors that a company can take advantage of to augment the chances of success with a new technological implementation. With Tesla, Inc. some studies attribute the success of the company to the timing of the technology. Elon Musk and his team implemented products in the 2000s that aligned with the needs and interests of consumers at the time. Not only was the system quality very good, but it also answered the desires of those who were interested in a clean energy, working model vehicle. Finally, the charismatic persona of Elon Musk and his team revolutionized the industry and made Tesla, Inc. a force to be reckoned with - "Tesla's CEO is the consummate engineer and salesman, so it's not surprising that he's assembled a team that's very good at both."[135] This emphasis on persona and public perception reflects Edison's approach to the incandescent light bulb and DC electric power.

The factors mentioned in this study were integrated within the model as those which influence American technology acceptance and align with American culture. Additionally, given that this example falls under the genre of clean, renewable energy, it becomes even more applicable to the greater research study.

6.3.3 Steve Jobs' NeXT Computer

Before co-founding Apple, Inc. Steve Jobs founded NeXT in 1985, an American computer company most notably responsible for the NeXT computer. Many are likely unfamiliar with this computer system or chose not to purchase it because it was innovative, yet pricey, and high-tech, yet overcomplicated. The NeXT computer was described as Jobs' noble failure. Although it was an unsuccessful example of technology implementation, it was instrumental in Steve Jobs' later success with Apple, Inc. He learned from the mistakes made with NeXT and re-started his career and brought Apple, Inc. to where it is today.

---

[134] "Tesla: Electric Cars, Solar Panels & Clean Energy Storage", (Tesla, Inc., 2018).
[135] "7 Reasons Why Tesla Has Been So Successful", (Steinbuch, January 2015).

The most frequent and substantial problems associated with the NeXT "Black Cube" computer were the price and timing of it. Jobs had failed to introduce the technology at a point when people were generally interested in high-technology, innovative solutions, especially if these solutions would come at an unreasonable cost. Some researchers have pondered Jobs' rationale, suggesting that Jobs encountered a dilemma: "Was it more important to create a machine with great technology, meet a $3,000 price point, or have it ready by 1987?"[136] Regardless, the inception of this device was unsuccessful – it solved problems that people did not know they had. As remarked in a Forbes 1991 article, "Jobs ha[d] made fundamentally wrong decisions that could well doom the venture."[137]

Another fundamental issue with the NeXT computer was that its message emphasized impractical needs. While Apple's Mac computer focuses on the creation of personal computers for everyday consumers, NeXT sought to construct the most powerful computers available for business and educational uses.[138] NeXT's message indicated that it was not designed for every consumer (unlike Tesla, Inc, in Section 6.3.2.), but rather for the elite. As for those who were interested in purchasing, they became hesitant with the pricing. In effect, Jobs' message was discerned as ineffective and NeXT ultimately failed.

The use of this case study of an unsuccessful technological implementation is that is shows that Tesla and NeXT succeeded and failed, respectively, for the same reasons. Tesla, Inc. harnessed the right message, implemented innovative automobile solutions at the right time, and captured public interest through the team's charismatic persona. NeXT, in comparison, had the wrong message, implemented an innovative technology that people did not want, and failed to capture public interest. Both of these studies were useful in proposing a TAM for American culture. They highlight that similar factors affect American user acceptance.

6.4 Proposed Solar Technology Acceptance Model

Combining the four themes derived from the literature review along with the case studies discussed previously, the following external variables were proposed as affecting American user

---

[136] Elmer-Dewitt, P., "Long-lost Video: Steve Jobs' Biggest Product Failure", (Fortune, 2016).

[137] Linn, Allison, "What Steve Jobs taught us: It's OK to fail", U.S. Business: NBC News, 2011).

[138] "Why did NeXT Fail? (Or Did It?)", (512 Pixels, 27 March 2012).

acceptance of solar technology implementation: system quality, system lifetime, perceived cost, perceived benefits, maintenance, reliability, public advocate, and aesthetic. A diagram outlining these external variables is shown below in Figure 47.
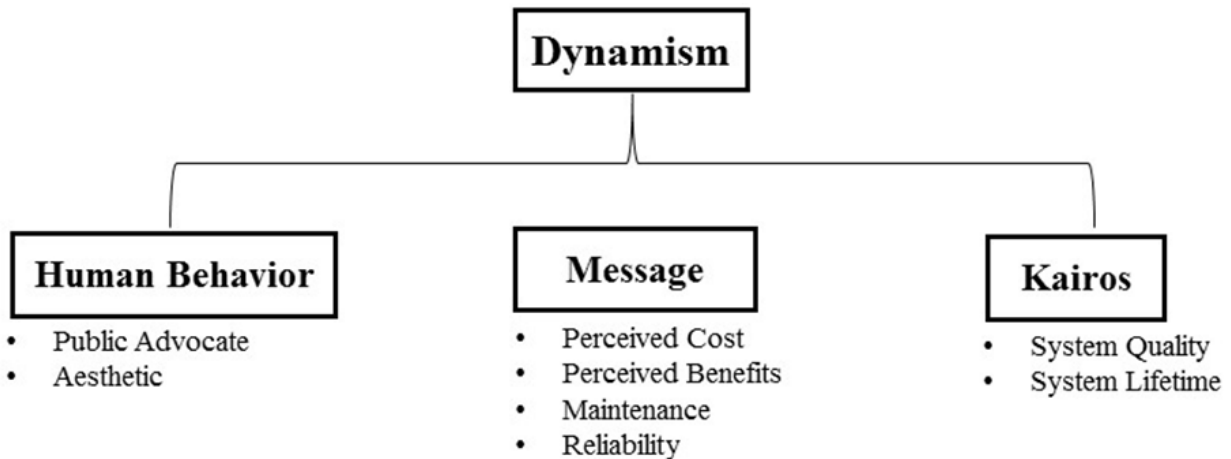
Figure 48. External variables derived from literature review themes to be integrated in U.S. solar TAM.

The above diagram depicts that the dynamic, fluid nature of any cultural or political context, such as that of American society, is continuously shaping the external variables which influence user acceptance. Under human behavior, public advocate and aesthetic were proposed to be correlated with how human values govern our interpretations and the manner in which we respond to messages. On a similar note, the message (central activity of a form) strongly influences the perceived cost and benefits of a solar technology, followed with maintenance and reliability, both of which are essential components to establishing a message to market solar energy. Finally, under kairos, we have system quality and system lifetime, depicting that the user perceived status or overall quality of a solar technology is influenced by the timing of its implementation.

Integrating the above external variables into a predictive model, we have a proposed United States solar technology acceptance model illustrated below in Figure 48.
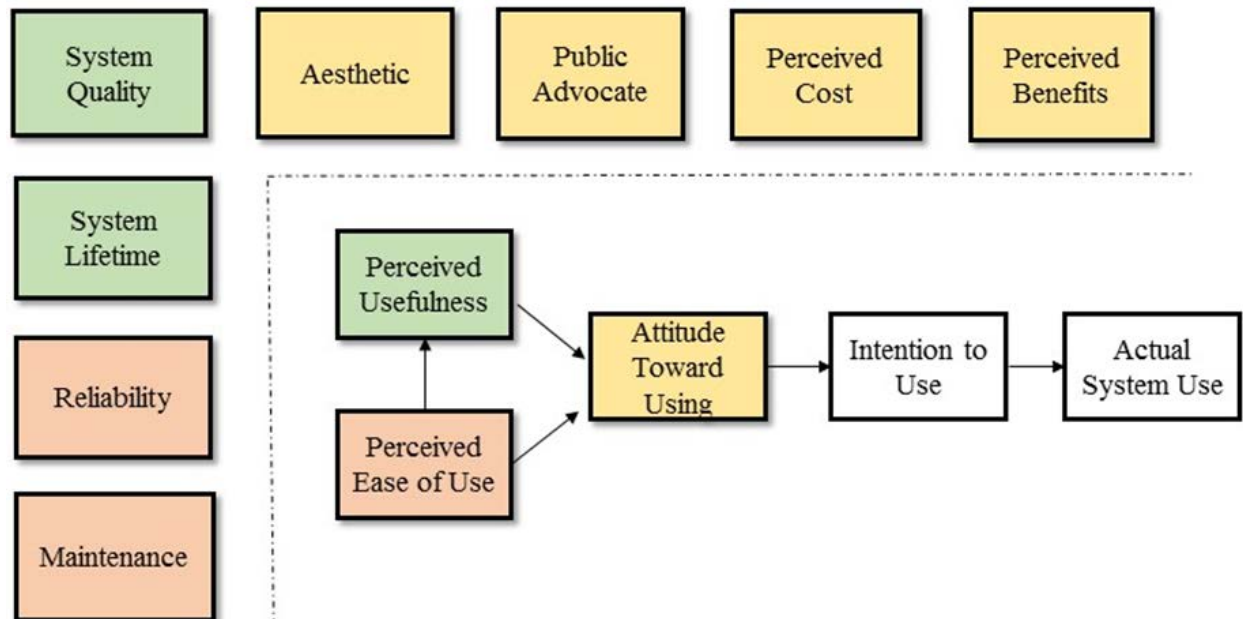
Figure 49. Proposed U.S. solar technology acceptance model

The color correlations illustrated in the model depict the factors which influence the user's perceived usefulness, ease of use, and attitude toward using a solar technology. For instance, aesthetic, public advocate, perceived cost, and perceived benefits are all variables that affect the user's attitude toward using the technology. Likewise, device reliability and maintenance influences the perceived ease of use. Finally, system quality and lifetime influence perceived usefulness. The proposed model reflects elements of the South Korea model, such as system quality and perceived benefits, while drawing upon American culture and values highlighted in the case studies of successful (Tesla, Inc.) and unsuccessful (Jobs and NeXT) technology implementation.

6.4.1 Empirical Validation

In order to begin to validate the proposed model, surveys were administered to 30 participants, 15 male and 15 female. The administered survey (Appendix H1) was used as a metric to quickly gauge public perception of solar technologies based on the external variables indicated in the model.

Of the 30 participants, 67% indicated that they are at least moderately familiar with solar energy technologies, while 10% responded that they are not at all familiar. Additionally, 57% (17)

of the participants specified that they are 21 years old or younger, 33% (10) are between the ages of 22 and 34, and the remaining 10% (3) are in the range of 35 and 54 years old. As further background, all participants were either students or faculty of Worcester Polytechnic Institute (WPI), the majority of which having at least some degree of a technical background and/or education.

The most substantial question in the administered survey was the following: Please rank the following factors as: Not important at all **(1)**, Moderately unimportant **(2)**, Neither important nor unimportant **(3)**, Moderately important **(4)**, or Very important **(5)** when deciding whether or not to make use of a solar technology: System Quality, Perceived Cost, Perceived Benefits, Reliability, Public Advocate, System Lifetime, Maintenance, and Aesthetic. A mean score and standard deviation summary is illustrated in the table below (Table 7).

Table 7. Table outlining the mean likert score and standard deviation of each of the external factors in the proposed U.S. solar TAM.

External Variable	Mean Score (Likert: 1 - 5)	Standard Deviation
System Quality	4.37	0.81
Perceived Cost	4.1	1.0
Perceived Benefits	4.03	1.0
Reliability	4.53	0.63
Public Advocate	2.77	0.73
System Lifetime	4.23	0.82
Maintenance	4.03	0.81
Aesthetic	2.6	1.33

Based on the results, the following conclusions were developed and will be interpreted further in the section that follows:

- Above all, participants value system quality, system lifetime, and reliability of solar energy technologies.
- Participants also view perceived cost, perceived benefits, and maintenance as moderately important when deciding whether or not to make use of a solar energy technology.
- In general, participants find public advocate to be of neutral importance with a relatively low standard deviation.
- Participants view solar technology aesthetic as the least important external factor, but it is also interesting to note that this yielded the greatest standard deviation in responses.

6.4.2 Interpretation and Conclusion

The empirical validation results reflect a general technical mindset of the participants, emphasizing system quality over system looks and aesthetics. There appears to be agreement from the participants that solar energy needs to be reliable and useful, and that the cost and benefits should both align favorably. It is also difficult to extrapolate consumer behavior from a generic survey. As Kahan et al. noted, once actual decisions with real consequences are put into play, consumer choice and individual actions may not follow stated (theoretical) preferences or idealist intentions.

In the future, I would administer a more comprehensive survey to better discern the most critical external variables and refine the model accordingly. Though promising, there is not enough empirical data to confirm the degree of predictability of the proposed U.S. solar TAM. Additionally, I would target a larger, more diverse audience to survey a larger population that is more representative of the United States. Through this approach, empirical results will likely change.

Appendix A: Material Structure of BiI₃

BiI₃ is an n-type material that has potential to be a successful semiconductor for use in photovoltaics. BiI₃ has a hexagonally closest-packed lattice with iodine centres, and the bismuth centres take up two-thirds of the octahedral voids of every other layer.[139] This structure is illustrated in Figure 49 below.
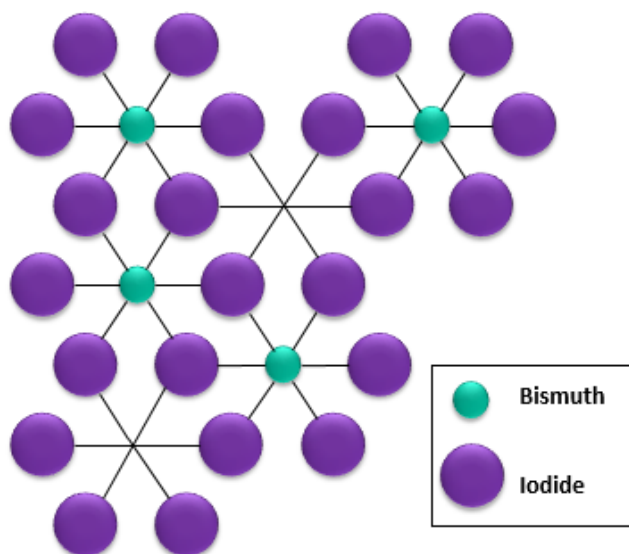
Figure 47. The lattice structure of BiI₃

Similar to silicon, bismuth triiodide's crystalline structure allows easy movement of electrons from atom to atom, making bismuth triiodide a good semiconductor. BiI₃ has a relatively high mass density, of 5.78 g/cm³ compared to other semiconductors like silicon with the mass density of 2.33 g/cm³. Because of this, BiI₃ has been investigated for use as hard radiation detectors and for X-ray imaging.[140] Additionally, BiI₃ has anisotropic optical and electronic properties, meaning that a different value is obtained when measured in a different direction.[141]

---

[139] Anna Lehner, et al, *Electronic structure and photovoltaic application of BiI₃, Applied Physics Letters (2015)*
[140] Ibid
[141] Ibid

Appendix B: Property Comparison of Materials

Table 8. Property Comparison Table

	COMPARISON OF SILICON, BiI3, AND PEROVSKITE PROPERTIES			
Property	**Silicon**	**BiI3**	**Methylammonium Lead Iodide**	**Definition**
Band gap	1.18 +/- 0.03 eV	1) 1.67 (optimal- 1.8 eV) 2) 1.79 +/- 0.05 and 1.80 +/- 0.05 3) 1.82eV	indirect bandgap of 60meV and direct bandgap of 1.51 eV	The energy difference between the top of the valence (outer electron) band and the bottom of the conduction (free electron flow) band. Electrons are able to jump from one band to another given an "energy lift" by some external force (e.g. sunlight or photon).
Thickness	0.5 micrometers	100nm/ 1 micrometer (BiI3, HTL, ETL)	200nm- efficiency= 31% at this thickness	The amount of material perpendicular to the direction of solar radiation (whether incoming or outgoing) necessary for efficient absorption
Electron Mobility	1400 cm^2/ (V*s)	260 +/- 50 or 1000 +/- 200 cm^2/(V*s)	~66cm^2/(V*s)	How quickly an electron can move through a metal or semiconductor when pulled by an electric field
Hole Mobility	450 cm^2/ (V*s)	260+/- 50 cm^2/Vs	~322 cm^2/V*s	The ability of a hole to move through a metal or semiconductor, in the presence of applied electric field
Hole Effective Mass	0.57/0.81 (m(h,dos)/m(0))	10.39	mh* = 0.29m0	The mass that it seems to have when responding to forces, or the mass that it seems to have when interacting with other identical particles in a thermal distribution
Electron Effective Mass	1.08	1.85	me* = 0.23m0	The mass that it seems to have when responding to forces, or the mass that it seems to have when interacting with other identical particles in a thermal distribution
Electron Diffusion Lengths	100-300 micrometers	1.9 or 4.9 micrometers	>1000nm or 1micrometer	The average distance the relevant charge moves in the semiconductor--influenced by the average distance the relative charge moves in the semiconductor and recombination/ extraction from the semiconductor
Light Absorption Coefficient	For wavelength 800nm, absorption depth=1.0x10^-3 cm^-1	16900 and 20,000 cm^-1 absorption doublet other absorption bands C and D at ca. 23500 and 27500 cm^-1	at 550nm, 1.5e+4 cm^-1, at 700nm, 0.5e+4 cm^-1 absorption coefficient= ~10^4 (600nm)	How deep light or electromagnetic radiation can penetrate into a material (that is absorption depth)
Lifetime	recombination of first surface=1000cm/s... **Ts= 1.49e-5 s and Teff=1.46e-5 s** 1ns to 1ms	180-230 ps for PVT films 190-240 ps- solution processed films 160-260 ps for single-crystal sample	~ 1 microsecond	The average time it takes for a minority carrier (hole or electron) to recombine with its counterpart (that is, that of the opposite charge)

Appendix C: Experimental Laboratory Procedures

Appendix C1: Cutting, Etching, & Cleaning

1. Find a space on the bench to work
2. Cut FTO-Glass into 1.9 cm x 2.4 cm rectangles
   a. These dimensions are 0.1 cm less than the allowed size to make sure they aren't too large for the gold evaporator
   b. Use the multimeter to find the conductive side
   c. Use a ruler and a marker to measure out the samples
   d. Use blade roller to cut along the lines (use the ruler to cut in a straight line)
   e. Use black tool to snap the samples in half. The white line should be on the bottom aligned with the crack and the crack side should be facing up.
   f. Make sure samples fit in the container for the gold evaporator
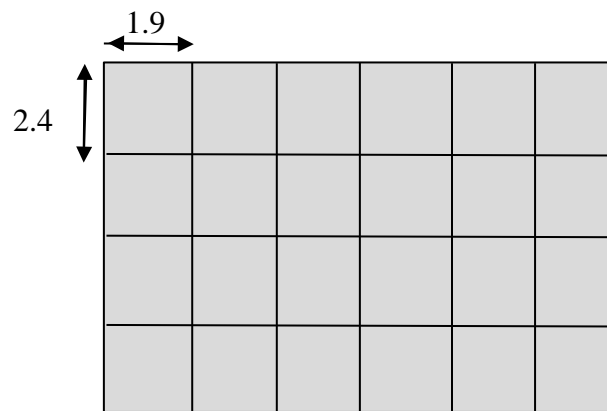
Figure 48. Sheet of FTO-glass with samples dimensions drawn on before cut into individual samples

3. Preparing to Etch
   a. Use KAPTOM tape (dark and shiny) to protect the 0.8 cm strip of sample we don't want to etch
   b. Place the tape on the FTO side so it covers the middle of the sample with no air bubbles
   c. Measure the 0.8 cm strip and gently cut the tape to size with the razor blade
   d. Peel excess tape away
   e. Put sample in petri dish and clean with DI water (from hose in the hood)

0.8 cm
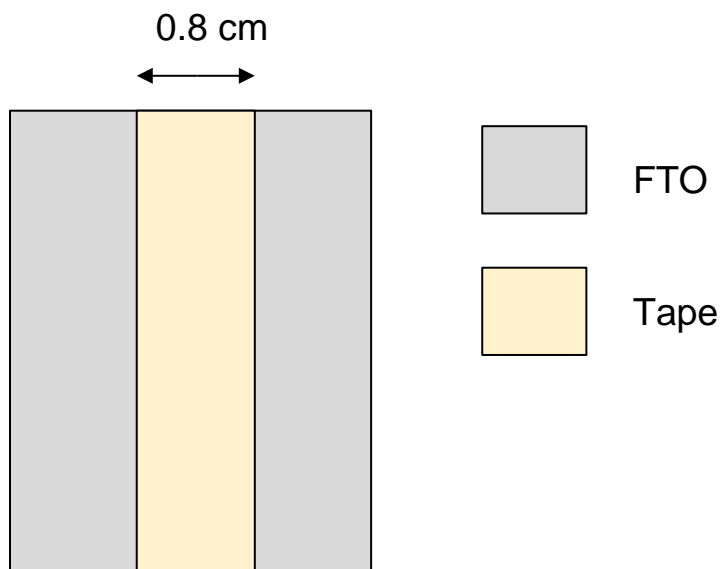
Figure 49. Diagram of sample prepared for the etching process

4. Etch
   a. Use spatula to scoop zinc on the exposed FTO; cover but don't use too much

Zinc   Tape   Zinc
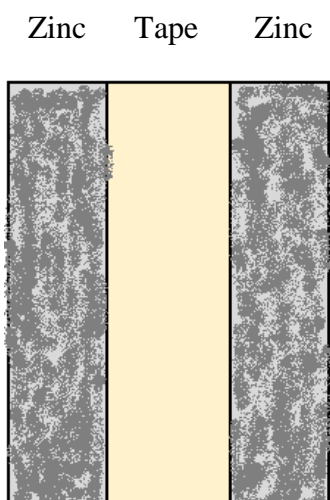
Figure 50. Diagram of how the zinc should be applied to the exposed FTO

   b. Make sure no one else's samples are around before HCl is added because the reaction will bubble
   c. Pipette 6M HCl onto the sample drop by drop
      i. HCl is available at 12M, dilute in half to make 6M
      ii. If available at 6M, still put some in a separate vial before you use it for the reaction to prevent zinc contamination from the tip of the pipet

d. When reaction has finished, wipe off zinc with a Q-tip

e. Rinse sample in petri dish with DI water

f. Pour water containing zinc waste into the zinc/HCl waste jug

g. Measure resistance

    i. If >500 kΩ, continue to cleaning procedure

    ii. If <500 kΩ, repeat steps 4a - 4e

5. Cleaning

    a. Take off tape

    b. Let samples sit in DI water in a petri dish

    c. Soap and water wash

        i. Dissolve detergent in DI water (will become fully dissolved when sonicated, just stir some before adding the samples in)

        ii. Sonicate for 30 minutes with sample in the mixture

        iii. Rinse off soap with DI water

        iv. Make sure you never let the samples dry, keep samples in DI water in between this and each of the following cleaning steps

    d. Boiling water rinse

        i. Fill beaker using DI water

        ii. Set hot plate to 200-300 °C, it will boil in ~15 minutes

        iii. Put sample in the beaker to rinse

        iv. The time you leave the samples in the hot water depends on how dirty they still are at this point

        v. Take out the samples with tweezers

    e. 1:1:1 isopropyl alcohol, acetone, and DI water rinse

        i. Pour enough of mixture into a beaker for all of the samples

        ii. Sonicate mixture with sample in it for 5 minutes

        iii. Rinse with DI water

        iv. Use a fresh amount of the mixture and repeat steps e.ii-e.iv two more times

    f. Soak in isopropyl alcohol

    g. Blow with air to dry

        i. Air hose located in the hood

Appendix C2: TiO$_2$ Electron Transport Layer

Compact-TiO$_2$

1. Prepare solution

    a. Make two separate solutions in two vials

        i. Vial 1: 0.15M

        ii. Vial 2: 0.3M

    b. Set pipet to 0.055 mL (55 microliters)

      i.   Vial 1: one pipet of diisopropyl titanium oxide

      ii.   Vial 2: two pipettes of diisopropyl titanium oxide

  c. Add 1 mL of 1-butanol in each vial (found in top left of base cabinet)

  d. Put both solutions in the sonicator for 5-10 minutes

2. Spin-Coating and Annealing

  a. Set up spin-coating instrument

      i.   Select Process

      ii.   #5

      iii.   Spin-Coating

      iv.   RPM = 2000

      v.   Time = 30 seconds

      vi.   Acceleration = 1000 RPM/second

  b. Put piece of tape on edge the of sample

Figure 51. Diagram of sample as it is prepared for TiO$_2$ spin-coating

  c. Put sample in the middle of the spin-coating instrument

  d. Turn on vacuum

  e. Pipet solutions to cover sample in a total of three rounds including

      i.   .15M, then anneal for 5 min at 125°C

      ii.   .30M, then anneal for 5 min at 125°C

      iii.   .30M, then anneal for 30 min at 500°C

          1. Take off tape after each round of spin-coating

          2. Cool sample after each annealing step

          3. Put sample on piece of foil when annealing with a petri dish to cover it.

3. Put samples in a labeled petri dish until the next layer can be put on.

Mesoporous-TiO$_2$,
1. Make a 20wt% solution
    a. Weigh ~0.5 grams of titanium paste, record mass from balance
    b. Solve equation for mass of ethanol needed for solution
        i. $M_p = 0.2(M_p) + 0.2M_e$
    c. Convert mass of ethanol to volume using density
        i. $M_e * (1 \text{ mL}/0.789 \text{ g}) = V_e$
    d. Mix paste and ethanol in a vial
    e. Sonicate for 40 minutes
2. Spin-Coating
    a. Set up spin-coating instrument
        i. Select process
        ii. #5
        iii. Spin-coating
        iv. RPM = 4000
        v. Time = 30 s
        vi. Acceleration = 1000 RPM/second
    b. Put piece of tape on edge of sample
    c. Put sample in the middle of the spin-coater
    d. Turn on vacuum
    e. Pipet solution to cover sample
    f. Run spin-coating instrument
    g. Turn off vacuum
    h. Take sample off
3. Annealing
    a. Preheat hot plate to 500 C
    b. Take tape off of sample
    c. Place on a piece of aluminum foil on top of the hot plate
    d. Cover sample with a petri dish
    e. Anneal for 1 hour
    f. Allow for samples to cool after annealing
    g. Put samples in a labeled petri dish until the next layer can be put on

Appendix C3: BiI₃ Semiconductor Layer

1. Make solution
   a. Label a new vial with date and concentration
   b. Weight 300 mg (0.3 g) of BiI_3 (BiI_3 in the vacuum desiccator) and put it in the vial
   c. DMF
      i. Take some out of container and put into vial to use for a couple days
      ii. Label it "clean DMF" with date
      iii. Pipette out 1 mL from the vial and add it to the vial with the BiI_3
   d. Clean a stir bar with acetone and add it to the vial
   e. Stir with a stir plate. The solution will be ready in a few hours.
      i. This process can be sped up to an hour by heating the hot plate to 60 ℃
   f. Filter solution
      i. Using syringe and 0.2 μm filter cap (from a box in the bottom cabinet to the right of the bench) extract the mixed solution from the vial
      ii. Eject filtered solution into a new vial
      iii. Label new vial with contents and date
      iv. Throw syringe and filter cap into the trash
2. Spin-Coating
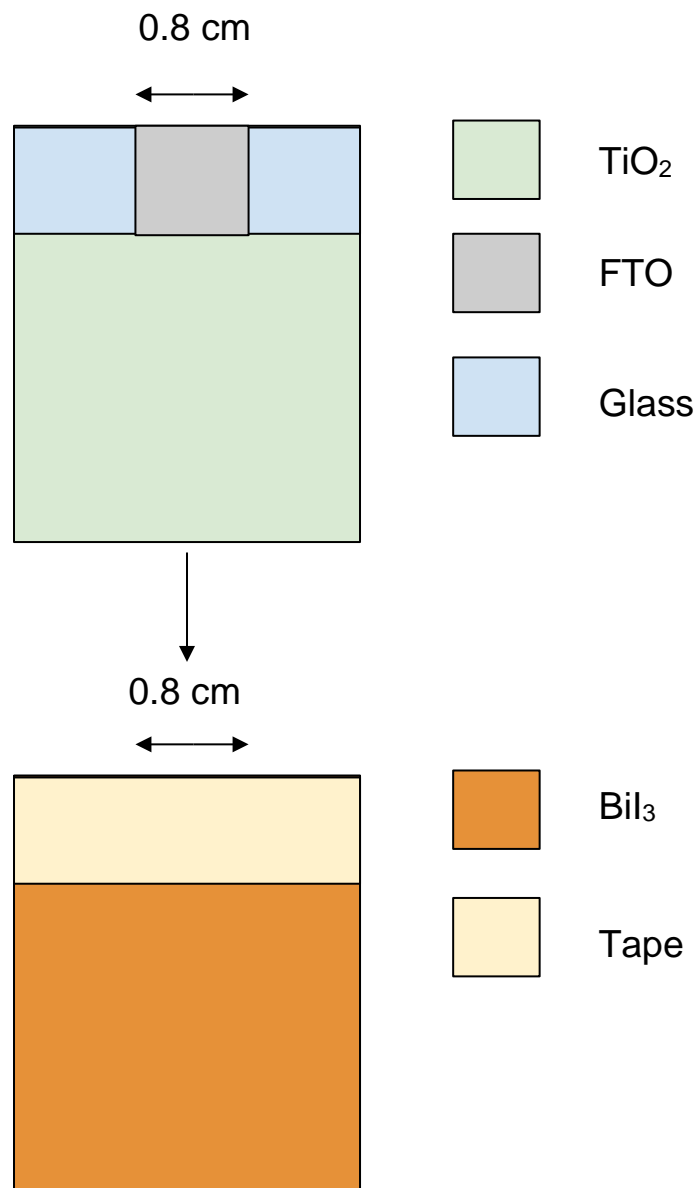
Figure 52. Diagram of sample before and after spin-coating BiI₃

a. Set up spin-coating instrument
     i.   Select process
    ii.   #5
   iii.   Spin-coating
    iv.   RPM = 1000
     v.   Time = 35 s
    vi.   Acceleration = 1000 RPM/second
b. Put piece of tape on edge of sample
c. Put sample in the middle of the spin-coating instrument

d. Turn on vacuum
e. Pipet solution to cover sample
f. Run spin-coating instrument
g. Turn off vacuum
h. Take sample off
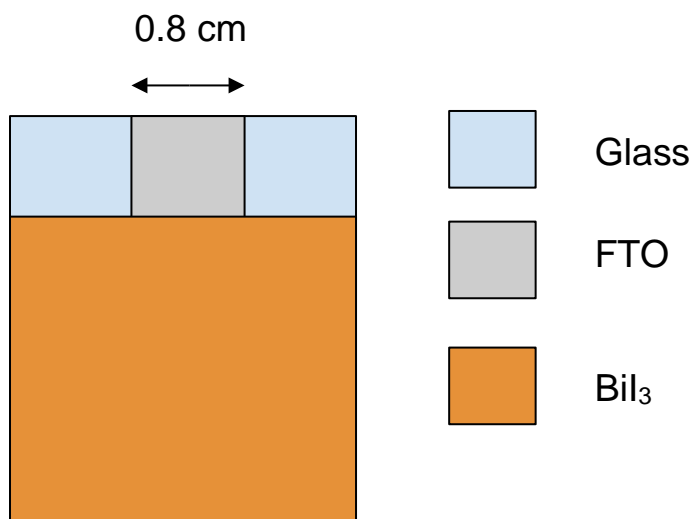
Figure 53. Diagram of sample after BiI₃ was spin-coated and the tape was removed. This is what the sample looks like while it is being annealed.

3. Annealing
   a. Cover whole hot plate with aluminum foil
   b. Preheat hot plate to 100 °C
   c. Take tape off of sample
   d. Place on a piece of aluminum foil on top of the hot plate
   e. Cover sample with a petri dish
   f. Anneal for 10 minutes
   g. Allow for samples to cool after annealing
   h. Put samples in a labeled petri dish until the next layer can be put on

Appendix C4: P3HT Hole Transport Layer

1. Make solution
   a. Label a new vial with date and concentration
   b. Weight up to 15 mg of P3HT (P3HT in the vacuum desiccator) and put into the vial
   c. 1,2-Dichlorobenzene
      i. Use syringe (in tool box) to draw 1 mL of solvent
      ii. Add to vial and mix
   d. Clean a stir bar with acetone and add it to the vial

      e.   Stir with a stir plate. The solution will be ready in 30 minutes.
2. Spin-Coating
    a. Set up spin-coating instrument
        i.   Select process
        ii.   #5
        iii.   Spin-coating
        iv.   RPM = 500
        v.   Time = 30 s
        vi.   Acceleration = 1000 RPM/second
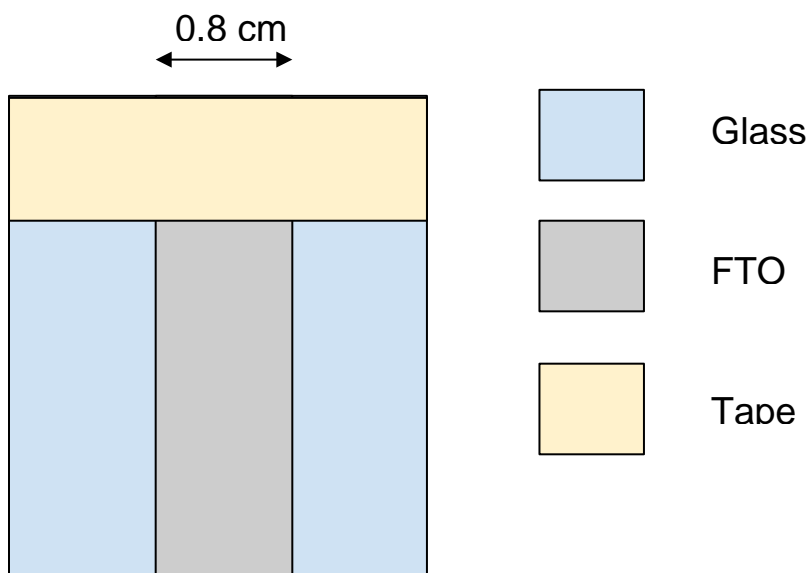   b. Put piece of tape on edge of sample
    c. Put sample in the middle of the spin-coating instrument
    d. Turn on vacuum
    e. Pipet solution to cover sample
    f. Run spin-coating instrument
    g. Turn off vacuum
    h. Take sample off
3. Annealing
    a. Cover whole hot plate with aluminum foil
    b. Preheat hot plate to 90 °C
    c. Take tape off of sample
    d. Place on a piece of aluminum foil on top of the hot plate
    e. Cover sample with a petri dish
    f. Anneal for 20 minutes
    g. Allow for samples to cool after annealing
    h. Put samples in a labeled petri dish until the next layer can be put on
4. Prep for Gold layer
    a. Evaporation
        i.   Cover with aluminum foil
        ii.   Cut out two strips to be covered with gold
        iii.   Put in a designated spot and let grad student know they are ready for evaporation

Appendix C5: Solar Cell Performance Testing Procedure

1. Setting up apparatus
    a. Put one ring stand on each of the sides of the solar simulator
    b. Attach a clamp to each of the stands
    c. Obtain sample holder from the tool box and hold it 13 cm in front of the lamp with the clamps
    d. Place the sample in the holder
    e. Touch the red probe to the FTO contact, and the black probe to the gold contact
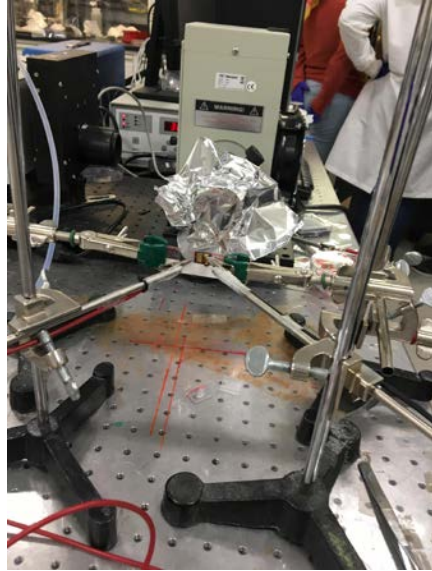
Figure 54. Sample testing apparatus

2. Turning on Program
    a. Turn on Computer
    b. Sign into your WPI account
    c. Search for EC-Lab and open that program
    d. Turn on the power switch for the lamp
        i. Make sure the opening for the light is closed as much as possible and there is a piece of aluminum foil covering the light unless you need it on (light on the sample for longer than needed can be bad for the performance of the cells)
    e. Press the lamp on button
    f. In EC-Lab click "load settings"
    g. Open up a file that would have similar testing parameters to the test you're going to do
3. Pre-Test for resistance
    a. Make sure the red probe is on the FTO contact and the black probe is on the gold contact
        i. For naming consistency, start with the cell closest to the FTO contact and call that "Cell 1" and "Cell 2" will be the one farthest from the FTO contact
    b. Attach the other end of the red probe to the black clamp of the Multimeter
    c. Attach the other end of the black probe to the red clamp of the Multimeter
    d. Turn the Multimeter to the omega to measure resistance
        i. If it's 0, the contacts to the sample need to be adjusted
        ii. If it's not 0, then the actual test can be run

4. Testing the cells
   a. Move the connections from the Multimeter to the probes that are connected to the potentiostat
      i. Red goes to red
      ii. Black goes to the blue and white (blue and white should be connected to each other)
   b. Turn on the potentiostat on
   c. Wait ~30 s to hear a "click" noise from the potentiostat
   d. Connect the potentiostat to the program
      i. Click "Connect" which is under the tab "Config"
   e. Click the green triangle to start the test
   f. Rename the file with the correct sample and cell number when the window comes up but don't press save yet
   g. Take the foil off of the lamp and open it up all the way
   h. Then press save to start running the test. The green triangle will turn into a red square
   i. Right click on the graph and switch to Ewe vs I
   j. Once the red square turns back to a green triangle, the test is done
   k. Close the lamp opening and recover the lamp with the foil
   l. Disconnect the potentiostat from the program
      i. Click "Disconnect" which is under the tab "Config"
   m. Turn off the switch the on the potentiostat
   n. Move the black probe to cell 2 and repeat steps 3 and 4
5. Shut down
   a. Press turn off lamp button
   b. Don't turn off power of the lamp box yet, wait until the fan on the lamp stops (about 20 minutes)
   c. Make sure potentiostat is disconnected and then turned off
   d. Turn off the EC-Lab program
   e. Log off of the computer
   f. Put samples away, make sure the areas of each cell have been measured and recorded
   g. Turn the power off of the lamp once the fan is off
6. Calculating Efficiency
   a. Export EC-Lab files to project files
   b. Export Project files to excel files
   c. In the excel document for each cell, make a new column next to the voltage column (Ewe/V) call it Positive V
      i. Multiply the existing voltage values by -1, drag down
   d. Make a new column next to the current column call it mA/cm^2

       i.   Divide the existing current by the area of that cell, drag down

e. Make a new column at the end, call it Power (mW/cm^2)

       i.   Multiply the Positive V column by the mA/cm^2 column, drag down

f. Make a new column to the right of the Power column

       i.   Divide the the Power column by 100 mW/cm^2 (total incident power) and multiply by 100%

      ii.   The power conversion efficiency is the maximum value in this column

             1. You can find this by using the =MAX command and selecting the range

Appendix D: Computational Modeling Input Files & Scripts

Appendix D1: BiI$_3$ Optimization

INCAR
System = BiI3
 ENCUT = 300.000000
 SIGMA = 0.100000
 EDIFF = 1.00e-05
 EDIFFG = -5.00e-02
 PREC = Normal
 ALGO = 38
 ISPIN = 2
 ISMEAR = 0
 ISTART = 0
 NSW = 500
 IVDW = 12
 IBRION = 2
 ISIF = 2
 LCHARG = .FALSE.
 LWAVE = .FALSE.

KPOINTS
KPOINTS
0
Gamma
3 3 1
0 0 0

POSCAR
Bi I
1.0
      7.55   0.0000000000   0.0000000000
      -3.77   6.538   0.0000000000
      0.0000000000   0.0000000000   20.65
Bi I
6 18
Direct
0.000000 0.000000 0.333241

0.666667 0.333333 0.000092
0.666667 0.333333 0.666574
0.333333 0.666667 0.333426
0.333333 0.666667 0.999908
0.000000 0.000000 0.666759
0.356590 0.002649 0.078976
0.997351 0.353941 0.078976
0.020607 0.689923 0.254358
0.669315 0.979393 0.254358
0.310077 0.330685 0.254358
0.646059 0.643410 0.078976
0.023256 0.335982 0.412309
0.664018 0.687274 0.412309
0.687274 0.023256 0.587691
0.335982 0.312726 0.587691
0.976744 0.664018 0.587691
0.312726 0.976744 0.412309
0.689923 0.669315 0.745642
0.330685 0.020607 0.745642
0.353941 0.356590 0.921024
0.002649 0.646059 0.921024
0.643410 0.997351 0.921024
0.979393 0.310077 0.745642

POTCAR (only first few lines)
 PAW_PBE Bi_d 06Sep2000
 15.0000000000000000
 parameters from PSCTR are:
  VRHFIN =Bi:
  LEXCH = PE
  EATOM = 1958.6135 eV, 143.9540 Ry

  TITEL = PAW_PBE Bi_d 06Sep2000
  LULTRA =   F   use ultrasoft PP ?
  IUNSCR =   1   unscreen: 0-lin 1-nonlin 2-no
  RPACOR =   2.200   partial core radius
  POMASS = 208.980; ZVAL =   15.000   mass and valenz
  RCORE =   2.500   outmost cutoff radius
  RWIGS =   3.090; RWIGS =   1.635   wigner-seitz radius (au A)
  ENMAX = 242.851; ENMIN = 182.138 eV

ICORE =   3   local potential
LCOR   =   T   correct aug charges
LPAW   =   T   paw PP
EAUG   = 442.899
DEXC   =   -.001
RMAX   =   2.959   core radius for proj-oper
RAUG   =   1.300   factor for augmentation sphere
RDEP   =   2.650   radius for radial grids
QCUT   = -4.225; QGAM   =   8.450   optimization parameters

Appendix D2: Oxidized BiI$_3$

INCAR
System = BiI3
 ENCUT = 450.000000
 SIGMA = 0.100000
 EDIFF = 1.00e-05
 EDIFFG = -5.00e-02
 PREC = Normal
 ALGO = 38
 ISPIN = 2
 ISMEAR = 0
 ISTART = 0
 NSW = 500
 IVDW = 12
 IBRION = 2
 ISIF = 2
 LCHARG = .FALSE.
 LWAVE = .FALSE.

KPOINTS
KPOINTS
0
Gamma
3 3 1
0 0 0

POSCAR for Calculation 1
Bi I O
 1.0000000000000000

```
7.5499999999999998    0.0000000000000000    0.0000000000000000
0.0000000000000000    7.5499999999999998    0.0000000000000000
0.0000000000000000    0.0000000000000000   20.6499999999999986
  6  16   1
Cartesian
 0.0000000000000000  0.0000000000000000   6.8814299999999999
 3.7766700000000002  2.1793300000000002   0.0019000000000000
 3.7766700000000002  2.1793300000000002  13.7647499999999994
 0.0033300000000000  4.3586700000000000   6.8852500000000001
 0.0033300000000000  4.3586700000000000  20.6480999999999995
 0.0000000000000000  0.0000000000000000  13.7685700000000004
 2.6822699999999999  0.0173200000000000   1.6308499999999999
 6.1956400000000000  2.3140700000000001   1.6308499999999999
-2.4454300000000000  4.5107200000000001   5.2524899999999999
 1.3610199999999999  6.4032700000000000   5.2524899999999999
 1.0944000000000000  2.1620200000000001   5.2524899999999999
 2.4520900000000001  4.2066100000000004   1.6308499999999999
-1.0910700000000000  2.1966500000000000   8.5141799999999996
 2.4223100000000000  4.4934000000000003   8.5141799999999996
 5.1012399999999998  0.1520500000000000  12.1358200000000007
 1.3576900000000001  2.0446000000000000  12.1358200000000007
 4.8710699999999996  4.3413500000000003  12.1358200000000007
-1.3212400000000000  6.3859500000000002   8.5141799999999996
 2.4189799999999999  0.1347300000000000  15.3975100000000005
 1.3279099999999999  2.3313899999999999  19.0191499999999998
-2.4156399999999998  4.2239300000000002  19.0191499999999998
 1.0977300000000001  6.5206799999999996  19.0191499999999998
 2.7326299999999999  3.3074699999999999  15.5474700000000006
```

POSCAR for Calculation 2
```
Bi  I  O
 1.0000000000000000
    7.5499999999999998    0.0000000000000000    0.0000000000000000
    0.0000000000000000    7.5499999999999998    0.0000000000000000
    0.0000000000000000    0.0000000000000000   20.6499999999999986
  6  16   1
Cartesian
 0.0000000000000000  0.0000000000000000   6.8814299999999999
 3.7766700000000002  2.1793300000000002   0.0019000000000000
 3.7766700000000002  2.1793300000000002  13.7647499999999994
```

```
0.0033300000000000  4.3586700000000000  6.8852500000000001
0.0033300000000000  4.3586700000000000  20.6480999999999995
0.0000000000000000  0.0000000000000000  13.7685700000000004
2.6822699999999999  0.0173200000000000  1.6308499999999999
6.1956400000000000  2.3140700000000001  1.6308499999999999
-2.4454300000000000  4.5107200000000001  5.2524899999999999
1.3610199999999999  6.4032700000000000  5.2524899999999999
1.0944000000000000  2.1620200000000001  5.2524899999999999
2.4520900000000001  4.2066100000000004  1.6308499999999999
-1.0910700000000000  2.1966500000000000  8.5141799999999996
2.4223100000000000  4.4934000000000003  8.5141799999999996
1.3576900000000001  2.0446000000000000  12.1358200000000007
-1.3212400000000000  6.3859500000000002  8.5141799999999996
2.6856000000000000  4.3759800000000002  15.3975100000000005
2.4189799999999999  0.1347300000000000  15.3975100000000005
1.3279099999999999  2.3313899999999999  19.0191499999999998
-2.4156399999999998  4.2239300000000002  19.0191499999999998
1.0977300000000001  6.5206799999999996  19.0191499999999998
6.2254300000000002  2.0272800000000002  15.3975100000000005
5.3032500000000002  1.8965500000000000  11.7907899999999994
```

POSCAR for Calculation 3

```
Bi  I  O
 1.0000000000000000
     7.5499999999999998  0.0000000000000000  0.0000000000000000
     0.0000000000000000  7.5499999999999998  0.0000000000000000
     0.0000000000000000  0.0000000000000000  20.6499999999999986
  6  16   1
Cartesian
 0.0000000000000000  0.0000000000000000  6.8814299999999999
 3.7766700000000002  2.1793300000000002  0.0019000000000000
 3.7766700000000002  2.1793300000000002  13.7647499999999994
 0.0033300000000000  4.3586700000000000  6.8852500000000001
 0.0033300000000000  4.3586700000000000  20.6480999999999995
 0.0000000000000000  0.0000000000000000  13.7685700000000004
 2.6822699999999999  0.0173200000000000  1.6308499999999999
-2.4454300000000000  4.5107200000000001  5.2524899999999999
 1.3610199999999999  6.4032700000000000  5.2524899999999999
 1.0944000000000000  2.1620200000000001  5.2524899999999999
-1.0910700000000000  2.1966500000000000  8.5141799999999996
```

2.4223100000000000 4.4934000000000003 8.5141799999999996
5.1012399999999998 0.1520500000000000 12.1358200000000007
1.3576900000000001 2.0446000000000000 12.1358200000000007
4.8710699999999996 4.3413500000000003 12.1358200000000007
-1.3212400000000000 6.3859500000000002 8.5141799999999996
2.6856000000000000 4.3759800000000002 15.3975100000000005
2.4189799999999999 0.1347300000000000 15.3975100000000005
1.3279099999999999 2.3313899999999999 19.0191499999999998
-2.4156399999999998 4.2239300000000002 19.0191499999999998
1.0977300000000001 6.5206799999999996 19.0191499999999998
6.2254300000000002 2.0272800000000002 15.3975100000000005
4.0488400000000002 3.7488100000000002 2.0382600000000002

POSCAR for Calculation 4
Bi I O
 1.0000000000000000
    7.5499999999999998   0.0000000000000000   0.0000000000000000
    0.0000000000000000   7.5499999999999998   0.0000000000000000
    0.0000000000000000   0.0000000000000000   20.6499999999999986
  6 17   1
Cartesian
 0.0000000000000000 0.0000000000000000 6.8814299999999999
 3.7766700000000002 2.1793300000000002 0.0019000000000000
 3.7766700000000002 2.1793300000000002 13.7647499999999994
 0.0033300000000000 4.3586700000000000 6.8852500000000001
 0.0033300000000000 4.3586700000000000 20.6480999999999995
 0.0000000000000000 0.0000000000000000 13.7685700000000004
 2.6822699999999999 0.0173200000000000 1.6308499999999999
 6.1956400000000000 2.3140700000000001 1.6308499999999999
-2.4454300000000000 4.5107200000000001 5.2524899999999999
 1.3610199999999999 6.4032700000000000 5.2524899999999999
 1.0944000000000000 2.1620200000000001 5.2524899999999999
 2.4520900000000001 4.2066100000000004 1.6308499999999999
-1.0910700000000000 2.1966500000000000 8.5141799999999996
 5.1012399999999998 0.1520500000000000 12.1358200000000007
 1.3576900000000001 2.0446000000000000 12.1358200000000007
 4.8710699999999996 4.3413500000000003 12.1358200000000007
-1.3212400000000000 6.3859500000000002 8.5141799999999996
 2.6856000000000000 4.3759800000000002 15.3975100000000005
 2.4189799999999999 0.1347300000000000 15.3975100000000005

1.3279099999999999   2.3313899999999999   19.0191499999999998
-2.4156399999999998   4.2239300000000002   19.0191499999999998
 1.0977300000000001   6.5206799999999996   19.0191499999999998
 6.2254300000000002   2.0272800000000002   15.3975100000000005
 2.7520600000000002   4.4503500000000003   8.5306099999999994

POSCAR for Calculation 5
Bi I O
 1.0000000000000000
    7.5499999999999998   0.0000000000000000   0.0000000000000000
    0.0000000000000000   7.5499999999999998   0.0000000000000000
    0.0000000000000000   0.0000000000000000   20.6499999999999986
  6 17   1
Cartesian
 0.0000000000000000   0.0000000000000000   6.8814299999999999
 3.7766700000000002   2.1793300000000002   0.0019000000000000
 3.7766700000000002   2.1793300000000002   13.7647499999999994
 0.0033300000000000   4.3586700000000000   6.8852500000000001
 0.0033300000000000   4.3586700000000000   20.6480999999999995
 0.0000000000000000   0.0000000000000000   13.7685700000000004
 2.6822699999999999   0.0173200000000000   1.6308499999999999
 6.1956400000000000   2.3140700000000001   1.6308499999999999
-2.4454300000000000   4.5107200000000001   5.2524899999999999
 1.3610199999999999   6.4032700000000000   5.2524899999999999
 1.0944000000000000   2.1620200000000001   5.2524899999999999
 2.4520900000000001   4.2066100000000004   1.6308499999999999
-1.0910700000000000   2.1966500000000000   8.5141799999999996
 2.4223100000000000   4.4934000000000003   8.5141799999999996
 5.1012399999999998   0.1520500000000000   12.1358200000000007
 1.3576900000000001   2.0446000000000000   12.1358200000000007
 4.8710699999999996   4.3413500000000003   12.1358200000000007
-1.3212400000000000   6.3859500000000002   8.5141799999999996
 2.6856000000000000   4.3759800000000002   15.3975100000000005
 2.4189799999999999   0.1347300000000000   15.3975100000000005
-2.4156399999999998   4.2239300000000002   19.0191499999999998
 1.0977300000000001   6.5206799999999996   19.0191499999999998
 6.2254300000000002   2.0272800000000002   15.3975100000000005
 0.6980300000000000   2.8095200000000000   18.8812199999999990

POSCAR for Calculation 6
Bi I O
 1.0000000000000000
     7.5499999999999998   0.0000000000000000   0.0000000000000000
     0.0000000000000000   7.5499999999999998   0.0000000000000000
     0.0000000000000000   0.0000000000000000   20.6499999999999986
   6 17   1
Cartesian
  0.0000000000000000 0.0000000000000000 6.8814299999999999
  3.7766700000000002 2.1793300000000002 0.0019000000000000
  3.7766700000000002 2.1793300000000002 13.7647499999999994
  0.0033300000000000 4.3586700000000000 6.8852500000000001
  0.0033300000000000 4.3586700000000000 20.6480999999999995
  0.0000000000000000 0.0000000000000000 13.7685700000000004
  2.6822699999999999 0.0173200000000000 1.6308499999999999
  6.1956400000000000 2.3140700000000001 1.6308499999999999
 -2.4454300000000000 4.5107200000000001 5.2524899999999999
  1.3610199999999999 6.4032700000000000 5.2524899999999999
  1.0944000000000000 2.1620200000000001 5.2524899999999999
  2.4520900000000001 4.2066100000000004 1.6308499999999999
 -1.0910700000000000 2.1966500000000000 8.5141799999999996
  2.4223100000000000 4.4934000000000003 8.5141799999999996
  5.1012399999999998 0.1520500000000000 12.1358200000000007
  1.3576900000000001 2.0446000000000000 12.1358200000000007
  4.8710699999999996 4.3413500000000003 12.1358200000000007
 -1.3212400000000000 6.3859500000000002 8.5141799999999996
  2.4189799999999999 0.1347300000000000 15.3975100000000005
  1.3279099999999999 2.3313899999999999 19.0191499999999998
 -2.4156399999999998 4.2239300000000002 19.0191499999999998
  1.0977300000000001 6.5206799999999996 19.0191499999999998
  6.2254300000000002 2.0272800000000002 15.3975100000000005
  2.8241900000000002 4.1600200000000003 15.4719700000000007

POSCAR for Calculation 7
Bi I O
 1.0000000000000000
     7.5499999999999998   0.0000000000000000   0.0000000000000000
     0.0000000000000000   7.5499999999999998   0.0000000000000000
     0.0000000000000000   0.0000000000000000   20.6499999999999986
   6 18   1

Cartesian
 0.0000000000000000 0.0000000000000000 6.8814299999999999
 3.7766700000000002 2.1793300000000002 0.0019000000000000
 3.7766700000000002 2.1793300000000002 13.7647499999999994
 0.0033300000000000 4.3586700000000000 6.8852500000000001
 0.0033300000000000 4.3586700000000000 20.6480999999999995
 0.0000000000000000 0.0000000000000000 13.7685700000000004
 2.6822699999999999 0.0173200000000000 1.6308499999999999
 6.1956400000000000 2.3140700000000001 1.6308499999999999
-2.4454300000000000 4.5107200000000001 5.2524899999999999
 1.3610199999999999 6.4032700000000000 5.2524899999999999
 1.0944000000000000 2.1620200000000001 5.2524899999999999
 2.4520900000000001 4.2066100000000004 1.6308499999999999
-1.0910700000000000 2.1966500000000000 8.5141799999999996
 2.4223100000000000 4.4934000000000003 8.5141799999999996
 5.1012399999999998 0.1520500000000000 12.1358200000000007
 1.3576900000000001 2.0446000000000000 12.1358200000000007
 4.8710699999999996 4.3413500000000003 12.1358200000000007
-1.3212400000000000 6.3859500000000002 8.5141799999999996
 2.6856000000000000 4.3759800000000002 15.3975100000000005
 2.4189799999999999 0.1347300000000000 15.3975100000000005
 1.3279099999999999 2.3313899999999999 19.0191499999999998
-2.4156399999999998 4.2239300000000002 19.0191499999999998
 1.0977300000000001 6.5206799999999996 19.0191499999999998
 6.2254300000000002 2.0272800000000002 15.3975100000000005
 1.9812200000000000 3.2477200000000002 17.2412999999999990

POSCAR for Calculation 8
Bi I O
 1.0000000000000000
    7.5499999999999998   0.0000000000000000   0.0000000000000000
    0.0000000000000000   7.5499999999999998   0.0000000000000000
    0.0000000000000000   0.0000000000000000 20.6499999999999986
  6 18   1
Cartesian
 0.0000000000000000 0.0000000000000000 6.8814299999999999
 3.7766700000000002 2.1793300000000002 0.0019000000000000
 3.7766700000000002 2.1793300000000002 13.7647499999999994
 0.0033300000000000 4.3586700000000000 6.8852500000000001
 0.0033300000000000 4.3586700000000000 20.6480999999999995

```
 0.0000000000000000  0.0000000000000000 13.7685700000000004
 2.6822699999999999  0.0173200000000000  1.6308499999999999
 6.1956400000000000  2.3140700000000001  1.6308499999999999
-2.4454300000000000  4.5107200000000001  5.2524899999999999
 1.3610199999999999  6.4032700000000000  5.2524899999999999
 1.0944000000000000  2.1620200000000001  5.2524899999999999
 2.4520900000000001  4.2066100000000004  1.6308499999999999
-1.0910700000000000  2.1966500000000000  8.5141799999999996
 2.4223100000000000  4.4934000000000003  8.5141799999999996
 5.1012399999999998  0.1520500000000000 12.1358200000000007
 1.3576900000000001  2.0446000000000000 12.1358200000000007
 4.8710699999999996  4.3413500000000003 12.1358200000000007
-1.3212400000000000  6.3859500000000002  8.5141799999999996
 2.6856000000000000  4.3759800000000002 15.3975100000000005
 2.4189799999999999  0.1347300000000000 15.3975100000000005
 1.3279099999999999  2.3313899999999999 19.0191499999999998
-2.4156399999999998  4.2239300000000002 19.0191499999999998
 1.0977300000000001  6.5206799999999996 19.0191499999999998
 6.2254300000000002  2.0272800000000002 15.3975100000000005
 2.0646700000000000  3.3697200000000000 10.3584499999999995
```

POSCAR for Calculation 9

```
Bi  I  O
 1.0000000000000000
     7.5499999999999998   0.0000000000000000   0.0000000000000000
     0.0000000000000000   7.5499999999999998   0.0000000000000000
     0.0000000000000000   0.0000000000000000  20.6499999999999986
   6  18   1
Cartesian
 0.0000000000000000  0.0000000000000000  6.8814299999999999
 3.7766700000000002  2.1793300000000002  0.0019000000000000
 3.7766700000000002  2.1793300000000002 13.7647499999999994
 0.0033300000000000  4.3586700000000000  6.8852500000000001
 0.0033300000000000  4.3586700000000000 20.6480999999999995
 0.0000000000000000  0.0000000000000000 13.7685700000000004
 2.6822699999999999  0.0173200000000000  1.6308499999999999
 6.1956400000000000  2.3140700000000001  1.6308499999999999
-2.4454300000000000  4.5107200000000001  5.2524899999999999
 1.3610199999999999  6.4032700000000000  5.2524899999999999
 1.0944000000000000  2.1620200000000001  5.2524899999999999
```

```
2.4520900000000001  4.2066100000000004  1.6308499999999999
-1.0910700000000000  2.1966500000000000  8.5141799999999996
2.4223100000000000  4.4934000000000003  8.5141799999999996
5.1012399999999998  0.1520500000000000 12.1358200000000007
1.3576900000000001  2.0446000000000000 12.1358200000000007
4.8710699999999996  4.3413500000000003 12.1358200000000007
-1.3212400000000000  6.3859500000000002  8.5141799999999996
2.6856000000000000  4.3759800000000002 15.3975100000000005
2.4189799999999999  0.1347300000000000 15.3975100000000005
1.3279099999999999  2.3313899999999999 19.0191499999999998
-2.4156399999999998  4.2239300000000002 19.0191499999999998
1.0977300000000001  6.5206799999999996 19.0191499999999998
6.2254300000000002  2.0272800000000002 15.3975100000000005
4.0601200000000004  4.5800099999999997  9.3981800000000000
```

POTCAR (only first few lines)
PAW_PBE Bi_d 06Sep2000
 15.0000000000000000
 parameters from PSCTR are:
  VRHFIN =Bi:
  LEXCH = PE
  EATOM = 1958.6135 eV, 143.9540 Ry

  TITEL = PAW_PBE Bi_d 06Sep2000
  LULTRA =   F   use ultrasoft PP ?
  IUNSCR =   1   unscreen: 0-lin 1-nonlin 2-no
  RPACOR =   2.200   partial core radius
  POMASS = 208.980; ZVAL   =   15.000   mass and valenz
  RCORE =   2.500   outmost cutoff radius
  RWIGS =   3.090; RWIGS =   1.635   wigner-seitz radius (au A)
  ENMAX = 242.851; ENMIN = 182.138 eV
  ICORE =   3   local potential
  LCOR   =   T   correct aug charges
  LPAW   =   T   paw PP
  EAUG   = 442.899
  DEXC   =   -.001
  RMAX   =   2.959   core radius for proj-oper
  RAUG   =   1.300   factor for augmentation sphere
  RDEP   =   2.650   radius for radial grids
  QCUT   =   -4.225; QGAM   =   8.450   optimization parameters

Appendix D3: DOS Graph Script

```python
import csv
import pymatgen as mg
import numpy as np
from pymatgen.io.vasp.outputs import Vasprun
from pymatgen.electronic_structure.core import Spin, Orbital
from pymatgen.electronic_structure.dos import Dos
import matplotlib
matplotlib.use('Agg')
import matplotlib.pyplot as plt

def get_dos(smear, labels):
    atom_header = []; orb_header = []
    orb_array = np.arange(1,nedos+1).reshape((-1,1))
    atom_array = np.arange(1,nedos+1).reshape((-1,1))
    element_counter = 0
    for i in range(len(natoms_list)):
        dosatom = np.zeros(nedos)
        for i_elem in range(natoms_list[i]):
            dos = dosrun.pdos[element_counter]
            keys = dos.keys()

            dicts = {'S': dos[keys[0]][Spin.up] + dos[keys[0]][Spin.down]}
            dictp = {'P': dos[keys[1]][Spin.up] + dos[keys[1]][Spin.down]}
            dictd = {'D': dos[keys[2]][Spin.up] + dos[keys[2]][Spin.down]}

            #Orbital resolved DOS
            orbSmeareds = Dos(dosrun.tdos.efermi, dosrun.tdos.energies,
dicts).get_smeared_densities(smear)
            orbSmearedp = Dos(dosrun.tdos.efermi, dosrun.tdos.energies,
dictp).get_smeared_densities(smear)
            orbSmearedd = Dos(dosrun.tdos.efermi, dosrun.tdos.energies,
dictd).get_smeared_densities(smear)
            #Matrix to store all orbital resolved DOS
            orb_array = np.append(orb_array, orbSmeareds.values()[0].reshape((-1,1)), axis=1)
            orb_array = np.append(orb_array, orbSmearedp.values()[0].reshape((-1,1)), axis=1)
            orb_array = np.append(orb_array, orbSmearedd.values()[0].reshape((-1,1)), axis=1)

            #Distinct atomic species resolved DOS
```

```
        dos_add = [ii + jj + kk for ii, jj, kk in zip(dicts.values(), dictp.values(), dictd.values())][0]
        #all_dos.append([dicts.values(), dictp.values(), dictd.values()])
        #Adding all dos per atomic species
        dosatom += dos_add
        dictatom = {'Atom': dosatom}
        #AtomSmeared stores DOS based of each distinct species. DOS of distinct species
involves addition
        #of DOS for each similar kind of atom
        AtomSmeared = Dos(dosrun.tdos.efermi, dosrun.tdos.energies,
dictatom).get_smeared_densities(smear)

        #Atom resolved DOS. #citatom__each_atom is to get DOS for each atom (not distinct
species)
        dictatom_each_atom = {'Atom': dos_add}
        AtomSmeared_each_atom = Dos(dosrun.tdos.efermi, dosrun.tdos.energies,
dictatom_each_atom).get_smeared_densities(smear)
        #Matrix to store all atomic DOS
        atom_array = np.append(atom_array, AtomSmeared_each_atom.values()[0].reshape((-
1,1)), axis=1)

        element_counter += 1
      #List to store DOS per distinct atomic species for automatic plotting
      dos_list.append(AtomSmeared.values()[0])

    #Finally add in Total DOS and E-Efermi energies to orb_array and atom_array matrices
    totup = Dos(dosrun.tdos.efermi, dosrun.tdos.energies,
dosrun.tdos.densities).get_smeared_densities(smear)[Spin.up]
    totdown = Dos(dosrun.tdos.efermi, dosrun.tdos.energies,
dosrun.tdos.densities).get_smeared_densities(smear)[Spin.down]
    totdos = totup + totdown

    e_ef = (dosrun.tdos.energies-dosrun.tdos.efermi).reshape((-1,1))

    orb_array = np.append(orb_array, totdos.reshape((-1,1)), axis=1)
    orb_array = np.append(orb_array, e_ef, axis=1)
    atom_array = np.append(atom_array, totdos.reshape((-1,1)), axis=1)
    atom_array = np.append(atom_array, e_ef, axis=1)

    #Build header for atomic DOS and orbital DOS
    for i, j in zip(natoms_list, labels):
```

```
        count = 0
        while count < i:
            atom_header.append(j)
            orb_header.append('%s-s'%j)
            orb_header.append('%s-p'%j)
            orb_header.append('%s-d'%j)
            count += 1

    atom_header = ', '.join(['NEDOS'] + atom_header + ['Total'] + ['E-Efermi (eV)'])
    orb_header = ', '.join(['NEDOS'] + orb_header + ['Total'] + ['E-Efermi (eV)'])

    #Write matrix to file
    np.savetxt('summary_orbital.csv', orb_array, header=orb_header, fmt='%1.7e', delimiter=',')
    np.savetxt('summary_atomic.csv', atom_array, header=atom_header, fmt='%1.7e',
delimiter=',')

    #return dos_list for automatic plotting
    return dos_list

def get_total_dos(smear):
    totup = Dos(dosrun.tdos.efermi, dosrun.tdos.energies,
dosrun.tdos.densities).get_smeared_densities(smear)[Spin.up]
    totdown = Dos(dosrun.tdos.efermi, dosrun.tdos.energies,
dosrun.tdos.densities).get_smeared_densities(smear)[Spin.down]
    totdos = totup + totdown
    return totdos

def plot_dos(labels):
    fig = plt.figure(figsize=(9.6,6))
    ax = plt.subplot2grid((1,1), (0,0))
    e_ef = (dosrun.tdos.energies-dosrun.tdos.efermi)
    plt.plot(e_ef, get_total_dos(smear), color='k', label='Total')

    for pp, label in zip(get_dos(smear, labels), labels):
        ax.plot(e_ef, pp,linewidth=1.5, label=label)

    ax.set_ylabel('Density of states')
    ax.set_xlabel('E-Efermi (eV)')
    tmp = raw_input("Enter X, Y limits separated by comma as xmin, xmax, ymin, ymax: ")
    limits = [float(ll) for ll in tmp.split(',')]
```

```python
    plt.axis(limits)
    plt.legend(loc='upper right', bbox_to_anchor=(0.95,0.95))
    plt.savefig("dos.png", format="png")


if __name__ == '__main__':
    print "Generating parsed DOS and a quick DOS plot\n"
    element_list = raw_input("Enter list of elements separated by space in the same order as in
POSCAR \n (Example: 'Bi S O' without quoutes): ")
    labels = element_list.split()
    smear = float(raw_input("Enter smearing (0.08 is a reasonable choice): "))

    dos_list = []
    dosrun = Vasprun("./vasprun.xml")
    nedos = len(dosrun.tdos.energies)
    with open("CONTCAR") as f:
        [f.readline() for _ in range(6)]
        line = f.readline()
        natoms_list = [int(aa) for aa in line.split()]

    get_dos(smear, labels)
    plot_dos(labels)
```

Appendix E: Compiled Raw Data

Table 9. Complied Raw Data

SAMPLES 1-18 ARE NOT INCLUDED IN THIS TABLE BECAUSE THEIR PURPOSE WAS
DIRECTED TOWARDS REPRODUCABILITY AND NOT FOR DATA ANALYSIS

Sample #	Cell #	TiO$_2$ Layer Type	BiI$_3$ Spin Coating Speed	Annealing Conditions	Pre/ Post-anneal	Jsc (mA/cm^2)	Voc (V)	Efficiency (%)
19	Cell 1	C	500	100 C on a hot plate for 10 mins	Pre-anneal	0.17	0.01	0.0043%
					Post-anneal	0.28	0.011	0.0008148%
	Cell 2				Pre-anneal	0.26	0.036	0.002362%
					Post-anneal	0.39	0.044	0.004375%
20	Cell 1	CM	500	100 C on a hot plate for 10 mins	Pre-anneal	N/A	N/A	0%
					Post-anneal	0.018	0.003	1.39x10-5%
	Cell 2				Pre-anneal	N/A	N/A	7.64x10-7%
					Post-anneal	0.008	0.0057	1.05x10-5%
21	Cell 1	CMM	500	100 C on a hot plate for 10 mins	Pre-anneal	N/A	N/A	1.39x10-5%
					Post-anneal	0.17	0.003	0.0001427%
	Cell 2				Pre-anneal	0.097	0.005	1.29X10-5%
					Post-anneal	0.26	0.0008	5.00X10-5%
22	Cell 1	C	1000	100 C on a hot plate for 10 mins	Pre-anneal	0.1	0.012	0.000307%
					Post-anneal	0.09	0.001	9.25x10-6%
	Cell 2				Pre-anneal	0.14	0.0066	0.002099%
					Post-anneal	0.23	0.019	0.0012029%
23	Cell 1	CM	1000	100 C on a hot plate for 10 mins	Pre-anneal	1.9	0.158	0.059%
					Post-anneal	2.51	0.185	0.091%
	Cell 2				Pre-anneal	0.7	0.095	0.0164320%
					Post-anneal	0.99	0.17	0.0398275%
24	Cell 1	CMM	1000	100 C on a hot plate for 10 mins	Pre-anneal	0.18	0.01	0.000468%
					Post-anneal	8.1x10-6	0.1	2.3x10-7%
	Cell 2				Pre-anneal	0.17	0.011	0.0004989%
					Post-anneal	0.24	0.003	0.0001972%
25	Cell 1	CMM	1500	100 C on a hot plate for 10 mins	Pre-anneal	0.25	0.032	0.0021700%
					Post-anneal	0.25	0.034	0.0021740%
	Cell 2				Pre-anneal	0.22	0.039	0.0003494%
					Post-anneal	0.22	0.016	0.0009520%
26	Cell 1	CMM	1500	100 C on a hot plate for 10 mins	Pre-anneal	1.32	0.179	0.047%
					Post-anneal	2.01	0.151	0.072%
	Cell 2				Pre-anneal	1.26	0.218	0.0494334%
					Post-anneal	2.5	0.25	0.1184880%

27	Cell 1	CMM	1500	100 C on a hot plate for 10 mins	Pre-anneal	0.25	0.02	0.0013%
					Post-anneal	0.28	0.018	0.0013028%
	Cell 2				Pre-anneal	0.24	0.01	0.0007242%
					Post-anneal	0.29	0.0086	0.0006641
28	Cell 1	CM	1000	250 C in box furnace for 10 mins	Pre-anneal	0.01	6.18x10-5	2.56x10-7%
					Post-anneal	0.09	0.0001	8.6x10-7%
	Cell 2				Pre-anneal	0.02	0.0006	1.37x10-7%
					Post-anneal	0.05	0.0001	8.49x10-7%
29	Both Cells							
30	Both Cells							
31	Both Cells							
32	Cell 1	CM	1000	200 C in box furnace for 15 mins	Pre-anneal	0.05	0.0004	0.000000%
					Post-anneal	0.17	0.006	0.000000%
	Cell 2				Pre-anneal	0.32	0.0065	0.000500%
					Post-anneal	0.22	0.0002	0.012%
33	Cell 1	CM	1000	200 C in box furnace for 20 mins	Pre-anneal	0.075	0.027	0.000486%
					Post-anneal	0.05	0.0004	0.00011%
	Cell 2				Pre-anneal	0.05	0.007	9.7x10-5%
					Post-anneal	0.017	0.0005	3.33x10-6%
34	Cell 1	CM	1000	150 C in box furnace for 10 min	Pre-anneal	0.2	0.006	0.0030%
					Post-anneal	0.1	0.009	0.00024%
	Cell 2				Pre-anneal	0.73	0.074	0.01350%
					Post-anneal	0.51	0.086	0.01100%
35	Cell 1	CM	1000	150 C in box furnace for 15 min	Pre-anneal	0.44	0.01	0.001%
					Post-anneal	0.35	0.012	0.00114%
	Cell 2				Pre-anneal	0.54	0.027	0.00350%
					Post-anneal	0.41	0.048	0.00510%
36	Cell 1	CM	1000	150 C in box furnace for 20 min	Pre-anneal	0.48	0.013	0.00140%
					Post-anneal	0.38	0.02	0.00216%
	Cell 2				Pre-anneal	0.51	0.016	0.002000%
					Post-anneal	0.61	0.026	0.00400%
37	Cell 1	CM	1000	100 C in box furnace for 10 min	Pre-anneal	0.64	0.053	0.00860%
					Post-anneal	0.42	0.11	0.01400%
	Cell 2				Pre-anneal	0.0021	0.0014	6.83x10-7%
					Post-anneal	0.33	0.053	0.00460%
38	Cell 1	CM	1000	100 C in box furnace for 15 min	Pre-anneal	0.8	0.056	0.013000%
					Post-anneal	0.43	0.088	0.00940%
	Cell 2				Pre-anneal	0.6	0.048	0.00750%
					Post-anneal	0.33	0.087	0.00720%
39	Cell 1	CM	1000	100 C in box furnace for 20 min	Pre-anneal	1.05	0.032	0.00862%
					Post-anneal	0.6	0.048	0.00740%
	Cell 2				Pre-anneal	0.53	0.005	4x10-5%
					Post-anneal	0.42	0.0007	2.67x10-5%

40	Cell 1	CM	1000	100 C on hot plate for 10 min	Pre-anneal	0.068	0.015	0.00026%
					Post-anneal	0.081	0.022	0.00042%
	Cell 2				Pre-anneal	N/A	N/A	0.00000%
					Post-anneal	0.003	8.62×10^{-5}	2.9×10^{-7}%
41	Cell 1	CM	1000	40 C in box furnace for 10 min	Pre-anneal	0.0006	0.0003	0.00000%
					Post-anneal	0.004	0.0008	4.6×10^{-7}%
	Cell 2				Pre-anneal	0.001	0.0003	0.00000%
					Post-anneal	0.0026	0.0008	0.00000%
42	Cell 1	CM	1000	50 C in box furnace for 10 min	Pre-anneal	0.086	0.034	0.00074%
					Post-anneal	0.112	0.057	0.00160%
	Cell 2				Pre-anneal	0.014	0.003	1.04×10^{-5}%
					Post-anneal	0.015	0.0043	1.6×10^{-5}%
43	Cell 1	CM	1000	60 C in box furnace for 10 min	Pre-anneal	0.25	0.018	0.00111%
					Post-anneal	0.01	0.0005	0.00000%
	Cell 2				Pre-anneal	0.24	0.025	0.00149%
					Post-anneal	0.002	0.005	0.00000%
44	Cell 1	CM	1000	70 C in box furnace for 10 min	Pre-anneal	0.002	0.0007	1.05×10^{-6}%
					Post-anneal	0.43	0.01	0.00114%
	Cell 2				Pre-anneal	0.0005	0.0002	0.00000%
					Post-anneal	0.16	0.03	0.00121%
45	Cell 1	CM	1000	80 C in box furnace for 10 min	Pre-anneal	0.23	0.023	0.00139%
					Post-anneal	0.41	0.043	0.004441%
	Cell 2				Pre-anneal	0.24	0.005	0.00029%
					Post-anneal	0.21	0.009	0.00049%
46	Cell 1	CM	1000	90 C in box furnace for 10 min	Pre-anneal	0.0005	0.0001	0.00000%
					Post-anneal	0.002	0.003	0.00000%
	Cell 2				Pre-anneal	0.001	0.0001	0.00000%
					Post-anneal	0.004	0.0004	0.00000%
47	Cell 1	CM	1000	100 C in box furnace for 10 min	Pre-anneal	0.0005	0.0001	0.00000%
					Post-anneal	0.003	0.0025	0.00000%
	Cell 2				Pre-anneal	0.0007	0.000226	2.2×10^{-8}%
					Post-anneal	0.0117	0.00013	0.00000%
48	Cell 1	CM	1000	100 C in box furnace for 10 min	Pre-anneal	0.249	0.00614	0.00028%
					Post-anneal	0.27	0.017	0.00118%
	Cell 2				Pre-anneal	0.1793	0.01013	0.00045%
					Post-anneal	0.23	0.011	0.00062%
49	Cell 1	CM	1000	SVA: 100 C for 10 minutes with DMF	Pre-anneal	0.0048	0.0097	1.2×10^{-5}%
					Post-anneal	N/A	N/A	N/A
	Cell 2				Pre-anneal	0.00339	0.0161	1.4×10^{-5}%
					Post-anneal	N/A	N/A	N/A

50	Cell 1	CM	1000	SVA: 100 C for 10 minutes with DMF	Pre-anneal	N/A	N/A	N/A
					Post-anneal	N/A	N/A	N/A
	Cell 2				Pre-anneal	N/A	N/A	N/A
					Post-anneal	N/A	N/A	N/A
51	Cell 1	CM	1000	SVA: 100 C for 10 minutes with DMF	Pre-anneal	0.00322	0.002413	1.1x10-6%
					Post-anneal	0.004	0.004	4x10-6%
	Cell 2				Pre-anneal	0.000166	0.000267	4.4x10-8%
					Post-anneal	0.01114	0.027	7.4x10-5%
52	Cell 1	CM	1000	SVA: 100 C for 10 minutes with DMF	Pre-anneal	0.574	0.053	0.0079%
					Post-anneal	0.483	0.047	0.00594%
	Cell 2				Pre-anneal	0.49	0.026	0.003%
					Post-anneal	0.0388	0.0266	0.00253%
53	Cell 1	CM	1000	SVA: 100 C for 10 minutes with DMF	Pre-anneal	0.34	0.027	0.0022%
					Post-anneal	0.295	0.025	0.0016%
	Cell 2				Pre-anneal	0.26	0.027	0.0018%
					Post-anneal	0.203	0.0287	0.00148%
54	Cell 1	CM	1000	SVA: 100 C for 10 minutes with DMF	Pre-anneal	1.89	0.14	0.062%
					Post-anneal	2.71	0.185	0.1146%
	Cell 2				Pre-anneal	1.27	0.134	0.04%
					Post-anneal	2.056	0.157	0.0856%
55	Cell 1	C	1000	SVA: 100 C for 10 minutes with DMF	Pre-anneal	N/A	N/A	N/A
					Post-anneal	N/A	N/A	N/A
	Cell 2				Pre-anneal	N/A	N/A	N/A
					Post-anneal	N/A	N/A	N/A
56	Cell 1	C	1000	60 C in box furnace for 10 min	Pre-anneal	0.82	0.0998	0.019 %
					Post-anneal	1.161	0.143	0.0382 %
	Cell 2				Pre-anneal	0.574	0.077	0.011 %
					Post-anneal	0.782	0.108	0.0208 %
57	Cell 1	C	1000	70 C in box furnace for 10 min	Pre-anneal	0.0119	0.008	2.2 x 10-5 %
					Post-anneal	0.0107	0.0092	2.43 x 10-5 %
	Cell 2				Pre-anneal	0.0079	0.0072	1.5 x 10-5 %
					Post-anneal	0.0099	0.0135	3.396 x 10-5 %
58	Cell 1	C	1000	70 C in box furnace for 10 min	Pre-anneal	N/A	N/A	7.16 x 10-6 %
					Post-anneal	N/A	N/A	3.178 x 10-7 %
	Cell 2				Pre-anneal	N/A	N/A	2.44 x 10-6 %
					Post-anneal	0.003	0.00024	0 %
59	Cell 1	C	1000	80 C in box furnace for 10 min	Pre-anneal	0.76	0.11	0.018 %
					Post-anneal	1.477	0.163	0.05277 %
	Cell 2				Pre-anneal	0.66	0.102	0.0144 %
					Post-anneal	1.23	0.133	0.0363 %

60	Cell 1	C	1000	80 C in box furnace for 10 min	Pre-anneal	0.573	0.0444	0.0061 %
					Post-anneal	1.097	0.107	0.0276 %
	Cell 2				Pre-anneal	0.136	0.099	0.00306 %
					Post-anneal	0.1896	0.119	0.00515 %
61	Cell 1	C	1000	100 C on hot plate for 10 min	Pre-anneal	0.046	0.068	0.00075 %
					Post-anneal	0.066	0.097	0.00152 %
	Cell 2				Pre-anneal	0.0201	0.0077	3.7 x 10-5 %
					Post-anneal	0.018	0.0092	4.178 x 10-5 %
62	Cell 1	C	1000	SVA: 100 C for 10 minutes with DMF with thermal anneal after	Pre-anneal	0.259	0.15	0.00794 %
					Post-anneal	0.263	0.209	0.0103 %
	Cell 2				Pre-anneal	0.242	0.116	0.0048 %
					Post-anneal	0.173	0.157	0.00634 %
63	Cell 1	C	1000	SVA: 100 C for 10 minutes with DMF with thermal anneal after	Pre-anneal	0.925	0.115	0.02368 %
					Post-anneal	1.492	0.182	0.0598 %
	Cell 2				Pre-anneal	1.725	0.155	0.06353 %
					Post-anneal	2.13	0.211	0.1092 %
64	Cell 1	C	1000	SVA: 100 C for 10 minutes with DMF with thermal anneal after	Pre-anneal	1.614	0.178	0.06861 %
					Post-anneal	2.153	0.285	0.14144 %
	Cell 2				Pre-anneal	1.306	0.164	0.04908 %
					Post-anneal	1.76	0.246	0.09588 %
65	Cell 1	C	1000	SVA: 100 C for 10 minutes with DMF with thermal anneal after	Pre-anneal	0.528	0.109	0.012836 %
					Post-anneal	0.881	0.164	0.03282 %
	Cell 2				Pre-anneal	0.58	0.112	0.01494 %
					Post-anneal	0.986	0.167	0.03881 %
66	Cell 1	C	1000	SVA: 100 C for 10 minutes with DMF with thermal anneal after	Pre-anneal	0.0036	0.00025	0 %
					Post-anneal	0.0103	0.015	4.16 x 10-5 %
	Cell 2				Pre-anneal	N/A	N/A	1.25 x 10-8 %
					Post-anneal	0.00043	0.0028	2.8 x 10-7 %

67	Cell 1	C	1000	SVA: 100 C for 10 minutes with DMF with thermal anneal after	Pre-anneal	0.132	0.1064	0.00325 %
					Post-anneal	0.139	0.137	0.004334 %
	Cell 2				Pre-anneal	0.0175	0.00125	$4.51 \times 10\text{-}6$ %
					Post-anneal	0.01	0.0032	7.96x10-6%
68	Cell 1	C	1000	40 C in box furnace for 10 min	Pre-anneal	0.0133	0.0019	4.37x10-6%
					Post-anneal	0.0089	0.0067	$1.48 \times 10\text{-}5$ %
	Cell 2				Pre-anneal	0.00359	0.0019	$1.59 \times 10\text{-}6$ %
					Post-anneal	0.0026	0.0021	$1.46 \times 10\text{-}6$ %
69	Cell 1	C	1000	40 C in box furnace for 10 min	Pre-anneal	0.002	0.0011	$2.37 \times 10\text{-}7$ %
					Post-anneal	0.00052	0.00133	$1.81 \times 10\text{-}7$ %
	Cell 2				Pre-anneal	0.055	0.00025	$3.16 \times 10\text{-}6$ %
					Post-anneal	0.092	0.004	0 %
70	Cell 1	C	1000	50 C in box furnace for 10 min	Pre-anneal	0.00496	0.0646	$8.24 \times 10\text{-}5$ %
					Post-anneal	0.0062	0.084	0.000137 %
	Cell 2				Pre-anneal	0.00815	0.033	$7.18 \times 10\text{-}5$ %
					Post-anneal	0.01	0.0436	0.000108 %
71	Cell 1	C	1000	50 C in box furnace for 10 min	Pre-anneal	0.0252	0.132	0.000897 %
					Post-anneal	0.025	0.098	0.00065 %
	Cell 2				Pre-anneal	0.044	0.065	0.000693 %
					Post-anneal	0.047	0.084	0.00099 %
72	Cell 1	C	1000	SVA: 100 C for 10 min with thermal anneal after	Pre-anneal	0.012	0.019	$5.78 \times 10\text{-}5$ %
					Post-anneal	0.0044	0.0047	4.8 x 10-6 %
	Cell 2				Pre-anneal	0.019	0.029	0.00014 %
					Post-anneal	0.008	0.008	$1.38 \times 10\text{-}5$ %
73	Cell 1	C	1000	SVA: 100 C for 10 min with thermal anneal after	Pre-anneal	2.06	0.09	0.048 %
					Post-anneal	2.57	0.193	0.134 %
	Cell 2				Pre-anneal	2.05	0.18	0.093 %
					Post-anneal	2.15	0.134	0.077 %

74	Cell 1	C	1000	SVA: 100 C for 10 min with thermal anneal after	Pre-anneal	0.0016	0.0048	1.68×10^{-6} %
					Post-anneal	0.0024	0.0041	2.73×10^{-6} %
	Cell 2				Pre-anneal	0.001	0.0072	1.83×10^{-6} %
					Post-anneal	0.0012	0.0085	2.89×10^{-5} %
75	Cell 1	C	1000	SVA: 100 C for 10 min with thermal anneal after	Pre-anneal	N/A	N/A	N/A
					Post-anneal	1.91	0.16	0.081 %
	Cell 2				Pre-anneal	0.8	0.163	0.031 %
					Post-anneal	0.947	0.186	0.047 %
76	Cell 1	C	1000	SVA: 100 C for 10 min with thermal anneal after	Pre-anneal	0.013	0.145	0.0005 %
					Post-anneal	0.016	0.116	0.00047 %
	Cell 2				Pre-anneal	0.002	0.002	1.14×10^{-6} %
					Post-anneal	0.0049	0.0093	1.09×10^{-5} %
77	Cell 1	CM	1000	SVA: 100 C for 10 min with thermal anneal after	Pre-anneal	0.027	0.04	0.00026 %
					Post-anneal	0.026	0.04	0.00026 %
	Cell 2				Pre-anneal	0.0047	0.02	2.30×10^{-5} %
					Post-anneal	0.0029	0.0081	5.51×10^{-6} %
78	Cell 1	CM	1000	SVA: 100 C for 10 min with thermal anneal after	Pre-anneal	0.162	0.032	0.0013 %
					Post-anneal	0.179	0.042	0.0019 %
	Cell 2				Pre-anneal	0.043	0.03	0.0003 %
					Post-anneal	0.041	0.024	0.00024 %
79	Cell 1	CM	1000	SVA: 100 C for 10 min with thermal anneal after	Pre-anneal	N/A	N/A	N/A
					Post-anneal	0.195	0.039	0.00197 %
	Cell 2				Pre-anneal	0.034	0.033	0.00027 %
					Post-anneal	0.027	0.025	0.000165 %
80	Cell 1	CM	1000	SVA: 100 C for 10 min with thermal anneal after	Pre-anneal	0.26	0.0005	0.00028 %
					Post-anneal	0.249	0.015	0.00097 %
	Cell 2				Pre-anneal	0.18	0.004	0.0002 %
					Post-anneal	0.14	0.006	0.00021 %
81	Cell 1	CM	1000	SVA: 100 C for 10 min with thermal anneal after	Pre-anneal	0.128	0.011	0.00037 %
					Post-anneal	0.194	0.084	0.0041 %
	Cell 2				Pre-anneal	0.038	0.021	0.0002 %
					Post-anneal	0.042	0.059	0.00061 %

Appendix F: Comprehensive Data

Appendix F1: Completed Data Set Graph

Figure 55. Graph of efficiency for all data.
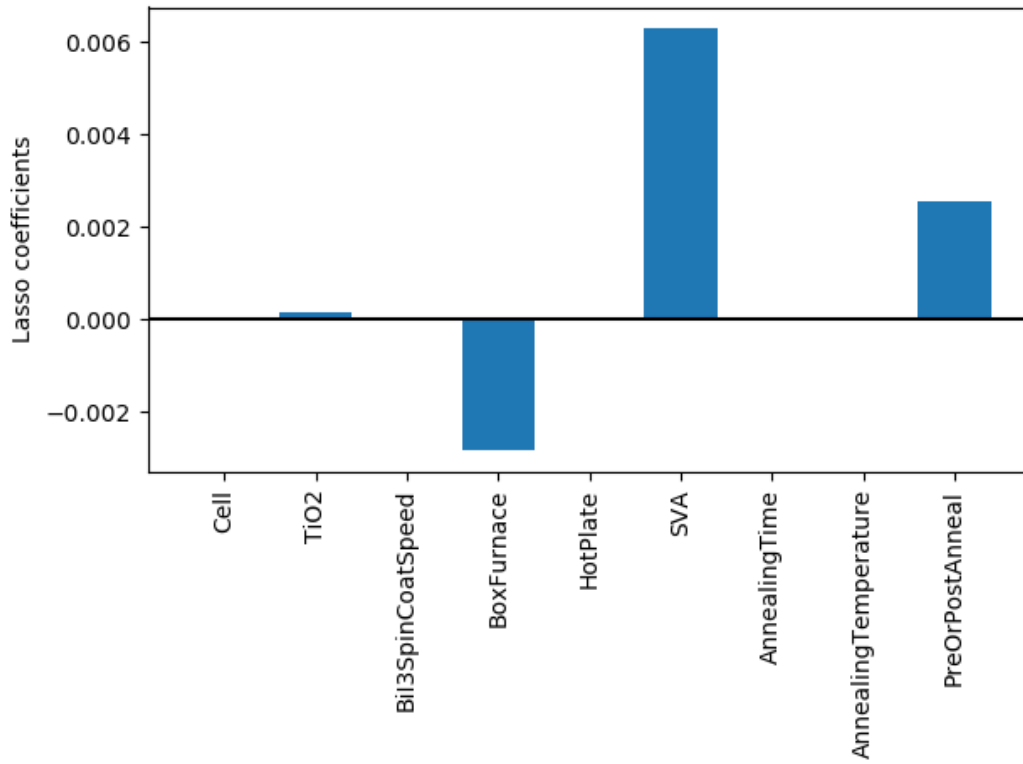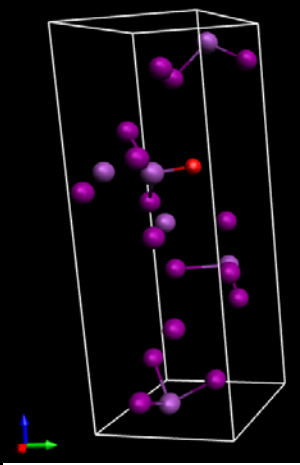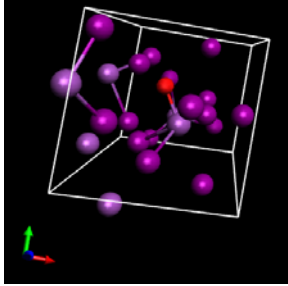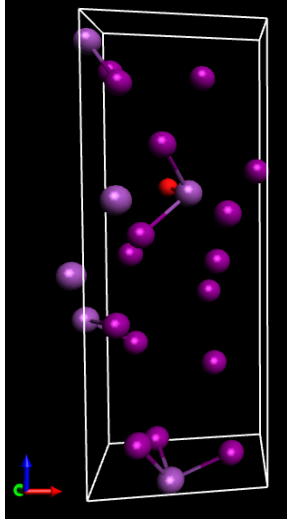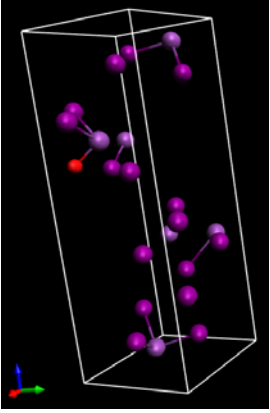
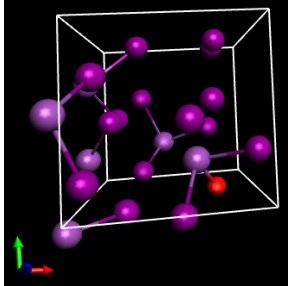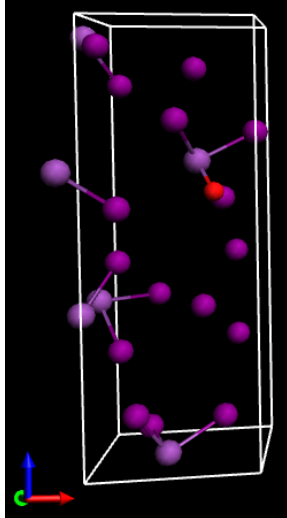**Appendix F2: Statistical Analysis Results**

Figure 56. A lasso linear regression model was made to understand which modifications were the most impactful in our research. Here is is shown that SVA and the post-anneal of samples had the biggest positive impact, where use of the bov furnace negatively impacted our results.
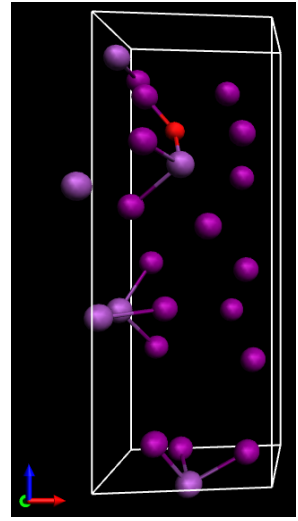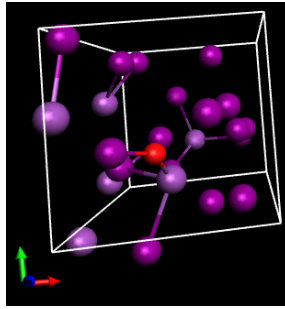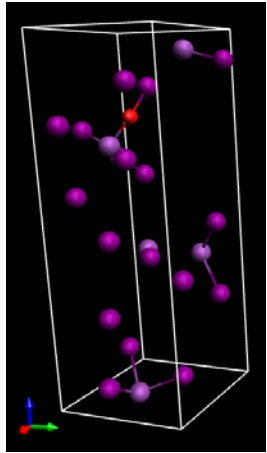
Appendix G: BiI₃ and Oxidized BiI₃ Optimized Geometries

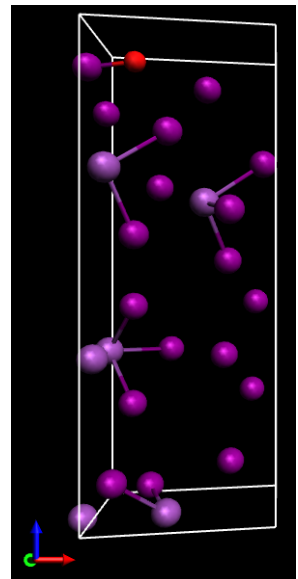*Table 10. Optimized Geometries of Oxidized BiI₃*

Calculation #	Optimized Geometry View 1	Optimized Geometry View 2	Optimized Geometry View 3
1			
2			

3			
4			
5			

6			
7			

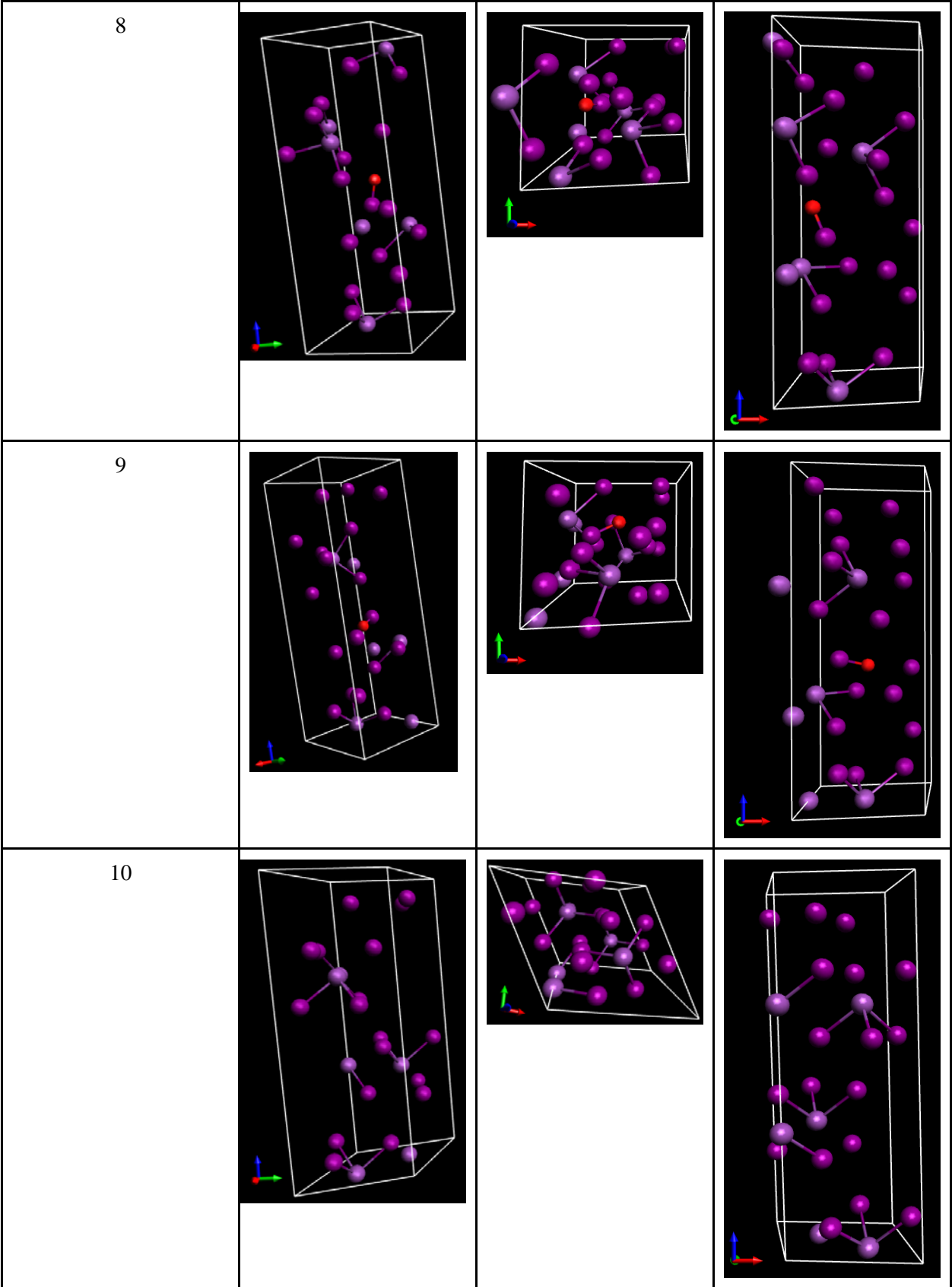| 8			
9			
10			
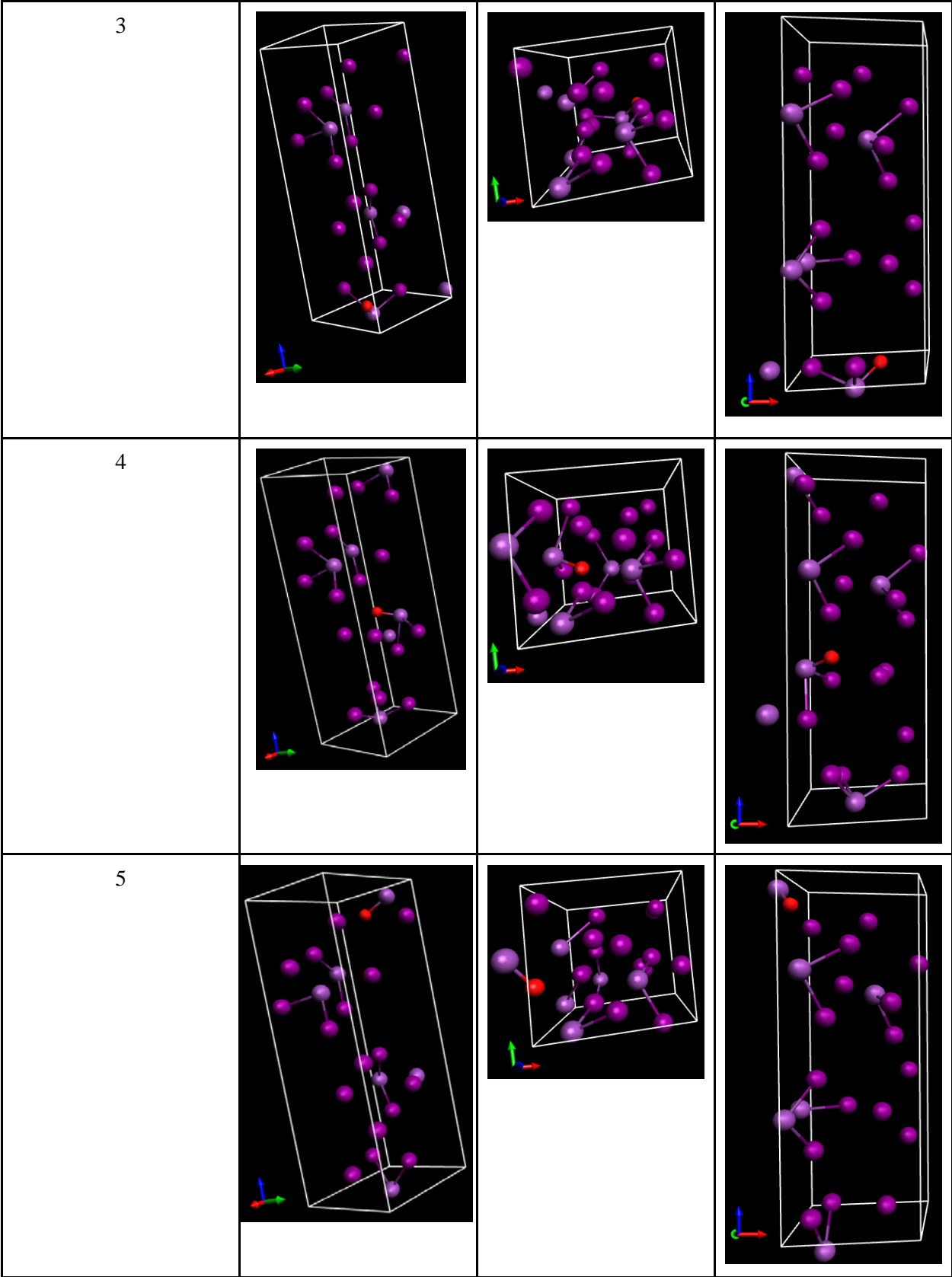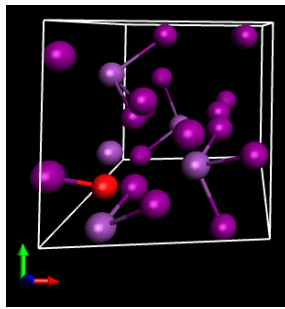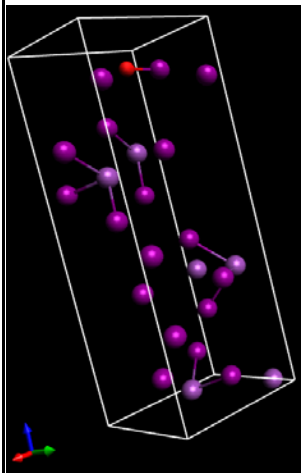
Appendix H: Solar Energy Technology Acceptance Survey

Appendix H1: Administered Condensed Version

Solar Energy Technology Acceptance Survey

Thank you for taking the time to complete this survey. Results will be used to gain a better understanding of public outlook on solar energy technologies and specifically the factors that influence solar adoption. All responses will remain anonymous.

Q1 Please indicate your gender.

○   Male

○   Female

○   Prefer not to say

Q2 Please select the age range with which you identify.

○   21 and Under

○   22 to 34

○   35 - 44

○   45 - 54

○   55 - 64

○   65 and Older

Q3 How familiar are you with solar energy technologies?

○   Extremely familiar

○   Very familiar

○   Moderately familiar

○   Slightly familiar

○   Not familiar at all

Q4 Please rank the following factors as: Not important at all **(1)**, Moderately unimportant **(2)**, Neither important nor unimportant **(3)**, Moderately important **(4)**, or Very important **(5)** when deciding whether or not to make use of a solar technology.

_____ System Quality
_____ Perceived Cost
_____ Perceived Benefits
_____ Reliability
_____ Public Advocate
_____ System Lifetime
_____ Maintenance
_____ Aesthetic